C O R R I G E N D A

Page	Line	Change	To read
21	8	transistors	transitions
27	27	(5 nsec)	(5 msec)
28	16	maximu	maxima
41	16	electrons	electron energy
48	10	$I-V_P$	$I-V_R$
49	21	$n = \sqrt{\Delta/\Delta'}$	$n = (\frac{\Delta}{\Delta'})^2$
53	6	(10^7 MW/cm^2)	(10^7 watts/cm^2)
53	26	c & ad.	c and d
54	10	given	produced
54	26	bean	beam
56	24	ref. 2	ref. 43
70	25	reterded	retarding
72	20	such a	a
73	5	miliampheres	milliamperes
78	17	current	a current
95	23	atom	atoms
110	6	a linear function	independent
112	5	relfectivity	reflectivity

INTERACTIONS OF LASER BEAM WITH SOLIDS

by

S. Rafi Ahmad

Oriel College

Oxford

Thesis Submitted for the Degree of

Doctor of Philosophy

in the University of Oxford

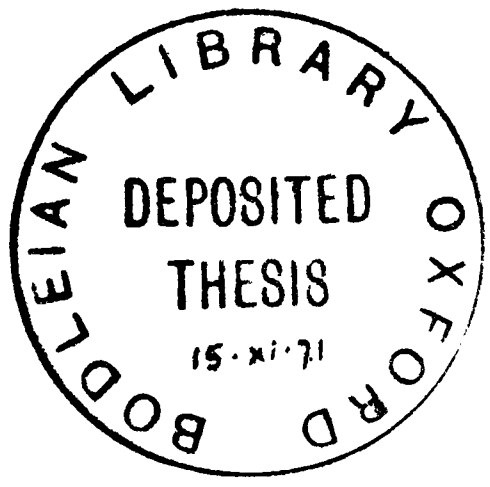

Department of Engineering Science,

Parks Road, OXFORD

March 1971

ABSTRACT

The present investigation is an extension of earlier work in this laboratory on the interaction of laser beams with metallic surfaces. It was conducted with a view to understanding the different processes involved in a laser surface interaction. Initial experiments (Chapter Five) were performed with low laser intensity, so that the Richardson effect was not prominent. The results were interpreted in terms of a double-photon photoeffect. The idea of such a double-photon photoeffect was also supported by the nonlinear optical absorption and double-photon photoconductivity in a CdS crystal (Chapter Eight).

The effect of linear absorption (single-photon absorption) process was investigated for metal surfaces and the results were interpreted in terms of a temperature rise of the target surface. When high intensity laser pulses were incident onto metal surfaces, the generation of a cloud of ionized particles was observed. The cloud was found to move away from the target in a plasma state. The various properties of this plasma and the mechanism of the generation of current signals by the directed motion of the different species of the charges in an applied electric field has been investigated in Chapter Six. In the same chapter, experiments on the reverse photoelectric effect (photoelectric emission from the surrounding metal parts by the high energy photons generated from the metal plasma) showed a positive contribution to the shape of the current signals by such electrons.

Finally, the controversial phenomena of 'rear-side

electron emission' was further investigated in Chapter Seven. It was concluded that the observed current recorded at a collector placed at the rear side of the target when the front surface was irradiated with a focussed Q-switched laser beam could be explained in terms of a capacitance effect. The electrostatic coupling between a collector and any neighbouring metal part, because of the stray capacitance between them, will be of considerable importance when a rapid voltage change of the collector is concerned.

The results of all the experiments were summed up and a general conclusion of the work was presented in Chapter Nine.

CONTENTS

ACKNOWLEDGEMENTS

The present work was carried out under the constant supervision of Dr. D. Walsh. I would like to express my deep gratitude for his advice and support throughout the course of the work.

I wish to acknowledge the help of the staff of the Electronics Workshop, especially Mr. G.N. Roger, and the staff of the General Workshop, in assembling and repairing equipment used in this work.

The technical assistance of Mr. J. Barton, Mr. P. Stannard and Mr. R. Stone is also acknowledged. Thanks are due to many of my colleagues and members of the Department with whom I have shared many interesting discussions.

Finally, I would like to express my thanks to Mrs. M. Matheson for her painstaking effort in skilfully typing this thesis.

This work was supported by the Colombo-Plan Authority and the Scholarship was sponsored by the Pakistan Atomic Energy Commission. Their generosity is gratefully acknowledged.

CHAPTER ONE

INTRODUCTION

Laser-induced emission from solid surfaces has been the subject of study for almost a decade. Photoelectric emission from solids of low work function has been known long before the discovery of lasers. The advent of laser light has provided us with an almost coherent source of light with much higher intensity than the ordinary source. This has geared up further study of photoelectric phenomena in solids. The development of Q-switched lasers has further made it possible to obtain almost unlimited power for a very short time interval, thus enabling the time-resolved investigation of the light-interaction with solids. Intense laser power has also made it possible to induce high currents from metal surfaces.

For metals with high work function, the predominant process of interaction with high power laser light is a heating effect. The laser-induced current is caused mainly by a thermionic process. Normal photoelectric emission from most metals initiated by a laser in the visible region is quite unlikely. But simultaneous absorption of multiple photons by the metal electrons and subsequent emission from the surface is a possible mechanism. Any such process, if it exists, will be overshadowed by the copious amount of thermionic emission. At low laser intensities, the thermionic mechanism can be made negligible and any laser-induced current, if observed, must be explained by a multiphoton-photoeffect. In semiconductors where the energy band gap exceeds the photon energy, the observed high photoconductivity can also be explained in terms of a multi-photon process.

It has been speculated that such a study may provide better insight into the electronic structure of the solids.

The laser is now considered to be an important tool for producing high currents from metals. In fundamental research or in electronic devices, where a time-correlated electron or ion current is required, high energy laser pulses can be used. The possibility of using such fast current pulses of very high amplitude as a remote-control switching device, probably in a high-voltage operation, may be considerable. The generation of an enormous amount of heat when a giant laser pulse interacts with solids is a well-established phenomenon. This property of laser beams has been employed not only in cutting, micro-welding and drilling hard solids but also in medical science, e.g. eye and ear surgery, etc. Furthermore, research is in progress in various places to use this laser-produced high temperature in initiating thermo-nuclear fusion reactions.

In view of the fact that laser-induced current and heat from solid surfaces may find use in science and technology, a detailed analysis of the mechanism of interaction with solid surfaces has been attempted in this work. The detection of charges was done by direct electrostatic probing. Lack of theoretical work on such probe measurements of the transient current made it impossible to be precise in estimating the absolute magnitude of the interaction parameters. Two separate processes of interaction have been considered to take place. The final stage of interaction has been oriented towards the concept of a thermo-mechanical ejection of plasma. The observed results have been explained in terms of the motion of charges of different polarity in

an applied electric field.

Though there exists quite a lot of experimental data on laser interactions with solids, no unique theory is available,so far, to account for it. The main difficulty in interpreting the observed results arises from the fact that the current is transient and the initiating agent acts for an extremely short time interval. Moreover, the laser produces charges of different polarity. The current detected by any electrostatic probe will be given by the combined motion of all the charged particles in the preferred directions. The energy distribution of the emitted electrons will be a complicated function of the initiating laser intensity. Recombination and re-radiation are expected to take place during the motion of the plasma. Secondary electron and ion production may contribute to the detected current. The rapid change in the space potential or the potential of any neighbouring electrode with respect to the earth is likely to induce current signals because of electrostatic coupling. The radiation from the laser-heated spot in a metal may scatter photoelectrons from the surrounding metal parts and the glass envelope. It is, however, suggested from the above considerations that highly sophisticated detecting techniques are necessary to formulate an empirical theory of laser interaction with solid surfaces.

The present work is oriented towards obtaining more information about the interaction and fitting the data to specific models. It is expected that a general explanation of the interaction mechanism can be suggested by comparing the observed results with the phenomenological models.

CHAPTER TWO

REVIEW OF THE PREVIOUS WORK

A huge amount of work has already been done on the various aspects of laser-induced emission. Various theories have been put forward and several models proposed to explain the mechanism of laser interaction with solid surfaces. Different experimental techniques have been employed to measure different parameters of the laser-induced emission. In this chapter a review of the relevant literature available at the start of the present work is made.

2-1 Electron Emission

Emission of electrons from solids under the influence of laser radiation was among the first experimental investigations with lasers. In the year 1963, Honig and Woolston (1), Lichtman and Ready (2), Verber and Adelman (3), and Giori et al. (4) reported independently the emission of electrons from solids when irradiated with focussed non-Q-switched laser beam. The phenomenon was interpreted as merely a thermionic effect. An accurate quantitative analysis of the results of these works was complicated by the fact that laser pulse consisted of many irregular short spikes (Fig. 2-1).

In 1965, Ready (5) first experimented with a Q-switched ruby laser. He calculated the peak temperature rise of a W surface and concluded that for laser intensities up to 25 MW/cm^2 the electron emission was purely thermionic. In a later work he employed a phenomenological model (6) to calculate amounts of material vaporized as a function of thermal properties of the laser pulse. He found a good agreement of his

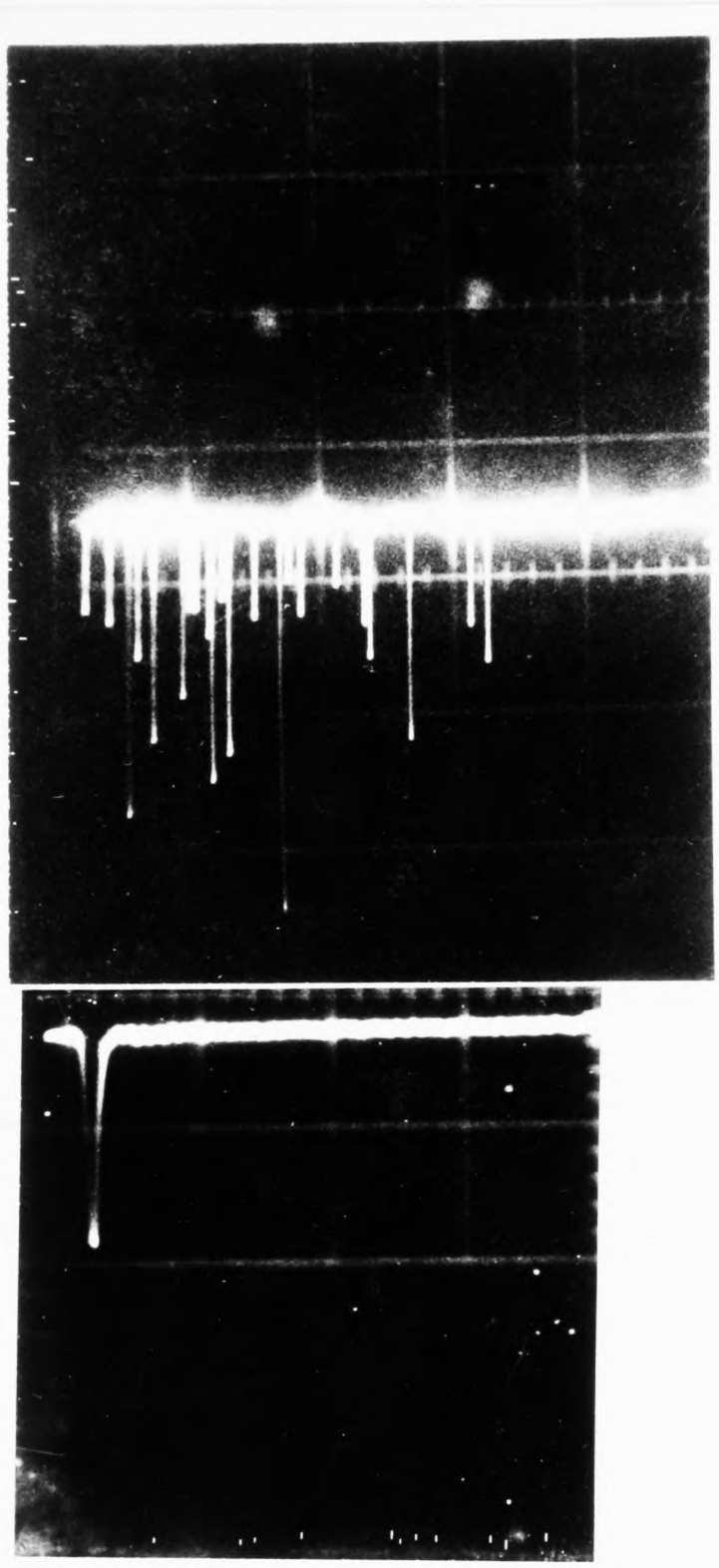

ORDINARY
MODE
OPERATION

Q-SWITCHED
OPERATION

FIG. 2.1. LASER SIGNALS RECORDED AT THE OUTPUT OF A PHOTODIODE.

results with the experimental observations.

Other experiments using a Q-switched ruby laser, reported by Knecht (7), Khan et al. (8), Richards (9) and others, show an additional electron emission pulse (Fig. 2-2) contrary to Ready's observation. Lichtman and Ready (2) investigated the possibility of photoelectric emission and field emission. They have found these processes to be unlikely causes of such high current. Richards (9) reviewed such a possibility for Q-switched laser. He also discarded the possibility of photoelectric emission or field emission. According to his suggestion, any additional peak other than the major thermionic peak in the current signal is caused by some process inherent in the laser-induced emission. Knecht (7) observed that the angle of the incident laser beam has a distinct effect upon the electron emission pattern. He suggested a direct laser field action in the emission process.

In recent works on this topic, multiphoton-photoemission process has become a popular field of investigation. It was thought that multiphoton-photoelectric studies might supply additional information in the electronic structure of solids. Sonnenberg et al. (10) observed an electron emission from Cs_3Sb which followed a square dependence on the light intensity of a Nd-doped glass laser. They explained this as a two photon-photoemission process. Teich et al. (11) reported a photocurrent versus intensity curve using Na and Ne-gas laser which was a mixture of one- and two-photon processes. Double photon absorption has been reported by Braunstein and Ockman (12) when Q-switched ruby laser was irradiated on CdS. Logothetis and Hartman (13) did a systematic study of the laser-induced electron emission from solids. According to

them, the electron emission from Au, stainless steel, KI, CsI and KCl for laser radiation of 1.17, 1.29 and 3.57 - eV photon energy at intensities lower than 15 MW/cm^2 can be explained in terms of two fundamental processes, e.g. thermionic emission and multiphoton-photoelectric emission. In a previous work, Logothetis and Hartman (14) observed three-photon photoelectric emission from evaporated gold films. For an incident ruby laser light of intensity 0.77 MW/cm^2 they calculated the quantum yield for two and three-photon photoemission. They estimated values of $\sim 10^{-9}$ and 10^{-13} electrons per incident photon respectively. Later, Walsh (15) made use of the results obtained by Logothetis and Hartman and, with an intuitive hypothesis and physical model, calculated the multiphoton emission time. He estimated that for multiphoton photoemission to occur, the photons must strike an atom within a time of approximately 10^{-13} seconds.

Along with the investigation of the mechanism of laser-induced electron emission, much work has been done to estimate the state of the electrons. Electron temperature has been estimated by various workers with different techniques. Allen (16), in his first report on electron and ion temperature, concluded that for incident laser beam intensities on solid targets in the range of 10^{10} to 10^{11} watts/cm^2, electron and ion temperatures lie between 10 and 20 eV. He also compiled a table of the electron temperature estimated by other workers. This is quoted here in Table I. In some of these works, laser power density has not been mentioned. But it is believed that the power density ranges between 10^{10} to 10^{11} watts/cm^2. Thus it can be observed from the table that no unique value

TABLE I

Investigator	Ref. No.	Temperature eV	Comments
Archbold, Hughes	17	$\geq$ 10	Spectroscopic
Burgess et al.	18	10<Te<130	Spectroscopic. Te = 40. Best justified.
Ehler	19	$\sim$ 30	Spectroscopic. Rough estimate.
Ambartsumyan et al.	20	$\sim$ 20	Spectroscopic. Rough estimate.
Schlier et al.	21	5<Te<30	Retardation potential.
Opower, Burlefinger	22	< 90	Time of flight.
Basov et al.	23	> 7	Hydrodynamic + experiment.
Alcock et al.	24	< 90	Neon gas break-through, X-ray ratio through foils.

for the electron temperature has so far been achieved. The value estimated lies between 10 to 90 eV roughly.

David et al. (25, 26) used a gas laser as a probe light and a Mach-Zender Interferometer to measure the phase shift due to laser-induced plasma refractivity. From their observation they estimated a particle density of electrons from a carbon surface initiated by laser beam of energy in the range 10 to 1000 joules/cm^2 to be $\sim 10^{12}$ electrons/cm^3. For a graphite surface the estimated electron density was much higher ($\sim 10^{19}$). No confirmed results have so far been reported on the electron density and its dependence on the parameters of the laser pulse and the surface material.

Another phenomenon which drew considerable interest was the so-called 'rear-side emission'. In 1966, Knecht (27) reported that electrons are also emitted from the rear side of metal foils when a laser beam is focussed onto the opposite side. He used 0.05 mm thick foils consisting of gold, tungsten and tantalum. The rear collector was placed inside a cylinder at one end of which the target was fixed, so that it was shielded from the radiation emitted from the laser-heated spot. He observed two peaks in the recorded current signal (Fig. 2-3). The explanation suggested for this was internal photon-assisted tunnelling effect. Later, Li and Isenor (28) found evidence against laser-induced spontaneous electron emission from the rear side of metal foils. With the introduction of adequate light shielding they were able to eliminate the initial sharp peak of the current signal recorded in the oscilloscope. But the slow thermionic peak reported by Knecht persisted even with shielding. According to Li and Isenor, Knecht's results can be ex-

plained by photoelectrons from surrounding metal parts. These electrons would be mainly a result of ultraviolet radiation from the micro-plasma generated at the laser-illuminated part of the foil. But the persistence of the second current peak even after introducing proper shielding kept the phenomenon a mystery. Further work on this interesting phenomena has been carried out and an explanation of Knecht's results is presented in Chapter Seven.

2-2 Ion Emission

Ion emission from solid targets when irradiated by laser beam was first reported by Honig and Woolston (1). An arc discharge initiated by the laser was developed between the target and a grid close to it, held at a positive potential. A second grid retarded electrons and the collector held at zero bias measured an ion current of up to 500 mA. Spectrographic study indicated singly charged ions. In their work they failed to observe ion emission from semiconductors. In a later work, however, Honig (29) detected ion emission from semi-conductor surfaces. Ready (2), Khan et al. (8) and Namba et al. (30) reported two peaks in the current signal recorded in an oscilloscope when the collector was biased negative with respect to the target (Fig. 2-4). The first sharp peak has been found to occur during the laser pulse, whereas the second peak occurred one or two microseconds later. From the time of flight experiment, Namba estimated ion energy corresponding to the first peak to be $\sim$ 100 eV and second peak to be $\sim$ 1 eV. According to Khan et al. the energy of the ions pertaining to the first peak should correspond to $\sim 10^4$ eV. This has been considered to be highly improbable for the laser-induced ions. They support the theory

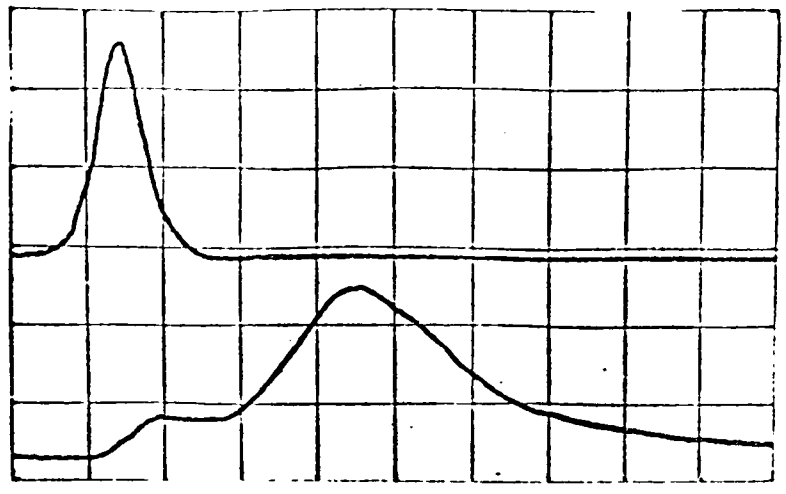

LASER
Electron emission (upwards) 100 ma/div.
Time-100 nsec/div.

FIG. 2.2. LASER INDUCED CURRENT SIGNAL FROM METAL (AFTER REF. 9).

AMPLITUDE SCALE - 10^{-1} V/div.
TIME SCALE - 1000 nsec/div.

FIG. 2.3. CURRENT SIGNAL RECORDED AT THE REAR SIDE OF A METAL FOIL (AFTER REF. 27).

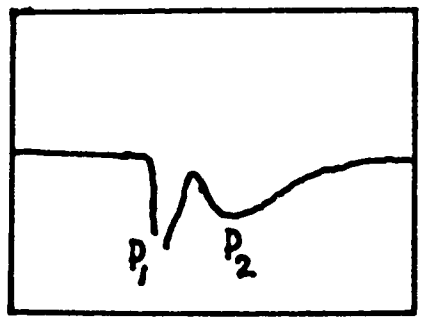

FIG. 2.4. TYPICAL OSCILLOSCOPE TRACE SHOWING LASER INDUCED POSITIVE-ION EMISSION FROM TANTALUM (AFTER REF. 30).

proposed by Lichtman and Ready (2) for the occurrence of the first peak. According to this proposition, the initial peak is caused by a reverse photoelectric effect. High energy photons are emitted when the laser beam heats the target up to a very high temperature. These photons cause photoelectrons from the metal collector. However, the second broader pulse has been indisputably considered to be due to pure ion emission from the target.

The properties of the laser-induced ions have been investigated by various workers. Langer et al. (31) used an electrostatic analyzer having a 90^{o} deflection angle and a particle path radius r_{o} = 10 cm. They observed that there is a light intensity threshold for the appearance of multi-charged ions. They also found that the maximum ion energy is the same whatever their ionization degree may be. With a peak flux of $\sim 6 \times 10^{10}$ W/cm^{2}, the maximum ion energy observed was $\sim$ 2 keV. They believe that the high ion energy cannot be accounted for by a purely thermal model. They suggested the existence of an accelerating electric field due to space charge separation.

With a similar technique, Schlier et al. (21) estimated ion temperature for carbon to be $\sim$ 50 eV and for tungsten $\sim$ 500 eV. Their experiment did not employ both a velocity selector and a time of arrival detector, like the previous workers. Moreover, because of shorter flight path (12 cm) in their experimental arrangement, the condition for validity of the analysis has been thought to be inaccurate.

Allen (16) in his report on electron and ion temperature, made use of the data collected by Langer et al. (31) and derived a method of inferring ion translational temper-

ature. According to this report, in inferring plasma temperature from the experimental data in any time of flight experiment, it is essential that there be a one-to-one correspondence between velocity and the time of arrival of a detected particle. Now, since the plasma emits particles for a considerable period of time, i.e. several hundred nano-seconds (independent of the duration of the laser pulse), this condition is not fulfilled. So, without taking this fact into consideration, measurement of ion temperature with this method will be an over-estimation.

Ion temperatures have been found to rise for a considerable length of time. It is believed that this is because the ions suffer many collisions between time of ejection from the target and time of escape from the plasma. The accelerating field has been considered to play an insignificant role for the high energies of ions.

Opower and Press (32) proposed a mechanism by virtue of which ions in laser-produced plasmas acquire high kinetic energy. According to them, the ions are accelerated by electrons which move out ahead of the plasma, the net result ultimately being the conversion of thermal energy of the electrons to kinetic energy of motion of the ions. The mechanism has been considered to be highly improbable by Allen (16).

No confirmed theory for the production of high energy ions has so far been put forward.

2-3 Other Radiations

When laser light is focussed onto any solid target, the target gets heated up and the incandescent solid emits radiation. At higher laser power the heated spot evaporates and

the ionization of neutral atoms and molecules takes place. Thus a plasma is formed and propagates away from the target. The plasma dissipates energy in the form of radiation. Linlor (33) took colour photographs of this plasma, which appeared blue. Ready (34) observed that for a laser pulse lasting for 45 nanoseconds the peak brightness of the plume of plasma occurred 120 nanoseconds from the start. Many workers have made spectroscopic analyses of the emitted radiation to estimate the electron and ion temperature. Archibold et al. (17) studied the light emitted from the laser hot spot with a spectroscope and recorded the event on a photographic plate at the end of the instrument. They achieved time resolution by sweeping the light from the target down the spectroscopic slit as the laser was firing. The analysis of the spectra showed a continuous emission of radiation from different metal targets, extending well into the ultraviolet. Richards (9) did a similar study. From his observation he concluded that the spectral lines emitted by a tantalum target are chiefly in the ultraviolet. In photographic plates of the spectra no significant emission lines in the visible region were observed.

Evidence for X-ray emission during the interaction of the focussed laser beam with target in air has been reported by Langer et al. (31). X-ray energy was estimated to be of about 2 keV. They found that the X-rays are generated at the laser-produced crater of the target.

2-4 Conclusion

A systematic survey of the electron and ion emission and other radiations has been made in this chapter. Most of the present works on laser interaction with solid surfaces

pre-supposes the fact that focussed laser light produces a vaporized cloud consisting of electrons, ions and neutral particles. The laser pulse further ionizes the neutral atoms and a 'plasma' is formed. In some recent works (35), hydrodynamical models have been presented to investigate the expansion of such a 'plasma' drop. In the present work the validity of the 'plasma' concept is verified and the value obtained for the plasma parameters are compared with the value calculated with such models.

Considering the fact that the existing knowledge of different mechanisms of laser interaction with solids may be useful in interpreting the experimental results, a brief theoretical account of different processes is given in the next chapter.

CHAPTER THREE

DIFFERENT PROCESSES OF LASER-INTERACTION WITH SOLID SURFACES

Laser beams can interact with solids in different possible ways. The free electrons of the solid surface will absorb the energy of the photons. The energy will be dissipated into the solid by interacting with the lattice phonons. Thus the temperature of the spot absorbing the laser photons will be raised. If the temperature can be raised high enough, thermionic emission of electrons can be achieved. For very high temperature rise ejection of ions, neutral particles or even the molten metal is possible. The free electrons may absorb two or more photons simultaneously and gain sufficient energy to cross the surface potential barrier, thus giving rise to photoelectric emission. The light emitted from the laser-heated spot may produce photoelectrons from the surrounding metal parts. A brief description of such mechanisms is presented below.

3-1 Thermionic Process

The temperature rise of a metal surface due to the absorption of laser radiation can be calculated by using the conventional one-dimensional heat transfer equation. In developing a temperature equation the following conditions must be fulfilled.

a) The heat flow is one-dimensional, i.e. the depth of penetration of the beam must be smaller than the transverse dimension of the spot being heated.

b) The beam energy is uniformly spread over the spot and is constant with time.

c) Loss of heat due to radiation or convection can be

negligible.

d) The thermal properties of the metal are independent of temperature.

The above conditions are only approximately fulfilled in the case of a giant laser pulse interacting with a metal surface. For ruby light the penetration depth into a metal is of the order of magnitude of a micron, whereas the focussed area is usually not smaller than $\sim 10^{-3}$ cm^2. The beam energy is not strictly uniform along the cross-section. But for the calculation of the order of magnitude of the temperature, and particularly the rate of change of the temperature, the assumption of uniformity can safely be made. The laser energy is not constant with time. The laser pulse can be approximated by a triangular pulse and the triangle can be divided into different intervals and the energy can be approximately considered to be constant for each interval (τ). The heat transfer equation can now be applied for each interval satisfying the condition b). The final temperature profile can be obtained from the envelope of the temperature profiles contributed by each different interval. For temperatures up to the vaporizing point of the metal the thermal properties can be approximated to be constant for such a calculation. At temperatures higher than that, such an approximation can not be valid and the temperature calculation will be exceedingly difficult.

Let the laser beam of power P act on the surface of a metal. This is equivalent to a flux of heat W on the surface ($x = 0$). The temperature rise of a semi-infinite slab extending over positive x for any time $t > 0$ is given by:

$$W = -K \frac{\partial T}{\partial x} \quad \text{per unit time per unit area} \qquad \ldots. \; 3\text{-}1$$

K = thermal conductivity of the metal.

The one-dimensional heat transfer equation is given by (36),

$$\rho c \frac{\partial T(x,t)}{\partial t} = K \frac{\partial^2 T}{\partial x^2} \qquad \ldots. \; 3\text{-}2$$

where

ρ = density of the metal

c = specific heat.

From eqns. 3-1 and 3-2 we obtain,

$$\rho c \frac{\partial W}{\partial t} = K \frac{\partial^2 W}{\partial x^2} \qquad \ldots. \; 3\text{-}3$$

If the absorption coefficient of the metal is represented by α, we have $W = \alpha P$. If we calculate the temperature rise for each constant laser power lasting for τ seconds, the boundary conditions for the solutions of the eqn. 3-3 can be written as:

$$W = W_o = \alpha P_a \qquad \text{at } x = o, \quad \text{for } o \leq t \leq \tau$$

$$W = o \qquad \text{at } x = o, \quad \text{for } t > \tau$$

If the initial temperature of the metal is taken to be zero, so that T represents the true rise in temperature then at the surface (x = o) a standard solution of equation 3-3 can be obtained (36) and we finally have

$$T(o,t) = \frac{2\alpha P_a}{K} \sqrt{\frac{Kt}{\pi \rho c}} \qquad \text{for } o \leq t \leq \tau \qquad \ldots. \; 3\text{-}4$$

and

$$T(o,t) = \frac{2\alpha P_a}{\sqrt{\pi \rho c K}} \left[t^{\frac{1}{2}} - (t-\tau)^{\frac{1}{2}} \right] \qquad \text{for } t > \tau \qquad \ldots. \; 3\text{-}5$$

Equations 3-4 and 3-5 were used to calculate the temperature rise of a tantalum surface. A specific case of a triangular-

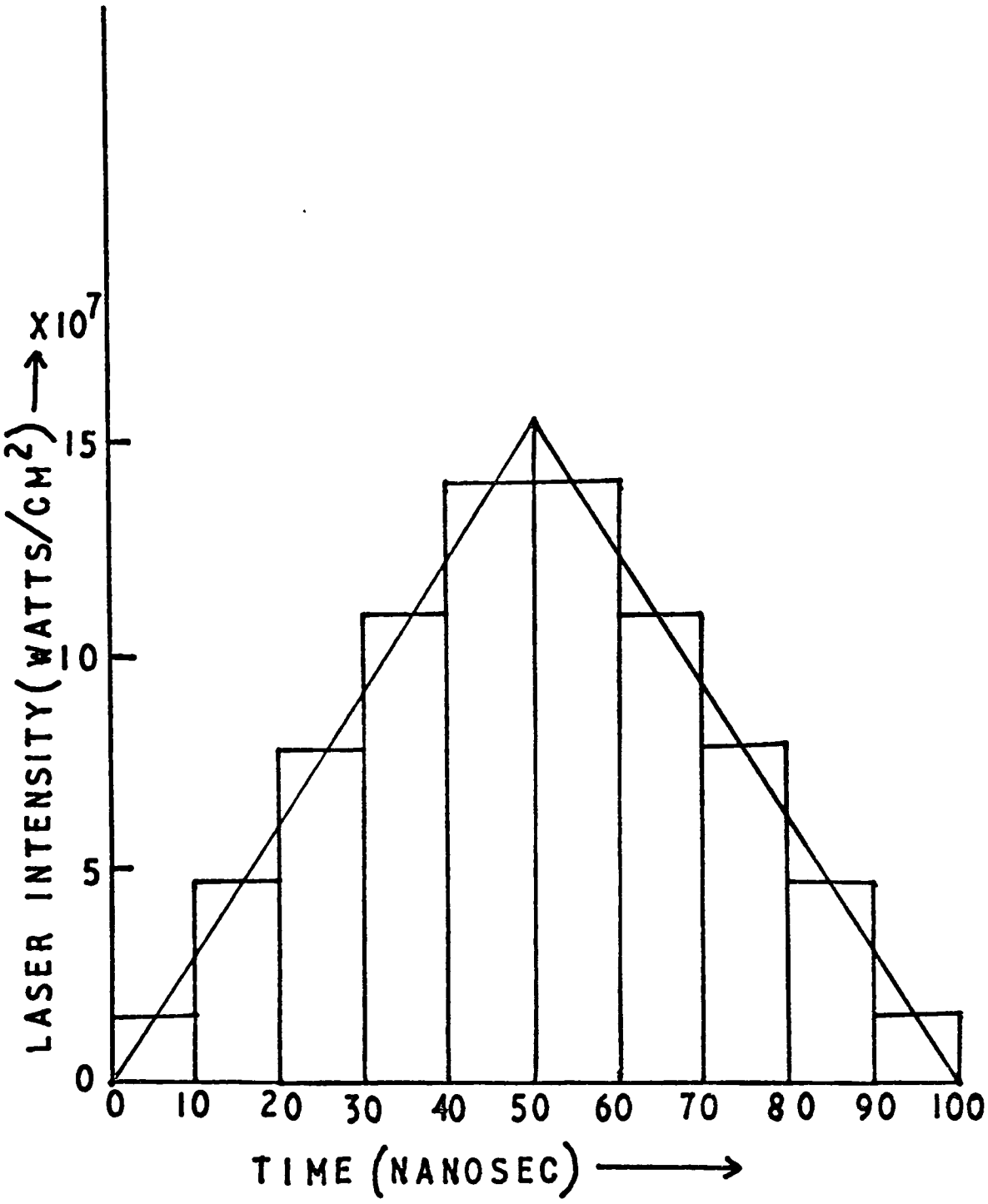

FIG. 3.1. THE SHAPE OF THE LASER PULSE USED TO CALCULATE SURFACE TEMPERATURE.

shaped laser pulse with peak power of $\sim 1.4 \times 10^8$ watts/cm^2 and lasting for approximately 100 nanoseconds was considered to be normally incident onto the surface. The constants of the metal are quoted below:

$\alpha = 0.46$

$\rho = 16.6$ gm/cm^3

$c = 0.15$ joules/gm/^oK

$K = 0.55$ joules/cm/sec/^oK.

The triangular laser pulse is divided into ten intervals, each with a constant laser flux lasting only for ten nanoseconds (τ), as shown in Fig. 3-1. The temperature rise for each square pulse of ten nanosecond duration was calculated and the total temperature rise due to the whole triangular laser pulse was obtained by combining the different contributions. The calculated temperature profile is shown in Fig. 3-2. The most uncertain parameter in this calculation was the focussed area. The area of the irradiated spot was measured under a travelling microscope. Some enlarged photographs of the eroded spot of the target are shown in Fig. 3-3. Since the spot was found to be not exactly circular, a considerable number of readings were taken and the average value of the spot diameter was obtained. Since the edge of the eroded spot was not strictly defined, an approximate error of 4-5% can easily be introduced in the measurement of the spot diameter. Thus the estimated area will be measured within an accuracy of $\sim \pm$ 20%. For the present calculation, an error of such magnitude in the area has been considered tolerable. The estimated area of the focussed spot was taken to be $\sim 5 \times 10^{-4}$ cm^2. The temperature of the spot has been found to rise rapidly with increasing energy

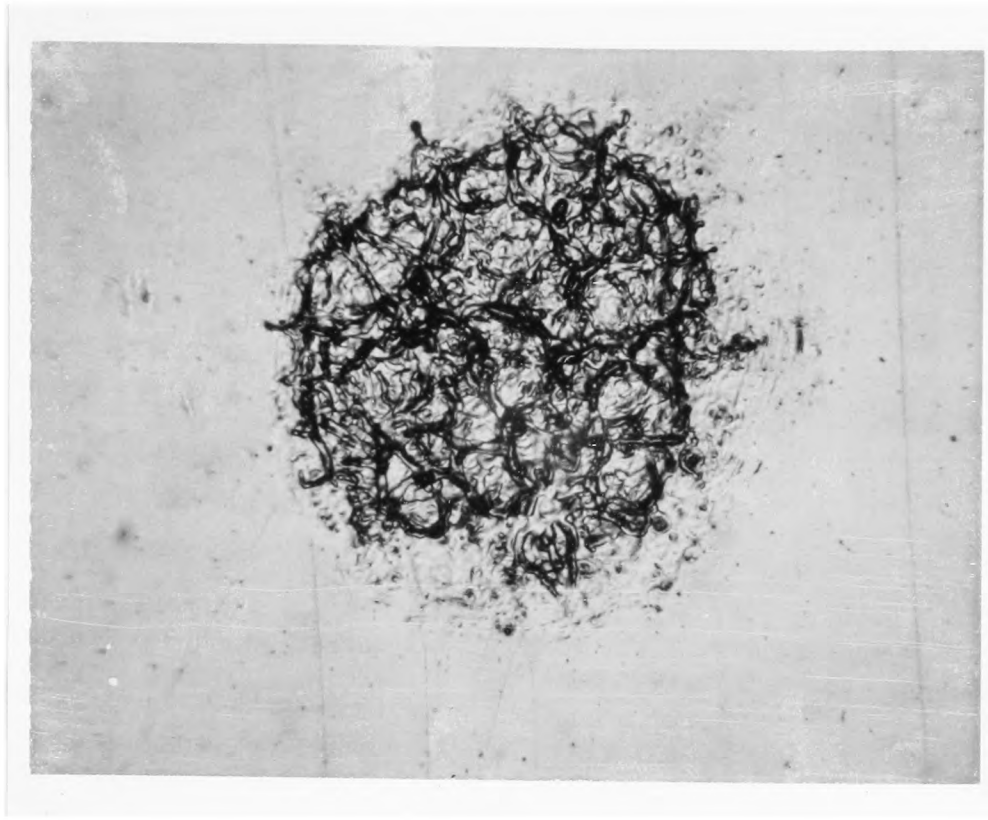

AFTER ONE SHOT

AFTER TEN SHOTS

Magnification - x113

FIG. 3.3. FOCUSSED LASER ERODED SPOT ON A Ta SURFACE.

influx. The temperature reached its maximum value of $\sim 13 \times 10^3$ ^{o}K within $\sim$ 60 nanoseconds. The temperature has been found to fall slowly and the spot appears to remain hot for a considerable length of time after the laser pulse ceased to deliver energy.

The melting temperature of Ta is known to be 3123^{o}K. The metal boils at around 5700^{o}K. From the temperature profile it can be estimated that the metal will normally boil off after approximately 25 to 30 nanoseconds from the initiation of the laser pulse. The heating process after that will be very much complicated because of the simultaneous existence of different phases. The concept of a temperature of a solid will no longer be valid. A phenomenological description of further heating of the solid and the production of a dense phase and the absorption of further laser radiation by the advancing cloud of particles from this dense phase will be given in Chapter Six while discussing the mechanism of the production and propagation of the plasma by laser heating.

It can be concluded from the above consideration that only for laser intensities which are low enough not to cause any surface damage, the calculation of temperature is expected to give a valid picture of the state of the metal electrons. The temperature calculation of a metal surface by a high powered laser pulse will be valid up to a time at which the transition of phase will take place. In such a transition the liquid phase may be ignored as the latent heat of fusion is much less than the latent heat of vapourization. If, however, the temperature of the metal surface can be estimated, the thermionic current can easily be obtained from the

Richardson-Dushmann equation. According to this, thermionic current at any temperature T will be given by

$$J = AT^2 \exp(-\beta/T) \quad \text{amps/cm}^2 \qquad \ldots. \; 3\text{-}6$$

where A = Richardson's constant = 60 amps/cm^2 degrees^2 (experimental value)

$\beta = 11600\,\phi$

ϕ = Work function = 4.2 eV (for Ta).

From the above equation it can be inferred that if the laser-induced emission of electrons from the metals is of a thermionic nature, the current-temperature law will be mainly governed by the exponential factor. A theoretical thermionic current profile is shown in Fig. 3-2.

3-2 Multiphoton Photoeffect

Photoelectricity is a well-known phenomenon. The corpuscular concept of light is the flow of bundles of photons or 'quanta' with negligible mass. The energy of such a quantum is given by $h\nu$, where h is Planck's constant and ν the frequency of the light derived from the classical concept. For normal photoelectric emission to take place, the photon energy must be higher than the work function ϕ of the solid surface. The work function gives a measure of the surface potential barrier which an electron has to overcome in order to escape into vacuum. The kinetic energy of the escaping electron will be given by the well-known photoelectric equation

$$E = h\nu - \phi. \qquad \ldots. \; 3\text{-}7$$

The threshold energy for photoemission ($h\nu = \phi$) will restrict photoelectric emission from most metals when irradiated by

light in the visible region of the spectrum. When, however, the incident photon density is very high the probability of simultaneous absorption of two or more photons by a single electron may become considerable. Such absorption will raise the electrons to energy states higher than the surface potential barrier and multiphoton photoemission will take place. The increase in photo-conductivity in semiconductors with a band gap E_g greater than the photon energy $h\nu$ can also be explained in terms of the multiphoton photoeffect. The concept of multiphoton-photoeffect arose quite recently as an attempt to explain the characteristics of the laser-induced electron emission from metals with high work function.

Very little theoretical work has, so far, been done on two-photon or three-photon-photoeffects. This is because, in such a calculation, a precise knowledge of the initial final and the intermediate electronic states is necessary. The theory presented by Adawi (37) is extremely complicated. The treatment of Logothetis et al. (13) considers a volume effect. The derivation of their result is quoted here.

If α_m is the m-photon absorption constant then the m-photon photoelectric current density is given by:

$$J_m = e \int_o^\infty I(x)p(x,E)\alpha_m \, dx \qquad \ldots. \; 3\text{-}8$$

where $I(x)$ = light intensity at x

$p(x,E)$ = the escape probability of an electron of energy E and generated at a depth x of the solid.

Double-photon photoelectric current has been calculated with the help of a specific model of the band structure of the

solid, as shown in Fig. 3-4. The expression for the current density is given as:

$$J_2 = \frac{e^5 E_a E_g f_{\ell c} f_{cv} D(2h\omega - E_o)^{\frac{1}{2}}}{4\pi\varepsilon_o{}^2 c^2 h^4 \omega^4 m^{\frac{1}{2}} \xi^2 (E_a - h\omega)^2} I^2 \qquad \ldots. \; 3\text{-}9$$

where $E_a = E_o - E_g$ (see Fig. 3-4)

ξ = index of refraction

D = average escape depth

and $f_{\ell c}, f_{cv}$ = oscillator strengths for the particular transistors.

The above equation, although it may be applicable to semiconductors, can not be applied to metals. In particular, the assumption that the bottom of the final band will coincide with the vacuum level, will restrict the applicability of the treatment to most solids. It can, however, be possible to study the behaviour of the multi-photon photoeffect in solids from the above treatment. It has been further postulated that an m-photon photoeffect will be proportional to the m^{th} power of the incident intensity.

In later chapters, experimental results will be used in phenomenological models of multi-photon photoeffect and the properties of such effects will be studied. In view of the complexity of the problem it has been considered advisable to study the nature of the photoeffect rather than attempt to evaluate the exact value of such a photocurrent.

3-3 Reverse Photoelectric Effect

It has been shown earlier in this chapter that the temperature of the laser-irradiated surface rises to a very high degree. Because of the development of high pressure in the heated zone, superheating of the dense material is possible.

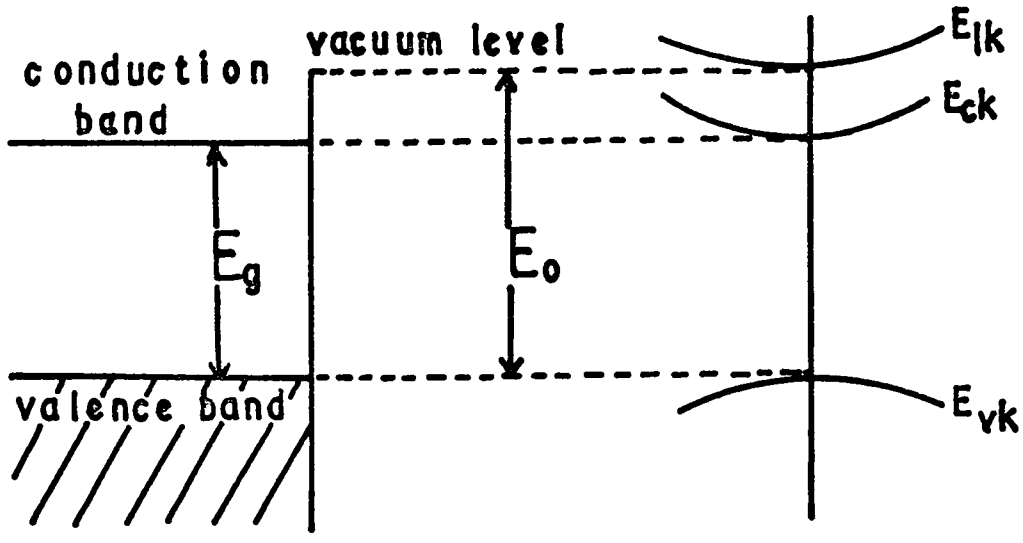

FIG. 3.4. ENERGY-BAND MODEL USED TO CALCULATE THE TWO PHOTON PHOTOELECTRIC EFFECT IN SEMICONDUCTORS. E_g - band gap. E_o - work function (AFTER REF. 13).

Furthermore, the high energy laser can very easily produce 'plasma' with a temperature of several thousands of degrees Kelvin. The incandescent solids will emit radiation. At a temperature $T^{\circ}K$, the maximum radiation will occur around a wavelength given by Wien's displacement law:

$$\lambda_m T = 2.898 \times 10^7 \quad \text{Å } ^{\circ}K.$$

Thus, as the temperature of the heated spot increases, it emits continuous radiation of increasing photon energy. At the boiling temperature of a metal (e.g. Ta boils at $\sim 5700^{\circ}K$) the photon energy corresponding to the most copiously emitted radiation will be $\sim$ 2.5 eV. These photons will not be able to produce appreciable photocurrent from metals of high work function. Though the tail of the black body radiation curve will contribute to photoelectrons from metals. Apart from that, during the motion of the laser-produced 'plasma', the charges will recombine and high energy radiation will be obtained. The plasma is expected to radiate chiefly in the ultraviolet region. The apparent colour of the plasma radiation has been found to be blue. Further heating of the ions and neutral atoms may cause ejection of electrons from the inner shells and result in soft x-ray emission. Evidence of such a process has been reported in the review chapter. Thus it can be concluded that there exist possible sources of high energy photons when laser light interacts with metals. These photons propagate in all directions and if some metal parts are exposed to them in the experimental system they will scatter electrons from them. If it is assumed that the radiation from the plasma is chiefly

in the ultraviolet region, the peak of the radiation curve will occur at around 5 to 6 eV. These photons are likely to produce a considerable amount of electron current from most of the metals. It is expected that the tail of the radiation curve may produce electrons of quite high energy. Electrons and ions, if occluded at the inside surface of the glass envelope of the experimental targets and collectors, may also be knocked out by such photons. For very high photon energy (e.g. soft x-rays), the possibility of knocking electrons from the interior of the metal (volume photo-electric effect) may be of considerable importance.

In the conventional method of detection of electron current by metal probes, the collector is strongly biased positive with respect to the target. Thus only the electrons emitted from the target will be accelerated towards the collector. The biasing was such as to overcome the space charge effect. Under these conditions, the reverse photo-electrons originating at the metal collector will not be able to move against the retarded voltage and hence will not contribute in the detection of laser-produced electron current. If the biasing condition is reversed so as to detect ion current flowing across the tube, the photoelectrons produced at the collector will be accelerated towards the target. The motion of the electrons from the collector to the target is equivalent to the motion of ions in the opposite direction. Thus, in this situation, the reverse photoelectric current is likely to give a positive contribution to the ion current. For this reason, the possibility of such a process has been investigated in Chapter Six.

3-4 Conclusions

It appears from the preceding description of the different mechanisms that the investigation of laser interaction with solids may involve different processes simultaneously. Thus, any attempt to explain the whole interaction mechanism by a unique process will be an oversimplification of the whole picture. The experimental results are, however, likely to indicate the predominant process at any particular stage of interaction. It is expected that thermionic current, photoelectric current and reverse photoelectric current, if all co-exist, will have different properties and different time correlation with the initiating laser pulse. Photoelectrons are likely to be detected at the early part of the laser pulse, though copious thermionic effect may mask the photoeffect. At the latter stage of the energy transfer from the laser pulse, the problem will be predominantly a 'plasma' diagnosis. If the quasi-neutral property of the 'plasma' persists for a time comparable to the time of production and emission of the electrons either by normal thermionic process or by photoelectric effect or by a thermo-assisted photoeffect, they are likely to appear as a separate peak in the current signal. In the detection of current from the plasma, motion of different species of charges in the preferred direction will be involved. So, in the analysis of the experimental results, this fact has to be taken into consideration.

CHAPTER FOUR

LASER SYSTEM

The investigation of laser interaction with solid surfaces required moderately high powered laser beams. One laser already in the Laboratory was used for this purpose. Another ruby laser system with a larger ruby rod and cavity was built as a spare laser source and for any future high power laser application. A brief description of the laser assembly is given below.

4-1 Laser Cavity

A schematic diagram of the ordinary mode laser system is shown in Fig. 4-1. The active material was a Meller ruby crystal which had the c-axis at 90° to the axis of the rod and with ends polished optically flat and parallel. A 2" x $\frac{1}{4}$" crystal for the first laser system and 4" x $\frac{1}{2}$" crystal for the second system were used. Both the crystals were doped with 0.04% Chromium atoms.

The ruby rod was fixed along one focus of a stainless steel elliptical cavity. The Xenon flash tube was fitted along the other focus. The cavity was placed inside a brass cylinder. Two end reflectors were placed to increase the light transfer to the ruby rod. Direct light from the flash tube and most of the reflected light from the wall of the cavity pass through the ruby to cause maximum population inversion.

The resonant cavity was formed by two optically flat dielectric mirrors. One of the mirrors had 99% reflectivity and the other 65%. The mirrors were aligned normal to the ruby crystal axis to an accuracy better than two minutes of

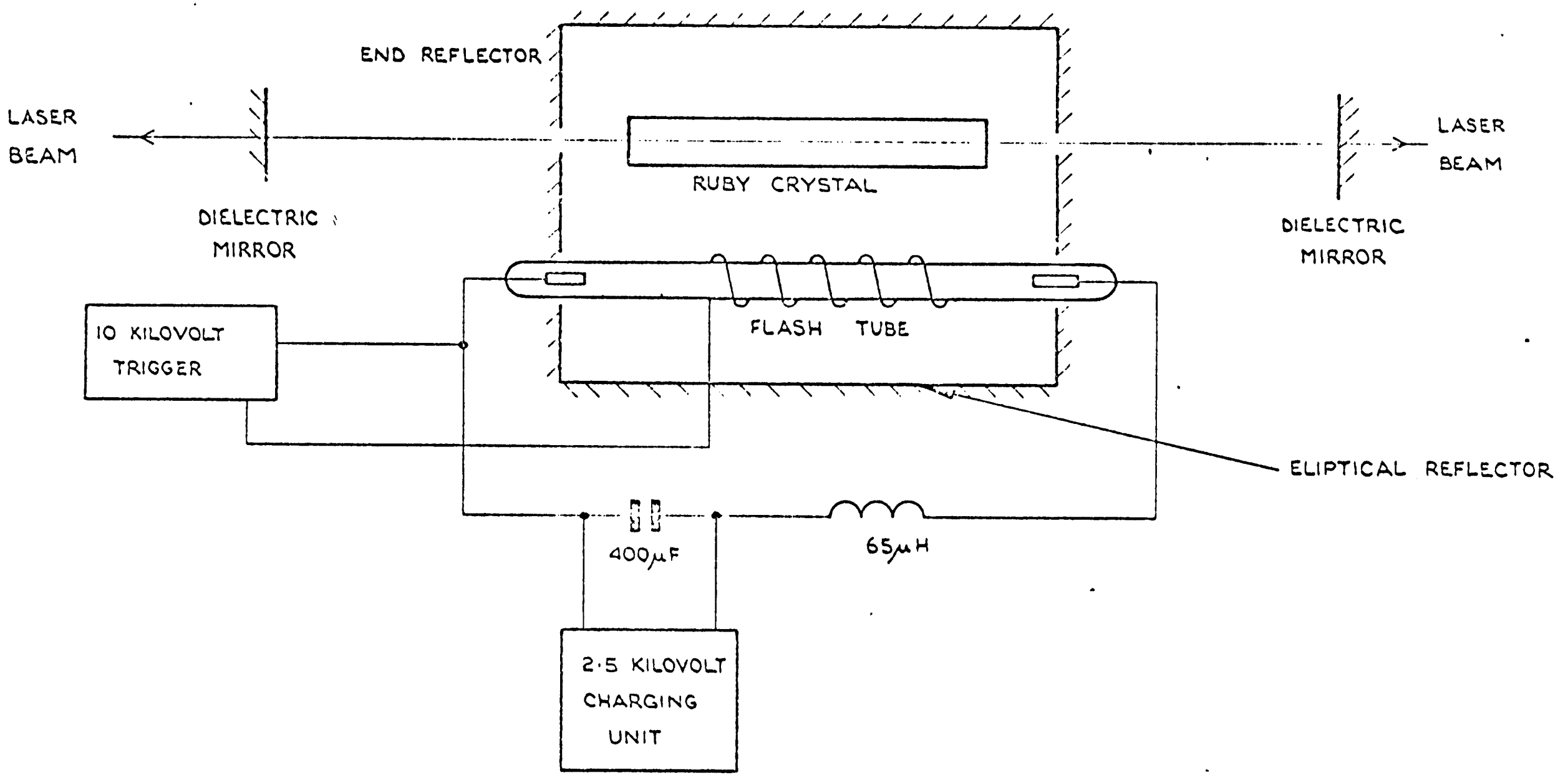

FIG. 4.1. SCHEMATIC DIAGRAM OF THE ORDINARY MODE LASER SYSTEM.

arc. The mirrors were mounted in holders whose angle can be accurately adjusted by means of screws.

The alignment was done independently by a He-Ne gas laser and an autocollimating light source and telescope. The telescopic method was found to be more convenient and accurate than the other. A schematic diagram of the telescope is given in Fig. 4-2.

Red light from a tungsten filament bulb is allowed to pass through a small hole and is focussed to a parallel beam by a 10 cm focal length bi-convex lens. The light returning in the opposite direction is focussed by this lens and partially reflected by a mirror onto the eyepiece where an image is observed.

For aligning the laser, the parallel beam of red light is passed along the axis of the ruby crystal. A part is reflected by the crystal face back through the telescope objective and viewed through the objective as a pair of bright spots (reflection from two faces of the mirror).

4-2 Pumping and Power Supply

The pumping or population inversion, as it is called, of the active material was accomplished by a flash tube. For the original laser system, British flash tubes by English Electric Valves, type XL 615/7/3, were employed and found to give excellent performance. For the detailed description of the power supplies for the original laser system, the work of Richards (9) is referred.

For the second laser system, a linear xenon flash tube, type FX47B (E,G8), of 6.5" arc length was used. The flash tube was driven by input energies up to 5000 joules. The energy was delivered through a current limiting inductor of

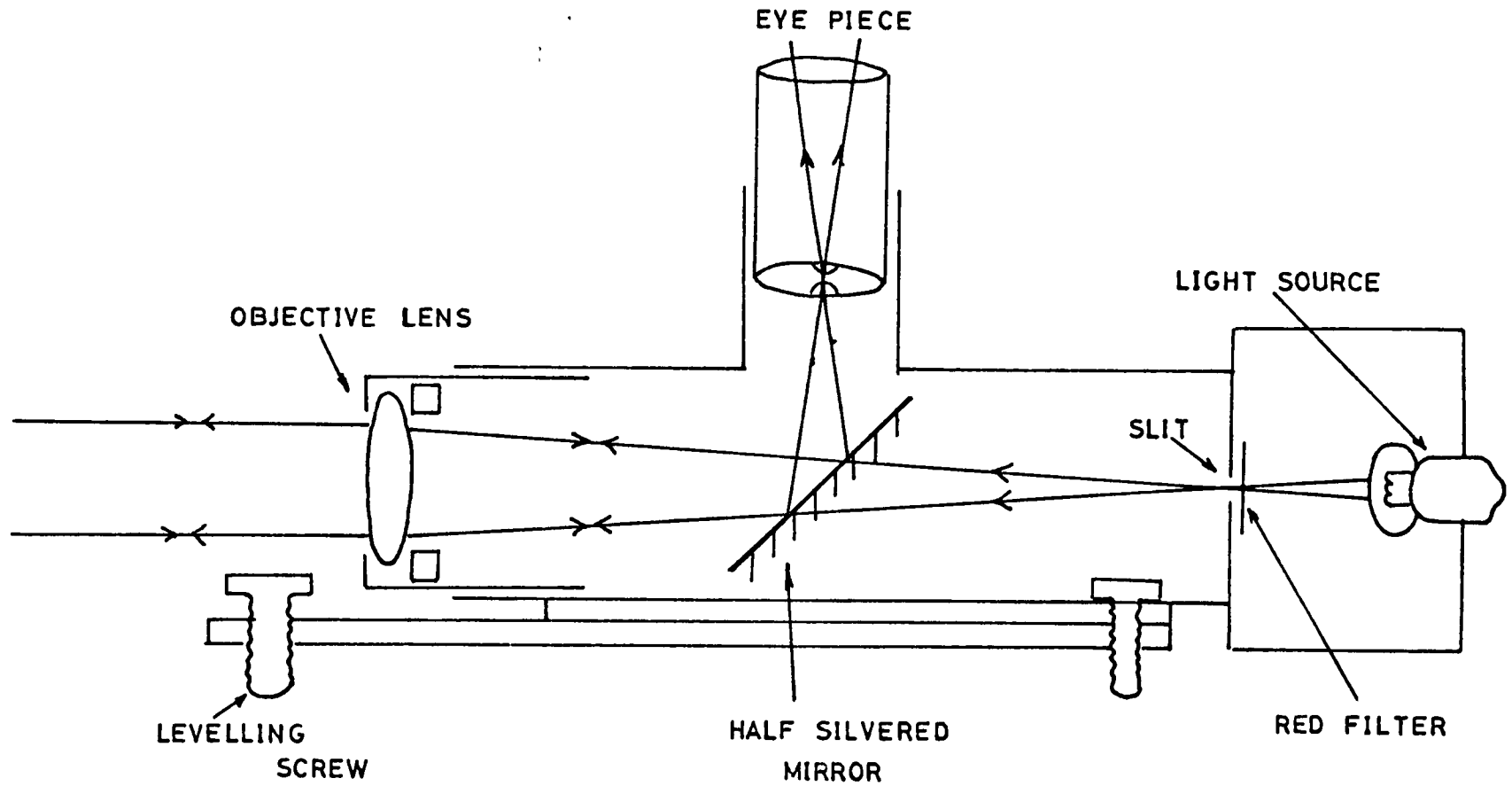

FIG. 4.2. LASER ALIGNMENT TELESCOPE.

104 micro-henries. The inductor was constructed of 16 gauge DSC copper wire wound on an insulating cylinder and was pasted with Araldite to hold them rigidly. The total value of the capacity of the condenser banks employed to feed energy to the flash tube was 1100 μF. The maximum operating voltage was 4 KV. The capacitor bank was charged by means of a simple voltage doubling circuit using silicon rectifiers. Independently powered relays and safety devices were incorporated. The circuit diagram is shown in Fig. 4-3. The charging could be done manually as well as automatically to any present value of the voltage. The flash tube was triggered by a simple thyratron (Mullard 2D21) circuit which discharged a 1100 μF capacitor charged up to 3 KV through the primary of a pulse transformer. A car ignition coil was used for this purpose. The secondary pulse of amplitude approximately 25 KV triggered the flash tube through a wire wrapped around the quartz envelope of the flash tube. The triggering could be done either manually for ordinary mode operation or electronically with a timing circuit for Q-switched operation employing rotating mirror.

4-3 The Q-Switched Operation

The flash tube emits radiation in the green region of the spectrum. This is absorbed by the Cr^{---} atoms in the ruby crystal. The atoms are excited and "pumped" up to the transitory levels $^4F_1$ and $^4F_2$, followed by a very rapid radiationless transition to the closed spaced levels ^2E. These have a long life time ($\sim$ 5 nsec.) so that if the pumping rate is adequate, an inversion of population would take place between ^2E levels and the ground state $^4A_2$. Due to relaxation oscillation the ^2E level gets depleted as soon as the

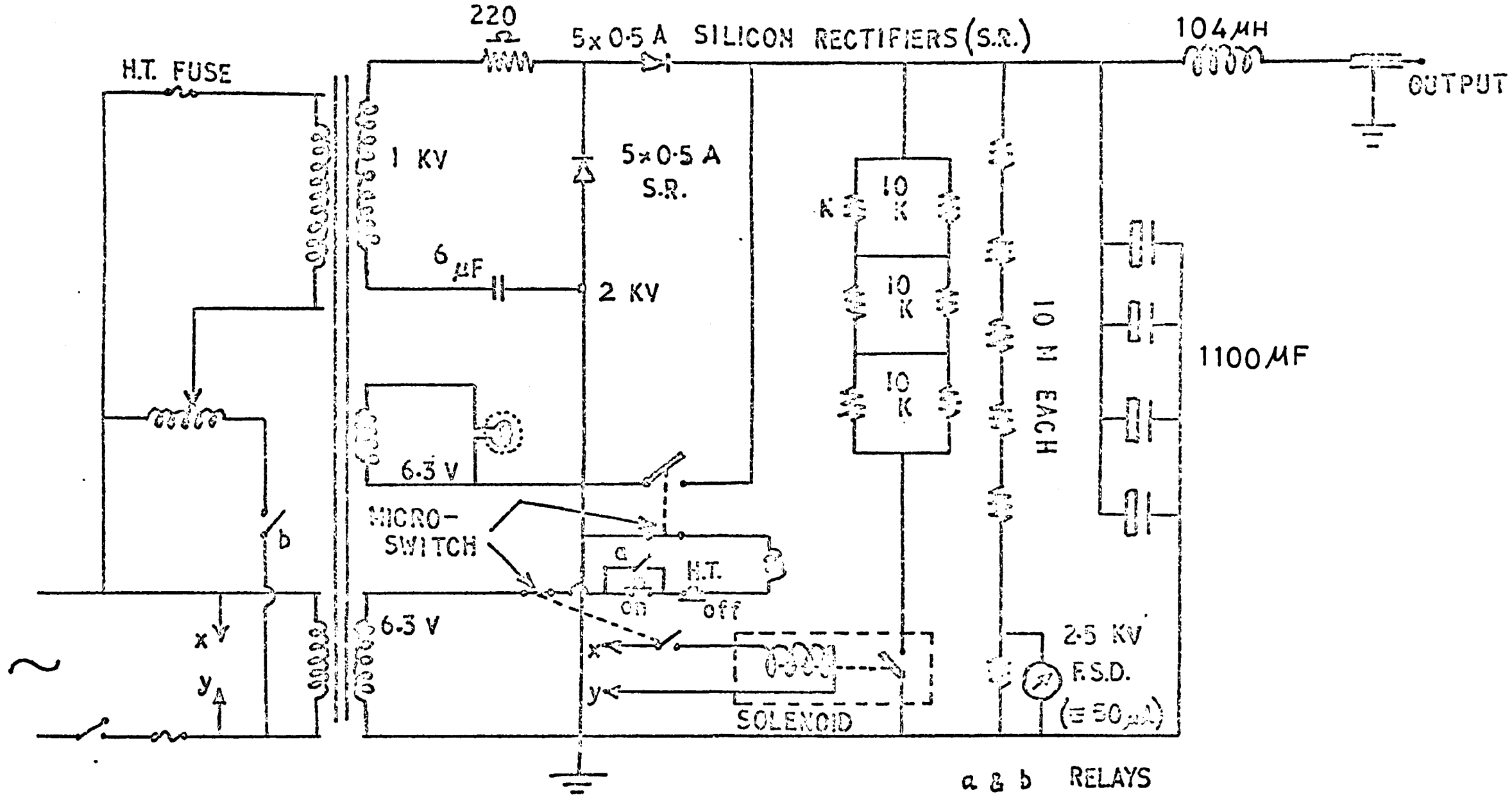

FIG. 4.3. CIRCUIT DIAGRAM OF THE CAPACITOR BANK.

oscillation begins. The population at the ^2E level then drops below the critical value required for oscillation until it is restored by the flash-pump source which persists for a millisecond or so. So it is clear that population inversion can not build up to a value much beyond the critical value for oscillation so long as the ruby lies in the resonating cavity during the build-up of the inversion. If the Q of the cavity is switched from a low to a high value prior to the generation of the laser pulse, a large amount of energy can be released in a single spike. This is the principle of the "Q-switching" to produce a "Giant" laser pulse.

Two different techniques were employed to obtain Q-switching. For the first laser system, a rotating mirror was used. The mirror was rotated so that when the flash pulse reached its maximu, the rotating mirror came exactly in parallel with the fixed mirror. As long as the two mirrors were not parallel, the Q of the cavity was spoiled and the population inversion built up beyond the critical value. As the rotating mirror became parallel to the fixed mirror, the excited atoms fell down in one single cascade. The synchronization of time of the rotation of the mirror with the peak of the flash light pulse was done electronically. The detailed description of the electronic circuitry is given in Ref. (9).

For the second laser system,a bleachable dye was used for Q-switching. The dye was a solution of cryptocyanine (I,I'-diethyl-4,4',carbocyanine iodide) in methanol. This dye has been found to have very high absorption at 6943 Å (38). Thus the dye at a certain concentration, when placed in the resonating cavity, will suppress oscillations until a

high level of population inversion is reached in the ruby. At such a high level of gains the oscillation will start and the intense light will bleach the dye in $\sim 10^{-9}$ sec. (39). Thus the dye becomes transparent and a sudden drop of the excited atoms takes place in a cascade to give an intense light lasting for a few tens of nanoseconds.

The advantage of using a dye for Q-switching is its simplicity. But the shot-to-shot reproduction of the laser pulse shape was found better with the rotating mirror system.

4-4 Detection and Measurement of Laser Pulse

For most of the present work it was necessary to know the absolute value of the laser power. The laser pulse was always used to trigger the current pulse in the oscilloscope. Moreover, it was necessary to record the laser pulse simultaneously with the current signal for detecting the change in the pulse shape from shot to shot. For the measurement of laser power an ADP power meter and a calibrated photodiode were used, both independently and simultaneously.

The ADP power meter was built in this laboratory. When a medium like ADP (Ammonium Dihydrogen Phosphate) is subjected to an optical electromagnetic field, a d.c. polarization is produced. The polarization is proportional to the square of the optical electric field, i.e. directly proportional to the power of the incident radiation. The polarization induces a voltage across the ADP crystal. To measure the signal produced in the crystal, an impedance-matching circuit was connected between the crystal head and the oscilloscope. The detailed description of the power meter and the calibration procedure is given in Ref. (9). The arrangement for the direct measurement of power simultaneously by the ADP

meter and the SGD(100) photodiode is shown in Fig. 4-4.

The photodiode was calibrated by Keuffel & Esser Co. The spectral response curve is shown in Fig. 4-5. Since direct laser light will damage the photodiode, a small fraction of the light was diverted to a matt surface with the help of a beam splitter. The scattered light from the matt surface was received by the photodiode at a certain angle. The fraction of the total light reaching the active area of the photodiode was calculated and the total power was directly measured from the output of the photodiode. The photocurrent was detected across a 100Ω resistor. The photodiode connections are shown in Fig. 4-6.

The calculation of the laser power from the output of the photodiode was done in the following way:-

Let the photodiode be placed at a distance d from the centre of the laser spot at the diffuser and at an angle θ from the normal to the plane of the diffuser (Fig. 4-7). From the beam splitter the laser light is incident onto the surface at right angles. If I denotes the brightness of the spot at the diffuser at any instant of time and is expressed in candelas/area, the flux of light into the photodiode F is given by Lambert's law as,

$$F = \frac{I.a.b.\cos\theta}{d^2} \text{ lumen.} \qquad \ldots. \ 4\text{-}1$$

where a is the area of the laser spot, and b is the active area of the photodiode. Let the initial laser power be P lumen/area. Thus the luminous flux at the surface θ is given by r.ρ.P lumen, where r is the reflection coefficient of the beam splitter and ρ is the reflection coefficient of the matt surface. The brightness of the spot is given in

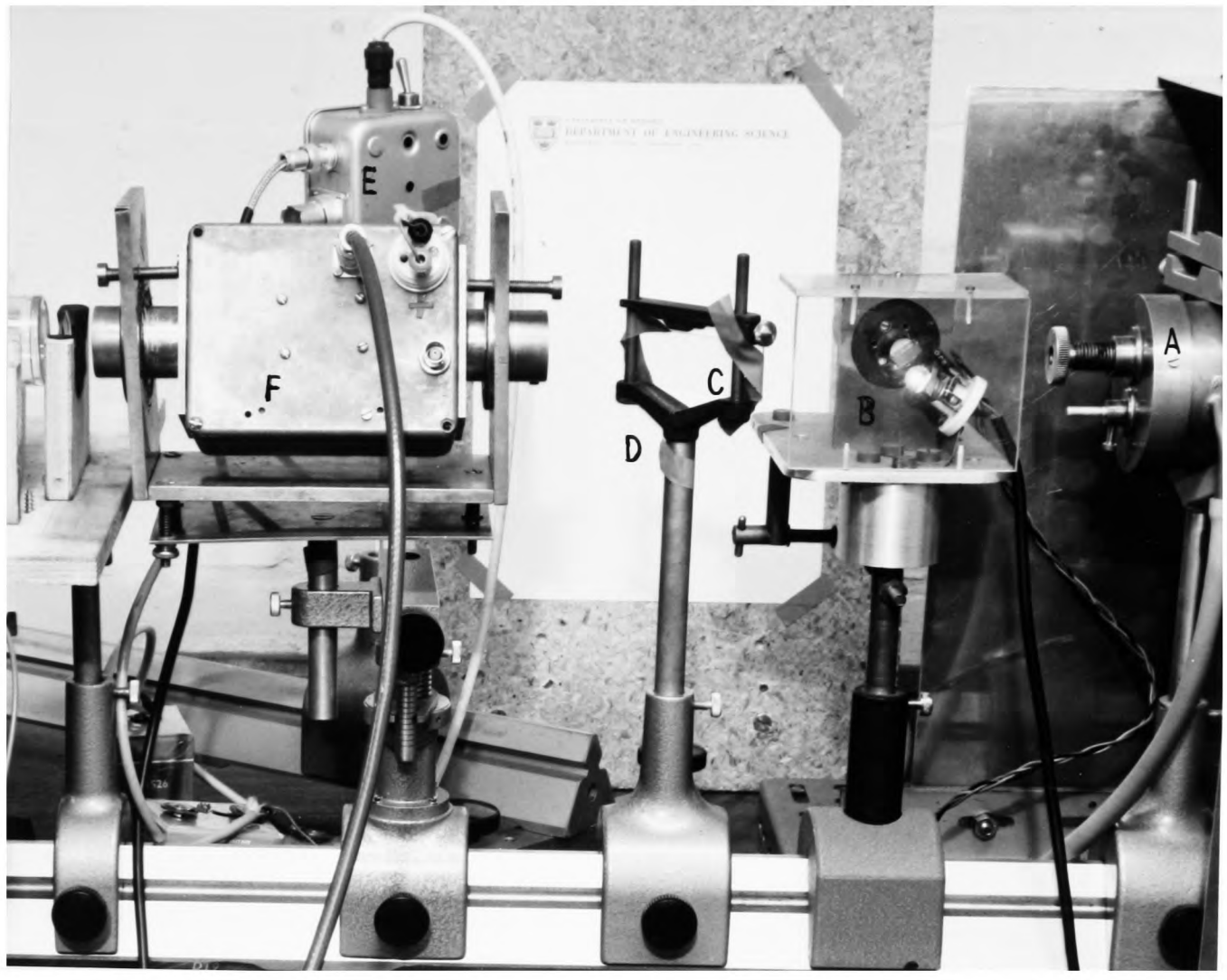

a) Photograph of the Arrangement.

A - Laser Cavity
B - Rotating Mirror
C - Beam Splitter
D - Matt Surface
E - SGD-100 Photodiode
F - ADP Power Meter

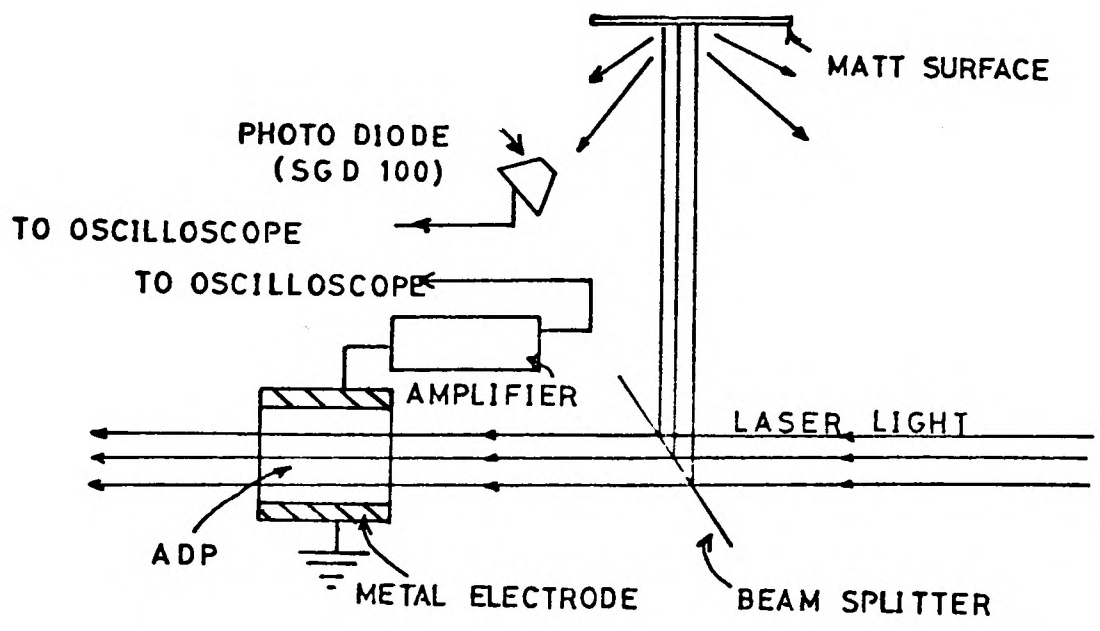

b) Schematic View.

FIG. 4.4. LASER POWER MEASUREMENT.

(Simultaneously by SGD-100 Photodiode and ADP Power Meter.)

CALIBRATED 2-8-67 SPECTRAL RESPONSE SGD-100 SERIAL NO. 7-1-11

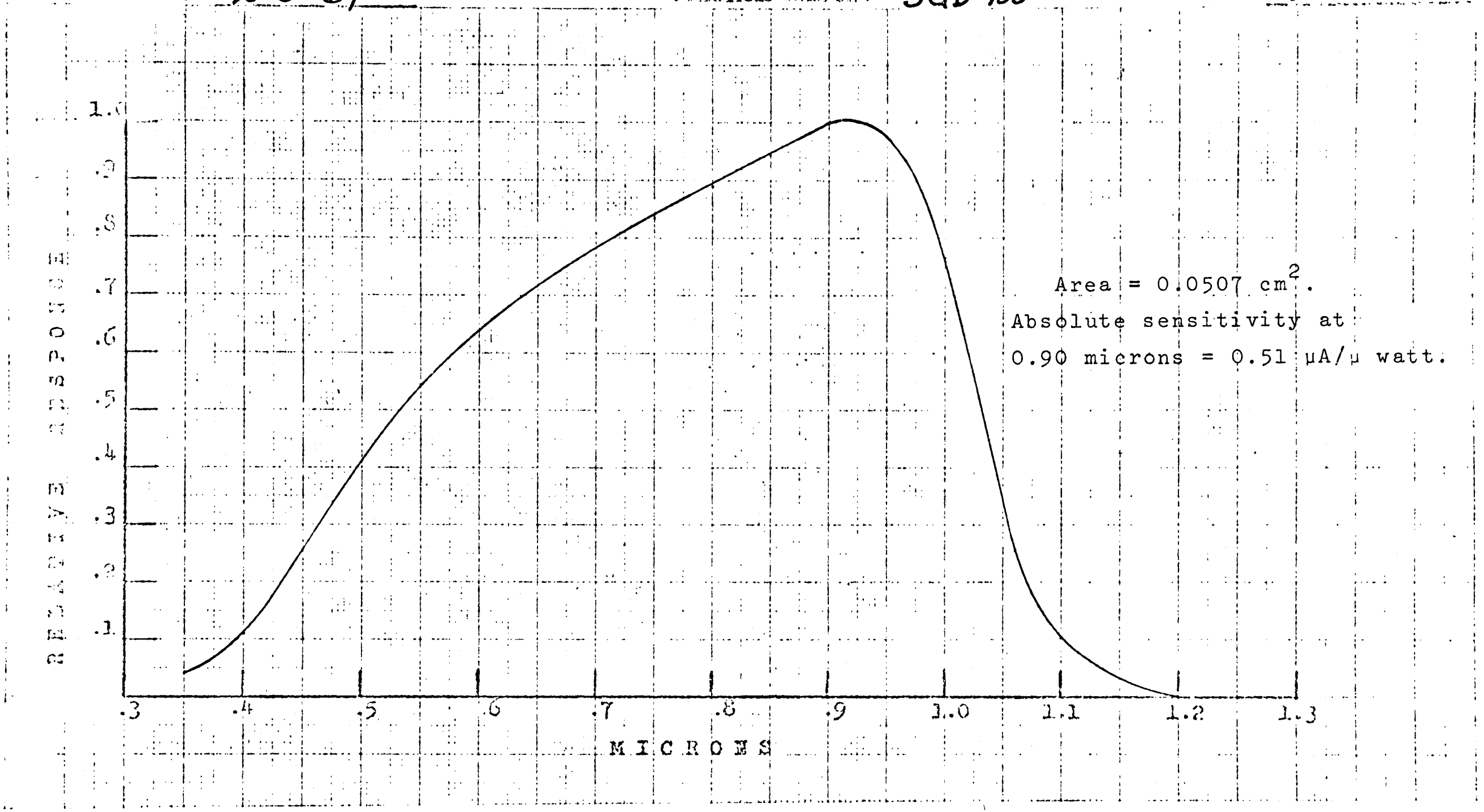

FIG. 4.5. SPECTRAL RESPONSE CURVE OF SGD-100 PHOTODIODE.

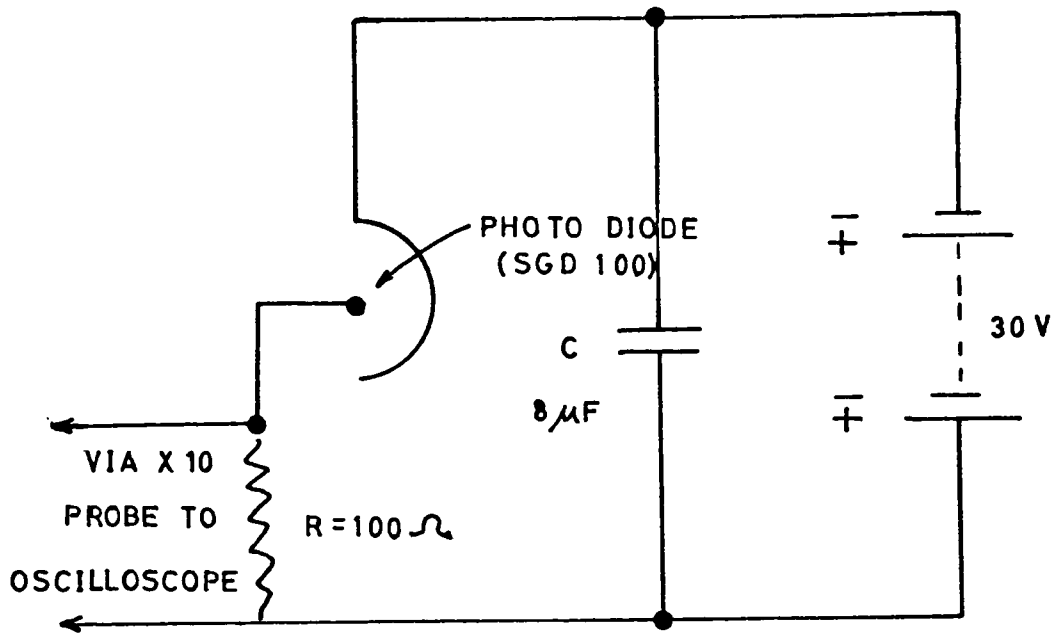

FIG. 4.6. PHOTO DIODE CONNECTIONS

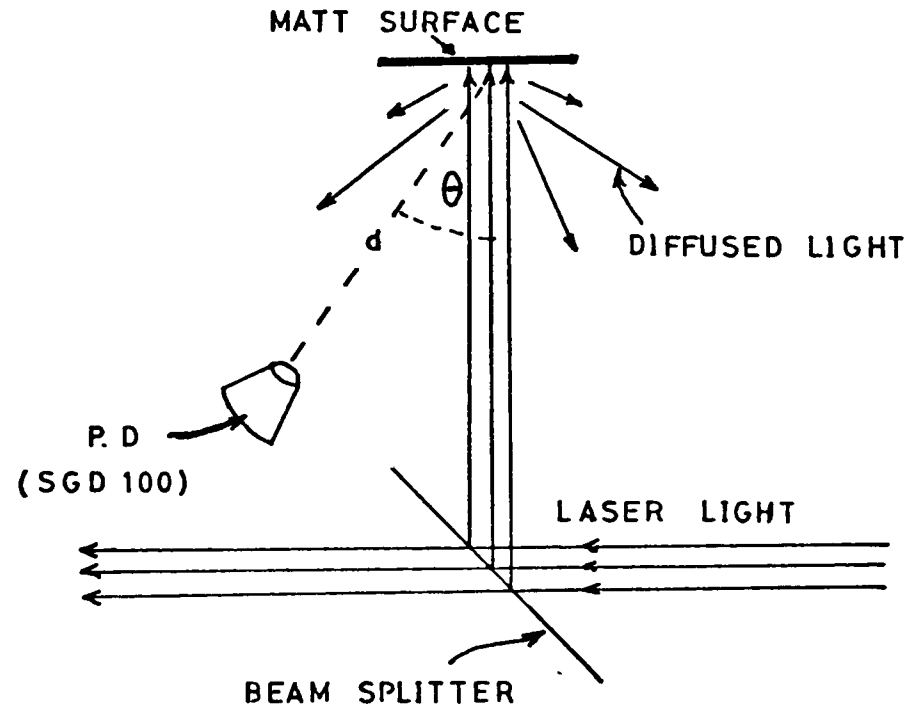

FIG. 4.7. ARRANGEMENT FOR THE CALIBRATION OF THE PHOTODIODE.

terms of the laser power as,

$$I = \frac{r.\rho.P}{2\pi} \text{ candela/area} \qquad \ldots. \ 4\text{-}2$$

From equation 4-1

$$F = \frac{r.\rho.P.a.b.\cos\theta}{2\pi d^2} \text{ lumen.} \qquad \ldots. \ 4\text{-}3$$

$$F = \frac{r.\rho.P.a.b.\cos\theta}{2\pi d^2 \times 620} \text{ watts} \qquad \ldots. \ 4\text{-}4$$

Thus, $\frac{r.\rho.a.b.\cos\theta}{2\pi d^2}$ watts of luminous flux in the photodiode corresponds to 1 watt/area of the initial laser power. From the frequency response curve (Fig. 4-5), the sensitivity of the P.d. at 0.69 μ was found to be 0.393 μA/μwatt. The current is passed through a 100Ω resistor, so that 1 watt of flux into the photodiode will correspond to a voltage signal of 38.5 volts. So that 1 watt/area of laser power will correspond to a voltage signal $\frac{r.\rho.a.b.\cos\theta}{2\pi d^2} \times 38.5$ volts. Thus for a photodiode signal of V volts, the total power will be given by

$$P = \frac{2\pi d^2 \times V}{r.\rho.b.\cos\theta \times 38.5} \text{ watts} \qquad \ldots.4\text{-}5$$

4.5 Ultra High Vacuum Technique

In atmospheric condition, or at very poor vacuum condition, secondary ionization of gas molecules by the laser-induced high energy particles and high frequency light is likely to take place. Also, physical adsorption of gas molecules or ions is likely to contaminate the target. This is likely to effect the detection of pure laser-induced emission from the target both as regards the intensity and the time response. To avoid this complication and to detect pure laser-induced current, most of the experiments were performed in ultra high vacuum. The experimental targets and the metal

anodes were assembled inside a glass envelope. Pyrex was chiefly used with electrical leadthroughs of tungsten. Sometimes, however, for the sake of convenience, Kodial glass was used with kovar conductors through it. One or two type EIP-12 ionization gauges (Mullard) were attached to each experimental tube. These gauges simultaneously pumped the tube and measured the pressure. The whole process of evacuating a tube down to a very low pressure is described below.

A schematic diagram of the baking and pumping system is shown in Fig. 4-8. The pumping was done in three different stages. The preliminary pumping was done with a molecular sieve. Rotary or diffusion pumps were not used to avoid possible contamination of the system by oil or mercury vapours. The active part of the molecular sieve is the pellets of calcium aluminium silicate. At liquid nitrogen temperature they absorb a large volume of gas. In several hours this pump reduces this pressure down to a few parts times 10^{-3} torr.

When the pressure fell below 10^{-2} torr, the getter ion pump (Ferranti, type No. FJD 8) was switched on and the valve B was opened. When the ion pump started to operate, the valve A was closed. The pressure went down to 10^{-6} torr in a few hours. Sometimes, however, minute leaks in the experimental tube or in the vacuum system did not let the pressure go below 10^{-4} or 10^{-5} torr. In this situation, a Mass Spectrometer Leak Detector (20th Century Electronics Ltd.) was used. Thus the tubes were checked carefully to ensure the absence of any leak before sealing off from the system. As the pressure went down below 10^{-6} torr, the oven was put on the

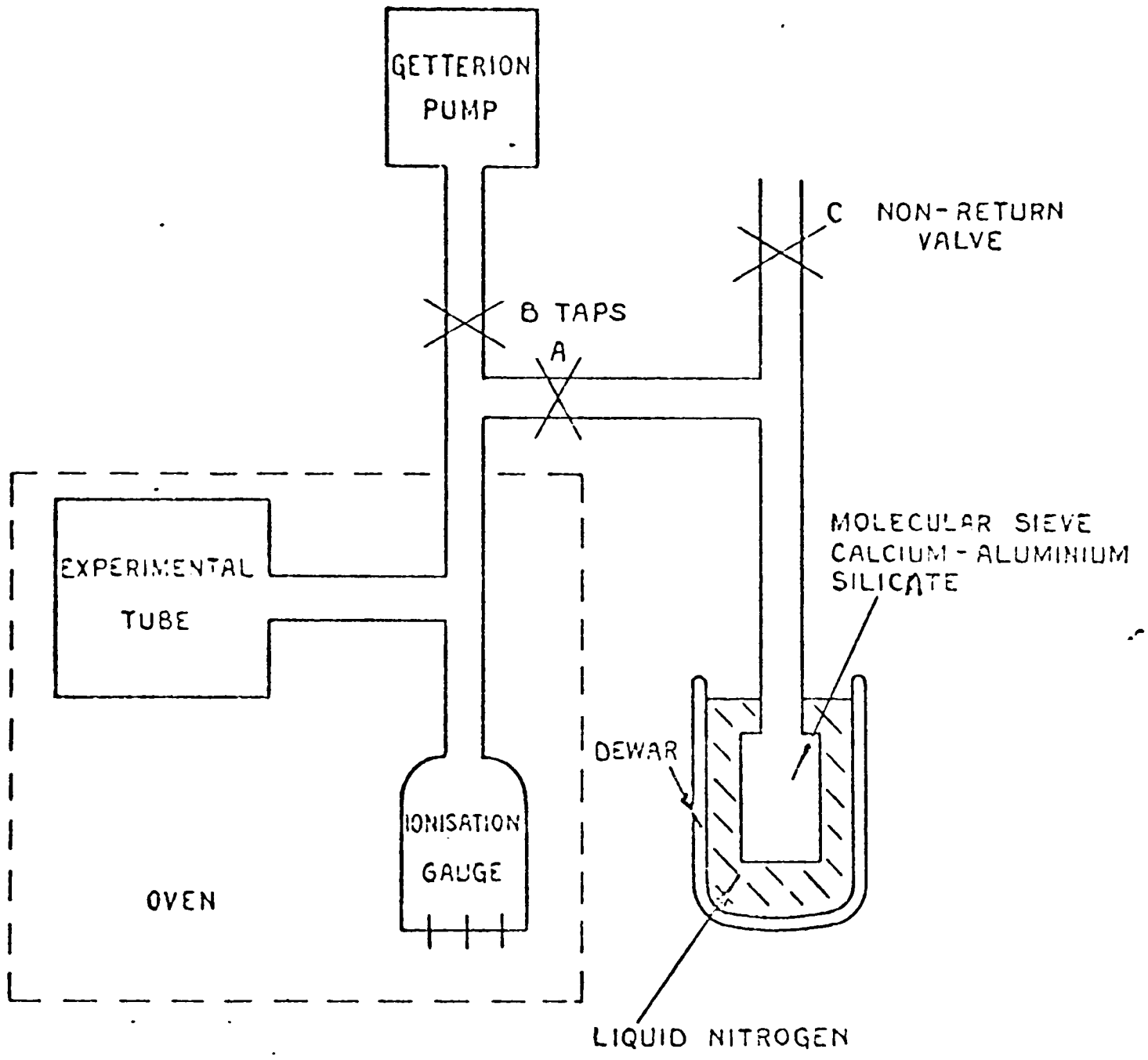

FIG. 4.8. ULTRA HIGH PUMPING AND BAKING SYSTEM.

platform to enclose the experimental tube and the ion gauges. The heating elements of the oven were connected in series with an Indicating Temperature Controller unit (Ether Ltd., type No. 990). A Pt. 13% Rh/Pt thermo-couple measured the temperature inside the oven. The temperature of the oven was raised up to 350°C in steps. The tube was baked at this temperature for a prolonged period. In this way the atoms and the molecules adsorbed in the wall of the glass tube were driven out and pumped away. The temperature controller consists of a high-resistance galvanometer fitted with an indicating-pointer. The pointer-arm operates a simple photo-electric system which controls the heating medium. With this, the tube could be baked at any desired temperature for any length of time within an accuracy of ∿ 5°C. After the baking the system was cooled down to room temperature gradually. A photograph of the system is shown in Fig. 4-9.

In the final stage of pumping, the ionization gauges were outgassed by heating the filament electrically to red heat. The getter was activated by evaporating zirconium onto the envelope from the heater element. The gauge was then switched on. With continuous pumping, pressure lower than 10^{-9} torr was achieved in the experimental tubes.

4.6 Dielectric Mirror Fabrication

The dielectric mirrors used to form the resonant optical cavity and also to attenuate the laser beam were found to be damaged by the laser beam and the atmospheric conditions. Thus it was found necessary to replace the mirrors from time to time for better performance. A vacuum evaporation plant installed in this laboratory was used to make these mirrors.

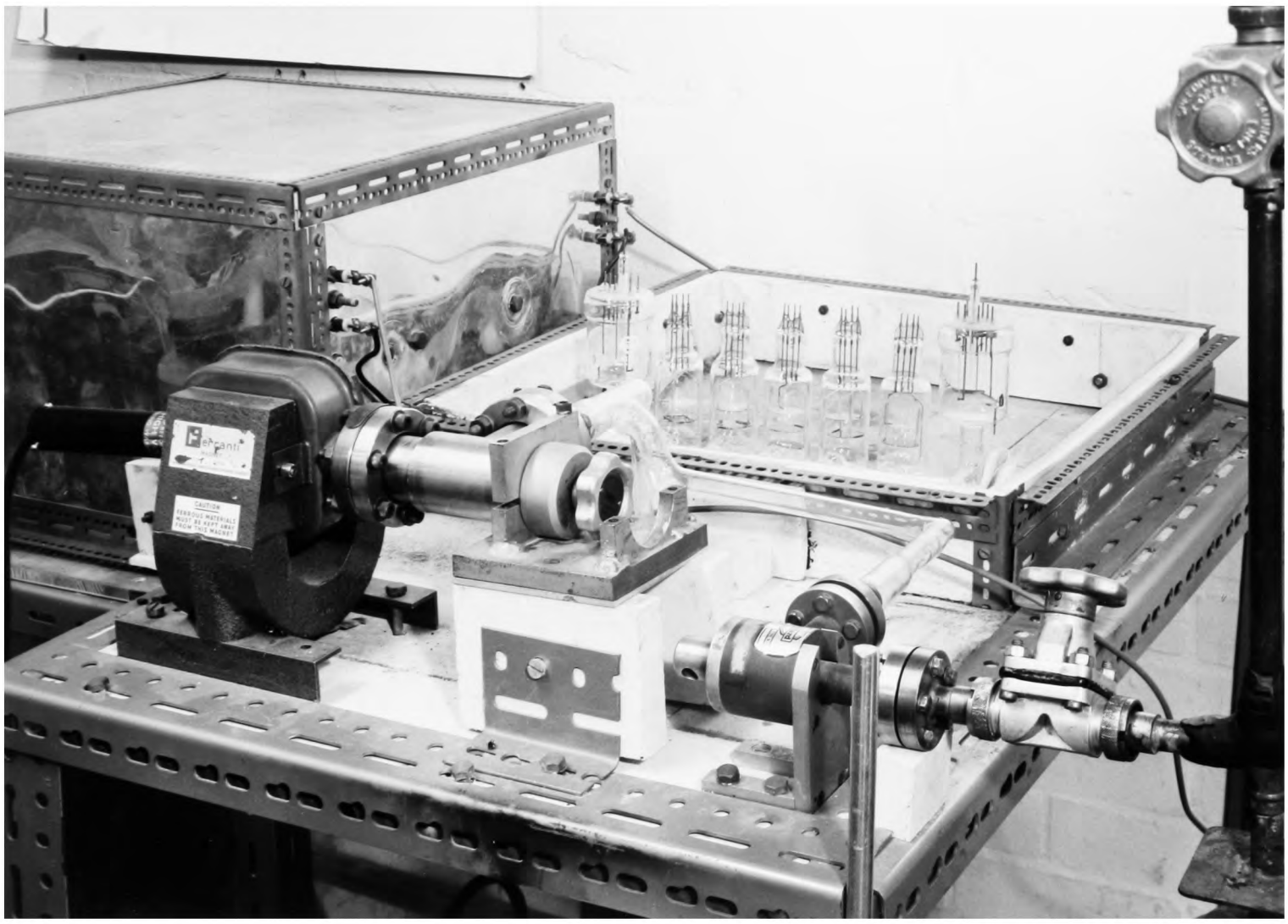

FIG. 4.9. PHOTOGRAPH OF THE ULTRA HIGH PUMPING AND BAKING SYSTEM.

Apart from the required reflectivity, the laser mirrors are required to have very low absorption coefficient, otherwise the intense laser radiation will vapourise the reflecting material of the mirror. Alternate layers of transparent dielectric materials of high and low refractive indices produce a reflecting surface with very low absorption coefficient. It is necessary to set the thickness of the layers accurately to a quarter of a wavelength of the light at which the maximum reflectivity is required.

The dielectric materials were evaporated onto a glass substrate which is optically flat. The substrates were properly cleaned before evaporating the materials onto them. The dielectric materials used are zinc sulphide of refractive index 2.4 and magnesium fluoride of refractive index 1.3. The evaporation was done at a pressure below 10^{-5} torr. The dielectric materials were evaporated from electrically heated molybdenum boats and deposited on the cooler substrate. The thickness of the layers was determined by observing the transmission of light through the coated substrate. The substrate was first coated with the high refractive index material until the transmission reached a minimum. The low refractive index material was then evaporated on top of this until the transmission reached a maximum. This process of alternate deposition of materials was repeated until the overall transmission reached the required value. A schematic diagram of the system in shown in Fig. 4-10. The light beam was chopped to eliminate the interference from other light, and passed through the substrate in the vacuum chamber. The output was focussed onto the slit of a monochrometer. The light was selected close to 6943 Å and was detected by the

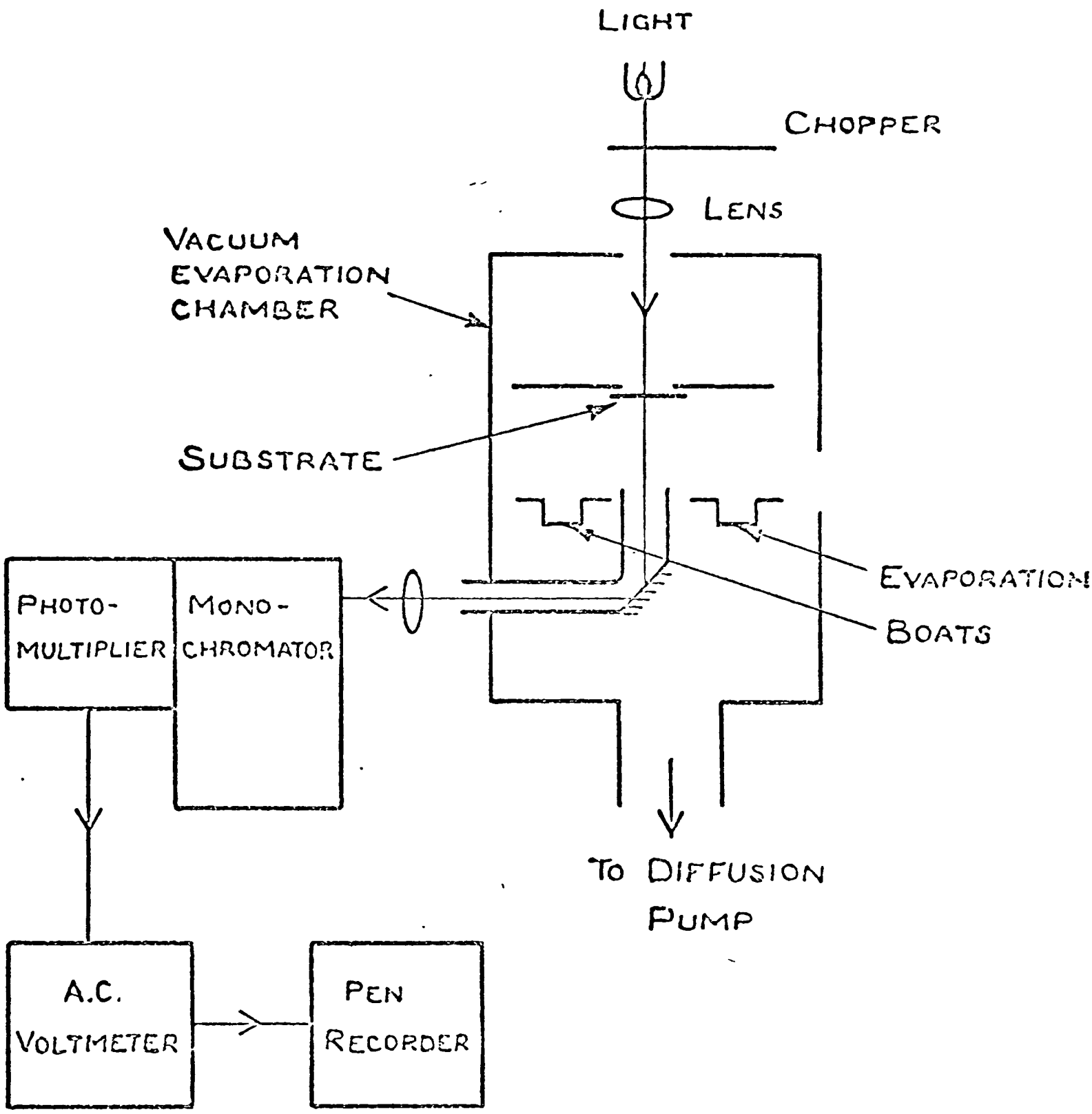

FIG. 4.10. DIELECTRIC MIRROR DEPOSITION SYSTEM.

photomultiplier. The output of the photomultiplier was fed into an A.C. valve voltmeter. ZnS was first evaporated, the transmission of light through the substrate decreased to a minimum value at a thickness of quarter wavelength of the light (6943 Å). At this stage the evaporation of ZnS was stopped and MgF_2 was evaporated to a thickness of another quarter wavelength, where the transmission increased to a maximum value, which was below the previous value of transmission. The process was repeated until the desired value of reflectivity was achieved.

To achieve a uniform coating, an arrangement to rotate the disc on which the substrate was mounted was made. For reflectivity higher than 98%, 12 to 14 layers of coatings were evaporated. The number of layers is limited in practice by the intensity of the monitoring light. Ultimately, the limiting factor is the noise level in the detecting system.

CHAPTER FIVE

INITIAL STAGE OF LASER INTERACTION WITH METALS

5.1 Introduction

A brief outline of the possible mechanism by which a laser beam interacts with the surface of a metal was given in Chapter Three. It was shown that for an intense beam of laser light, lasting for a few tens of nanoseconds, the irradiated region will reach the boiling temperature within a couple of nanoseconds. The concept of temperature and the thermionic emission within this time will be valid if a local thermal equilibrium between the excited electrons and the lattice can be assumed to be achieved within this time. An estimation of the time required for an excited electron to reach an equilibrium with the lattice can be made from the following consideration.

The mean free time τ between collisions for electrons in a good conductor (e.g. Ta) is of the order of 10^{-14} to 10^{-13} seconds. The ratio of the mass of an electron to that of a T_a atom is $\sim$ 1:3 x 10^5; and the same fraction of the energy of an excited electron is transferred to the lattice at each collision. Thus roughly 10^6 collisions must take place before a thermodynamical equilibrium is reached. Such a process of thermalization may take any time between 10 to 100 nanoseconds. If some of the electrons absorb sufficient energy so that at any instant of time before reaching the equilibrium they reach the surface with energy in a direction normal to the surface, they may escape over the work function barrier. Such an emission will be an instantaneous process as far as the present experimental measurements are concerned.

For current signals produced by such electrons are expected to have a peak to peak time correlation with the initiating laser pulse. The number of excited electrons which stay inside the metal longer than the thermalization time will contribute to the concept of a temperature of the activated spot as a whole. Thus for any delayed emission of electrons from the laser illuminated spot of a metal surface, the Richardson equation may be applied.

Light is absorbed in metals by internal photoeffect (40), raising the electrons to higher energy states in the conduction band. If the energy of the photon ($h\nu$) is greater than the work function (ϕ) of the particular metal surface then the excited electrons will have sufficient energy to escape into the vacuum through the surface barrier. With ruby photons ($h\nu$ = 1.78 eV), the excitation of any electron from the Fermi level (at $0^{\circ}K$) to the vacuum level is energetically impossible for most of the metals. For a metal like Ta with work function $\phi \tilde{\sim} 4.1$ eV, the rate at which the energy of an excited electron is dissipated in the lattice is of the order of 10^{7} joules/sec. For a typical laser pulse of $\sim$ 100 nsec. duration and 1 to 10 MW/cm^{2} in amplitude, the rate at which energy is delivered to an atomic dimension is very much smaller than the speed of thermalization. Thus it appears that most of the excited electrons will be cooled down before being emitted out of the surface barrier by the successive (or simultaneous) absorption of multiple photons. It was reported in Ref. 15 that if the photoelectric emission from metals are considered to be due to absorption of n number of photons by a single electron before it makes any transition, the photons must be absorbed within approximately 10^{-13} sec.

Though the probability of a multi-photon photoemission process at very low intensity appears to be remote, recent observations on intensity dependent interaction have shown that at moderately high intensity the probability of such a process may be of considerable importance. For example, two photon and three photon photoelectric processes have been reported to take place in Ref. 13, when metal surfaces were illuminated with laser light. In the present work, the effect is further investigated.

5.2 A Theoretical Account of the Multi-photon Photoeffect

If a clean metal surface is illuminated with a beam of laser light of intensity sufficiently low to keep any Richardson effect negligible, then any electron emission must be attributed to a photoelectric process. Since a photoelectric process from metals with $\phi > h\nu$ must involve simultaneous absorption of more than one photon, a precise theoretical treatment will be extremely complicated. The expression for a double-photon photoelectric current given in Eqn. 3-9 (Chapter Three) can only be applied for insulators and semiconductors. For metals, a similar analysis would require more sophisticated mathematical technique and to apply it for the quantitative analysis of the results a knowledge of the band structure and the electronic states involved in the interaction will be required. However, the analysis presented in Ref. 13 may be used as a guide line to study the multi-photon process in metals as far as the behaviour of the emission current with respect to the incident photon density is concerned.

From the single-photon photoelectric studies it is known that for a metal surface with work function ϕ, the

threshold energy for photoelectric emission is $h\nu \gtrsim \phi$. If it is assumed that at high incident photon density, the probability of n number of photons being absorbed by an electron within the time it requires to make a transition (to a higher energy state) is considerably high, the problem may be treated as if a single photon of total energy $nh\nu$ is being absorbed. The results can be treated in terms of a single-photon process with the energy balance equation given by:

$$E = nh\nu - \phi \qquad \ldots\ (5\text{-}1)$$

where E = the kinetic energy of the emitted electron.

From the above equation it can be seen that a two-photon photoelectric emission process from a metal surface with work function $\phi < 3.56$ eV (e.g. Al has a work function ~ 3.0 eV) is energetically possible for ruby photons ($2h\nu = 3.56$ eV), whereas for metals like Ta ($\phi \gtrsim 4.1$ eV), W ($\phi \gtrsim 4.5$ eV) etc. at least three photons must be absorbed for photoemission to take place. It is obvious that the quantum yield, η (no. of electrons emitted per incident photon), at a particular intensity of the incident laser beam, will be higher for a two-photon process than that for a three-photon process. Thus if photoelectric emission is observed from high work function materials, the current is expected to be considerably lower than that obtained from a metal surface with work function $\phi < 3.56$ eV. For example, Al and Cu have roughly the same absorption coefficient (single-photon) at ruby frequency. Since Cu has a work function $\phi > 3.56$, the photo-electric emission, if it takes place, must be predominantly due to a three photon process. Thus the amplitude of the

photocurrent from Cu is expected to be much smaller than that from the Al for the same incident intensity. The remarks made above are rigidly true only for an idealized case of absolutely pure, polished and clean metal surface near absolute zero. In practice the contribution in the photocurrent by lower order effect from the impurity atoms and assisted by the thermal energy (room temperature Fermi-distribution of the electrons) may be of considerable importance. Though the actual dependence of the photo-electric current with the parameters of the laser beam and the materials is not known, it can be considered from the phenomenological point of view that an n-photon photocurrent will depend on the n^{th} power of the incident intensity. The relation can be stated as:

$$J = bI^n \quad \text{amps/cm}^2 \qquad \ldots\ (5\text{-}2)$$

where I = laser intensity in watts/cm^2

and b = a constant which takes account of all the interaction parameters.

Thus the number of photons involved in a particular interaction can be estimated from a study of the intensity dependence of the photocurrent.

The quantum yield of a particular process can be estimated from Eqn. 5-2 in the following way:

For a double photon process the photocurrent equation will be $J = bI^2$. Thus the ratio of the current density to the laser intensity will be $J/I = bI$. If n_e represents the total number of electrons per sec. per unit area, the current density may be expressed as $J = 1.6 \times 10^{-19} n_e$. The incident intensity can also be expressed in terms of the number of photons n_p per sec. per unit area. For ruby photons of energy

$1.78 \times 1.6 \times 10^{-19}$ joules, the intensity $I = 1.7 \times 1.6 \times 10^{-19} n_p$. Thus the quantum yield for a two photon process can be expressed as:

$$\eta = \frac{n_e}{n_p} = 1.78\ bI \qquad \ldots\ (5\text{-}3)$$

Here b is expressed in $\frac{\text{amps/cm}^2}{(\text{watts/cm}^2)^2}$.

If the photoelectrons would have all been emitted by an unique process (for example, a two photon process only) and all from the Fermi level, all the electrons would have the same energy. For retarded potential the current would have a sharp cut-off voltage V_R given by $eV_R = (nh\nu - \phi)$. But since the electrons may also be emitted from both below and above (at $T > 0^{\circ}K$) the Fermi level and since there exists a finite probability of still higher order photoeffect (however small), the emitted electrons will have a distribution of energy.

For a Maxwellian distribution of electron energy the current at any retarded voltage V_R will be given by:

$$J = J_o \exp(-eV_R/kT_e) \qquad \ldots\ (5\text{-}4)$$

where J_o = saturation current

k = Boltzmann constant

T_e = electron temperature.

Thus for a Maxwellian distribution a plot of ℓnJ vs. V_R will be a straight line. From the slope of such a straight line, an estimation of the electron temperature can be made.

At higher incident intensity the Richardson effect may be high enough to give rise to a detectable current. It must be concluded that any Richardson effect must always be associated with the photoeffect in the cases where such

studies are concerned. The thermionic electron may be distinguishable from the photoelectrically emitted electrons as the former is expected to be a slower process because of the finite thermalization time. However, if the current signal can be identified as due to a thermionic process, the energy distribution of such electrons will be Maxwellian. The temperature rise of the target can be estimated from the study of the retarded potential characteristics of the current and can be compared with the calculated temperature at a particular laser intensity.

5.3 Experimental Arrangement

For the investigation of various parameters of the interaction and different characteristics of the laser induced current the vacuum tube used is shown in Fig. 5.1. Four different tubes were made with different target materials, viz. W, Ta, Cu and Al, and with kovar collectors. The individual tubes were joined together and the whole assembly of tubes were baked and evacuated down to a very low pressure ($\sim 10^{-9}$ torr). This made it convenient to do experiments with different materials at similar atmospheric conditions. All the tubes had similar electrode configurations.

The collector, in the form of a circular disc, was held at 1.2 cm. away from the target. A laser beam from the Q-switched laser system, as described in Chapter Four, was fired onto the target through an optical window and through a hole of diameter 1 cm. cut at the centre of the collector. The laser induced current flowing across the electrodes was passed through an external resistor which connected the target and the collector by the external feedthroughs. Bias

FIG. 5.1. VACUUM TUBE WITH FOUR DIFFERENT TARGET MATERIALS.

voltage was applied from a dry cell which was shunted by a 16 μF capacitor. A typical experimental arrangement is shown schematically in Fig. 5.2.

The voltage signal generated across the resistor was monitored by an oscilloscope (Type 551, with type L plug-in units) and recorded photographically. A part of the laser beam was deflected to a mat surface. The diffused light from the mat surface was received by a calibrated photodiode. The photodiode signal was fed to the remaining channel of the dual beam oscilloscope and recorded simultaneously with the current signal.

The pressure inside the tube was maintained below $\sim 10^{-9}$ torr by constantly pumping with the help of two ionization pumps (Type EIP-12 Mullard) attached to the tube. To avoid emission from the contaminated surface, before recording any current signal the target was irradiated several times with the unfocussed laser beam so that the absorbed atoms and molecules were driven off from the surface and pumped out by ionization pumps.

In the case where the current signals were recorded for different values of the incident laser intensity, the intensity was varied by introducing dielectric coated mirrors of different reflectivity. The laser signal was recorded for every measurement of the current amplitude. Thus the magnitude of the laser power was directly measured along with the value of the resulting current. Though the absolute magnitude of the laser power was estimated within an accuracy of roughly ± 20%, the relative variation of the laser intensity and the amplitude of the current pulses were measured within an accuracy of ± 5%. Thus a precise picture of the dependence of the current with the laser intensity will be

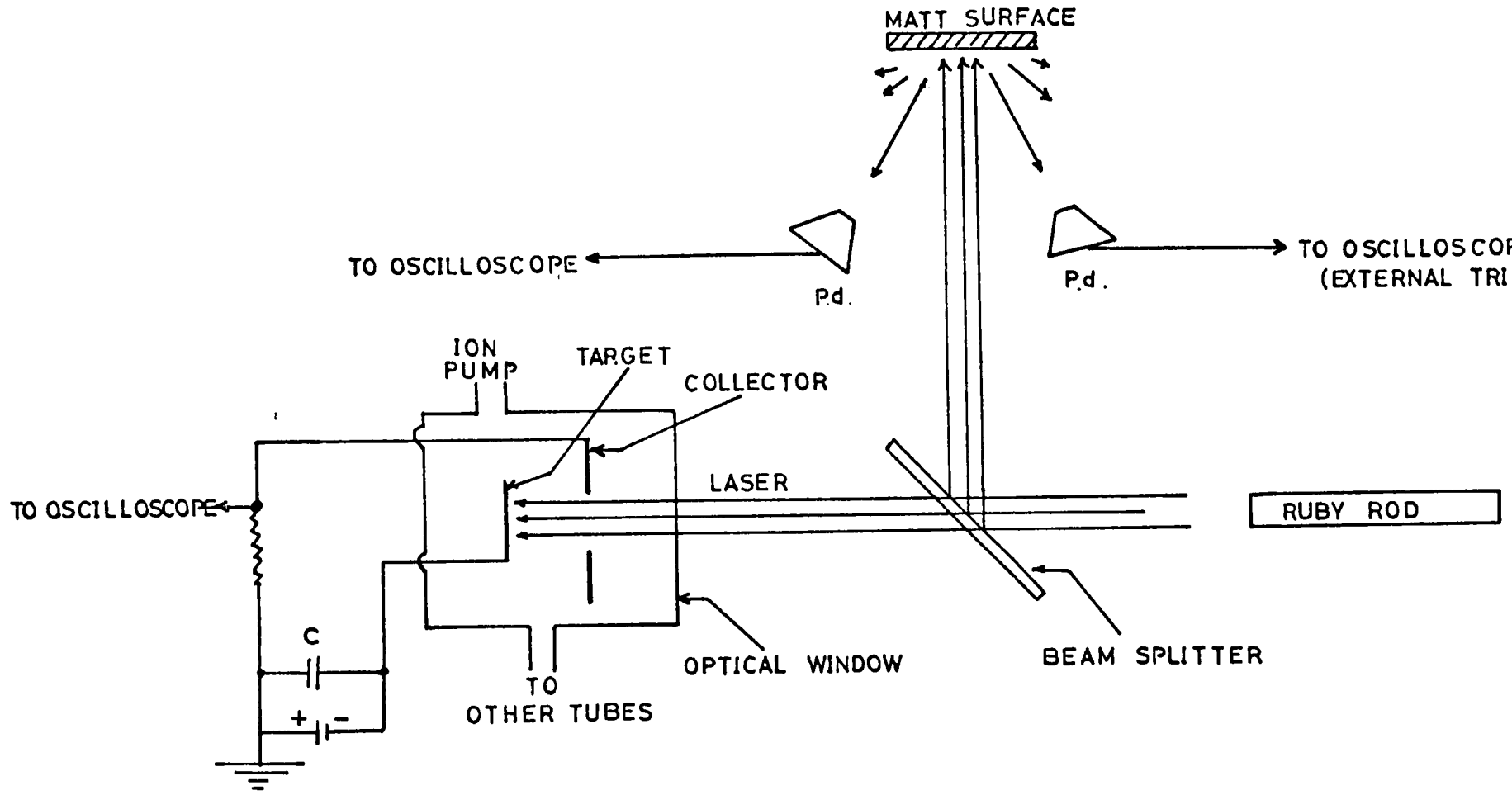

FIG. 5.2. SCHEMATIC DIAGRAM OF THE EXPERIMENTAL ARRANGEMENT.

obtained from the experimental results.

In the case where several shots of laser beam of the same intensity were required to study the emission in different circumstances, enough care was taken to record the current for the same laser intensity throughout the experiment. It was found that the laser power varied by ± 8 to 10% from shot to shot. So several readings were taken and the current which corresponded most closely to the particular value of the laser power was considered.

Finally, for the accurate detection of the signals the reaction time of the detecting circuit was kept as small as possible. The limiting factor, however, was the 12 nanosec. rise time of the oscilloscope plus another 6 nanosec. rise time of the plug-in unit.

5.4 Experiments to Investigate Multi-photon Process

To study the photoelectric effect from metal surfaces with work function $\phi > h\nu$ of the incident photon, incident laser intensity was kept much below the threshold value at which Richardson effect may be of considerable importance. Considering that a double photon photoelectric process is energetically possible from Al ($\phi \simeq 3$ eV) for the ruby photons, the amplitude variation of the current pulse with the laser intensity was studied for this metal.

From the recorded current signals it was observed that for laser intensity below $\sim$ 2 MW/cm^2, a single pulse, almost coincident with the laser pulse, was produced (Fig. 5.3). Thus the emission process appears to be instantaneous, which is a characteristic of a photoelectric process.

The power density of the illuminating beam of cross-sectional area of 0.13 cm^2 was varied in the range from 0.1

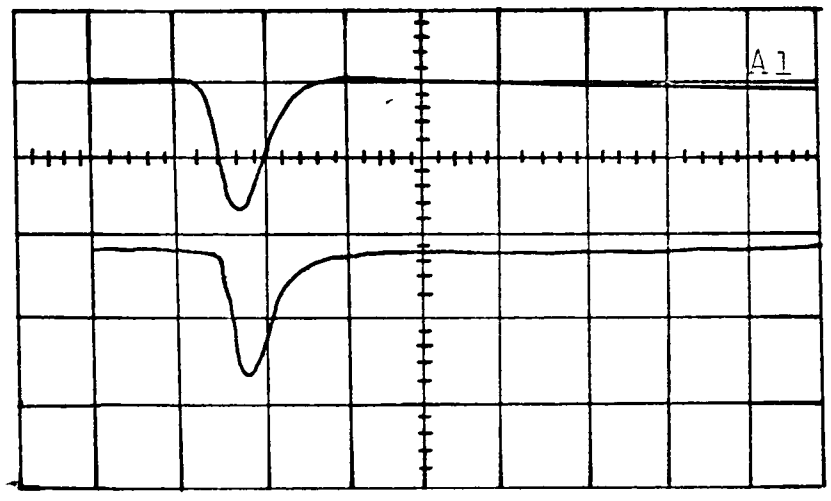

UPPER - Laser pulse

LOWER - Current pulse

TIME SCALE -
100 nsec/cm.

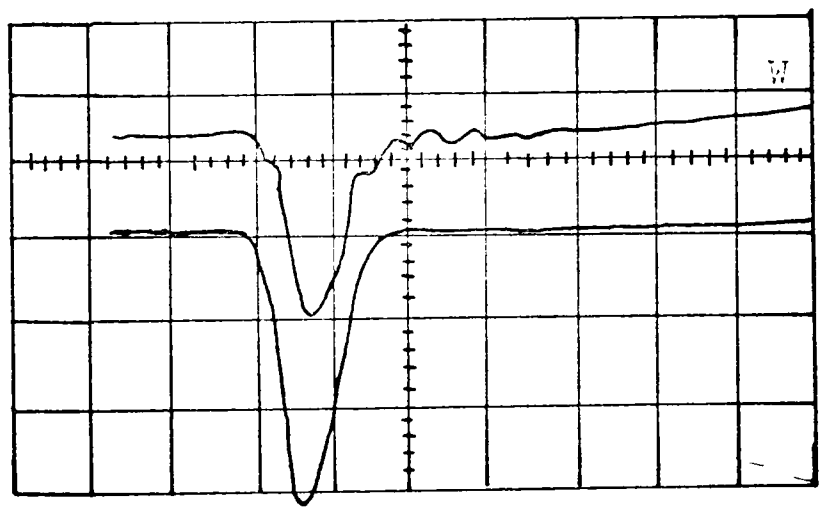

UPPER - Current pulse

LOWER - Laser pulse

TIME SCALE -
100 nsec/cm.

FIG. 5.3. OSCILLOGRAMS OF CURRENT SIGNALS INDUCED BY LASER PULSE OF INTENSITY BELOW 2 MW/cm^2.

to 2 MW/cm^2. At these intensities of the beam, the calculated temperature of the target surface is not expected to rise above 310 ± 60 ^{o}K. Thus any thermionic effect was negligible throughout the experiment. The current density J corresponding to the peak of the current pulse was plotted against the corresponding values of the peak laser intensities in a log-log scale. The experimental points fitted a straight line, as shown in Fig. 5.4. The slope of the straight line was found to be 2. The result clearly indicates a non-linear electron emission and a double photon process in Al can be inferred. A similar double photon process of emission from stainless steel ($\phi \tilde{\sim} 5$ eV) by 3.57 eV photons was reported in Ref. 13.

Photoelectric emission was also studied for a W surface. The results of a similar experiment are shown in the same figure (Fig. 5.4). The slope of the log J vs. log I plot was found to be 2.2, which also indicated a double photon process. W has a single photon photoelectric threshold at about 4.5 eV, thus a third order effect was expected. A similar contradiction between the observed and expected results was also reported by Logothetis et al. (13). They observed a double photon photoeffect from KCl with the valence band-vacuum level energy difference equal to $\sim$ 8 eV, when activated by 3.57 eV photons.

From the results of Logothetis et al it can be inferred that a three photon photocurrent is likely to be three to four orders of magnitude smaller than a double photon process for the same incident intensity. Thus if there exists a three photon effect in the experiment with the W target, the current will be below the sensitivity of the

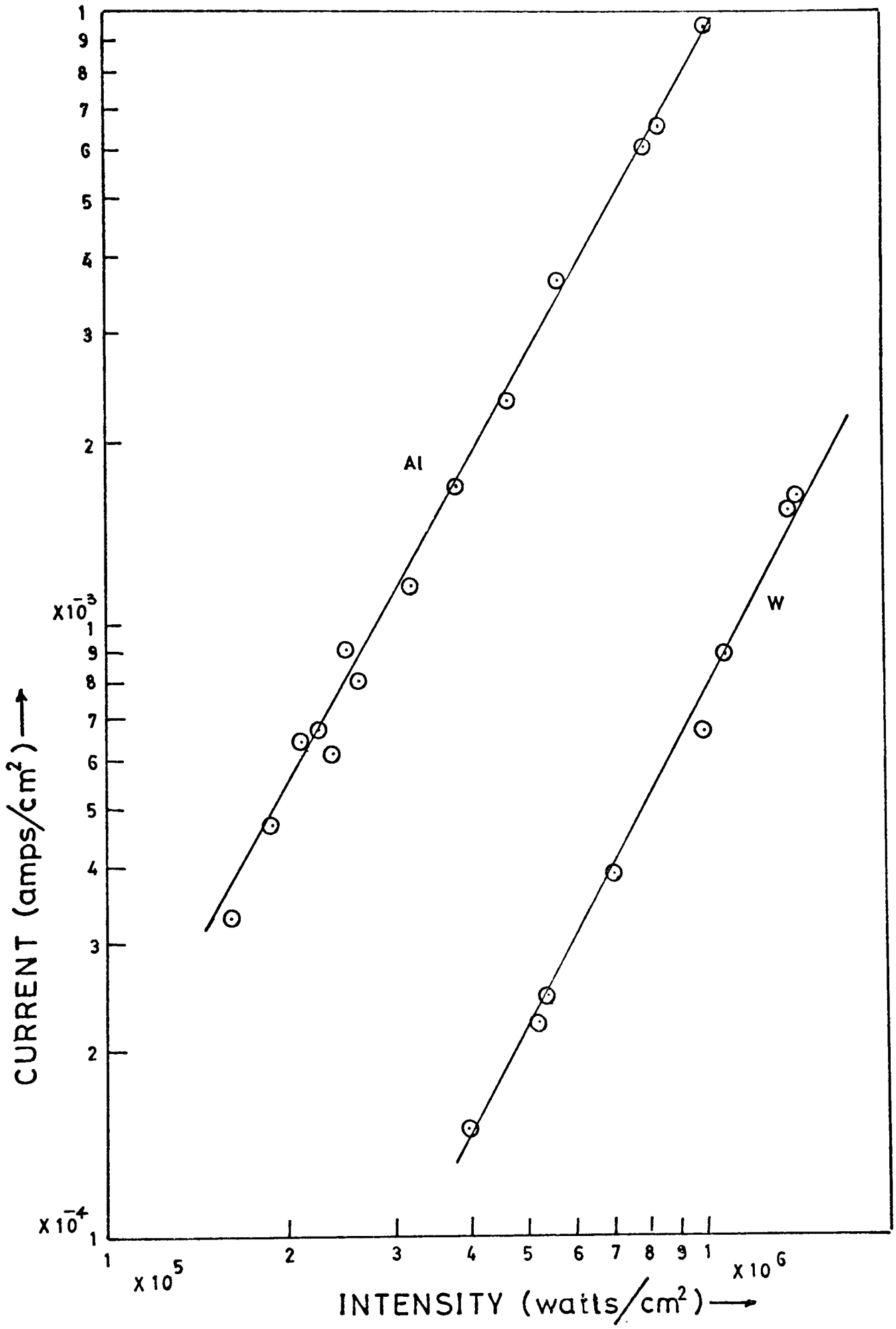

FIG. 5.4. CURRENT DENSITY VERSUS LASER INTENSITY.

present detecting system ($\sim 10^{-6}$ amps/cm^2). The observed current from W can possibly be due to a double photon process from impurity atoms or from the high energy tail of the Fermi distribution. It is important to mention that the anomaly in Logothetis' work (with KCl) was also assumed to be due to a lower order emission process from the impurities or defects in the KCl films.

From the straight line of Fig. 5.4 (for Al), the current density was noted for the corresponding values of the laser intensity. The current was plotted against the square of the incident intensity (Fig. 5.5). The slope of the straight line (b) was found to be $\sim 1.1 \times 10^{-14}$. Using Eqn. 5-2, the quantum yield was calculated and found to be $\sim 2 \times 10^{-8}$ electrons/photon at an incident intensity of 1 MW/cm^2. Compared to the results of Logothetis et al. it can be inferred that the double photon quantum yield from alkali halides (e.g. KCl, KI, etc.) is roughly an order of magnitude higher than the quantum yield from aluminium.

5.5 Photoelectric Emission from Different Metals

Current induced by low intensity laser light from different metal surfaces were compared in this experiment. The metals studied were W, Ta, Cu and Al, as introduced in the experimental tube of Fig. 5.1. Current signals were recorded for the same incident intensity of the laser beam from all the targets. The incident intensity was 0.4 MW/cm^2. At this power the calculated temperature rise of any metals studied here did not exceed $\sim 5^{\circ}$C. At least five readings were taken for each target and the average value of the current was considered. The results are shown below against their approximate values of the absorption coefficients at

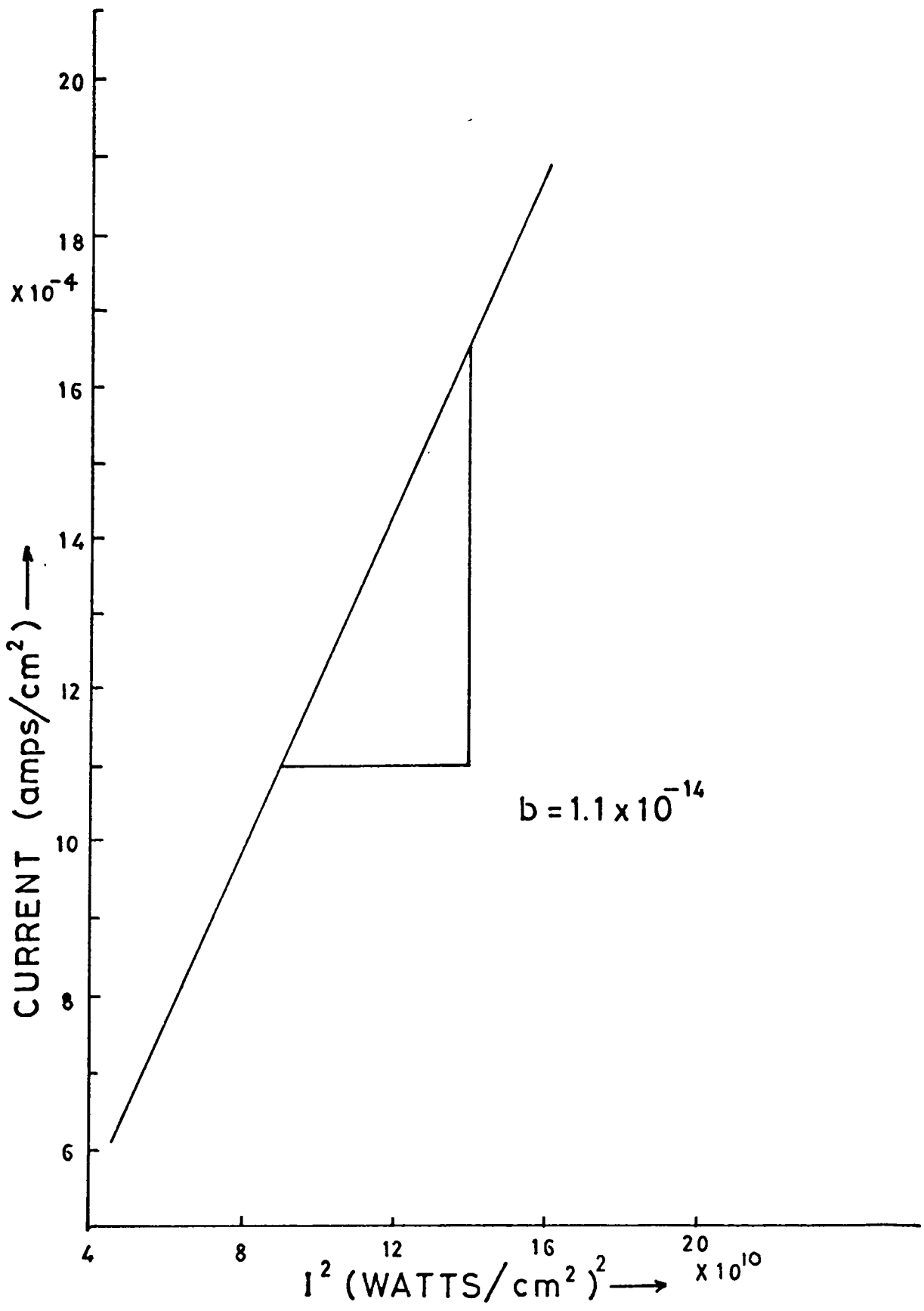

FIG. 5.5. CURRENT DENSITY VERSUS (INTENSITY)^2.

the ruby frequency and the work functions.

Metals	Absorption Coefficient at 0.7μ	Work function ϕ eV	Observed Current (Peak Value) amps. x 10^{-4}
W	0.46	4.52	1.5
Ta	0.40	4.10	4.8
Cu	0.13	4.10	3.1
Al	0.18	3.10	12.0

The observed current was not corrected for the reflection from the surface. When the absorption coefficient is taken into consideration it can be seen that the current from Al is only an order of magnitude higher than the current from metals like Ta or W. If a double photon process is assumed to take place in Al, then the observed current from W or Ta is still too high to account for a still higher order process. It can be mentioned, however, that current of similar magnitude has alos been observed from W when irradiated by ruby laser of the same order of magnitude by Knecht (7), and from Ag by Farkas et al. (41).

The results suggested that with the present experimental conditions a three photon process cannot be detected. The contribution by two photon process (probably from the impurity atoms or regions of low work functions) will mask any higher order effect.

5.6 Energy Distribution of the Emitted Electrons

The current signals were monitored by applying retarded voltage. The applied voltage was changed by 0.5 volts for each measurement of the current. The retarded voltage characteristics were studied for electron emission from all

the four materials, viz. W, Ta, Cu and Al. For this study the laser beam was not focussed and the intensity of the beam was kept always at about 5 MW/cm^2. The amplitude of the current was plotted against the retarded voltage in a semi-log graph. The experimental points fitted a straight line up to a retarded potential of $\sim$ 4 volts, as shown in Fig. 5.6. The results indicated that the electrons pertaining to the initial peak have a Maxwellian energy distribution. A very similar observation was made by Knecht (7) for a W target though the slope of the $I-V_p$ plot in the present case of W corresponds to temperature ($\sim 1.93 \times 10^4$ ^oK) which is slightly less than the value estimated by Knecht ($\sim 2.9 \times 10^4$ ^oK).

It is important to note that the electron temperature estimated for Al is $\sim 2.4 \times 10^4$ ^oK, which is higher than the temperature calculated for Ta and W. From the figure it is also noticeable that the emission from Al contains more high-energy electrons than the emission from W or Ta.

5.7 Discussion of the Results

The results clearly indicate a non-linear electron emission process from metal surfaces initiated by a low powered laser beam. Throughout the experiments the laser intensity was kept below the level at which the Richardson effect would be prominent. The results are interpreted as a double-photon process, though the actual mechanism of such a process from high work function materials like W, Ta, etc. is not clearly understood.

Gy. Farkas et al. (41) and Knecht (7) suggested independently that a similar observation of instantaneous

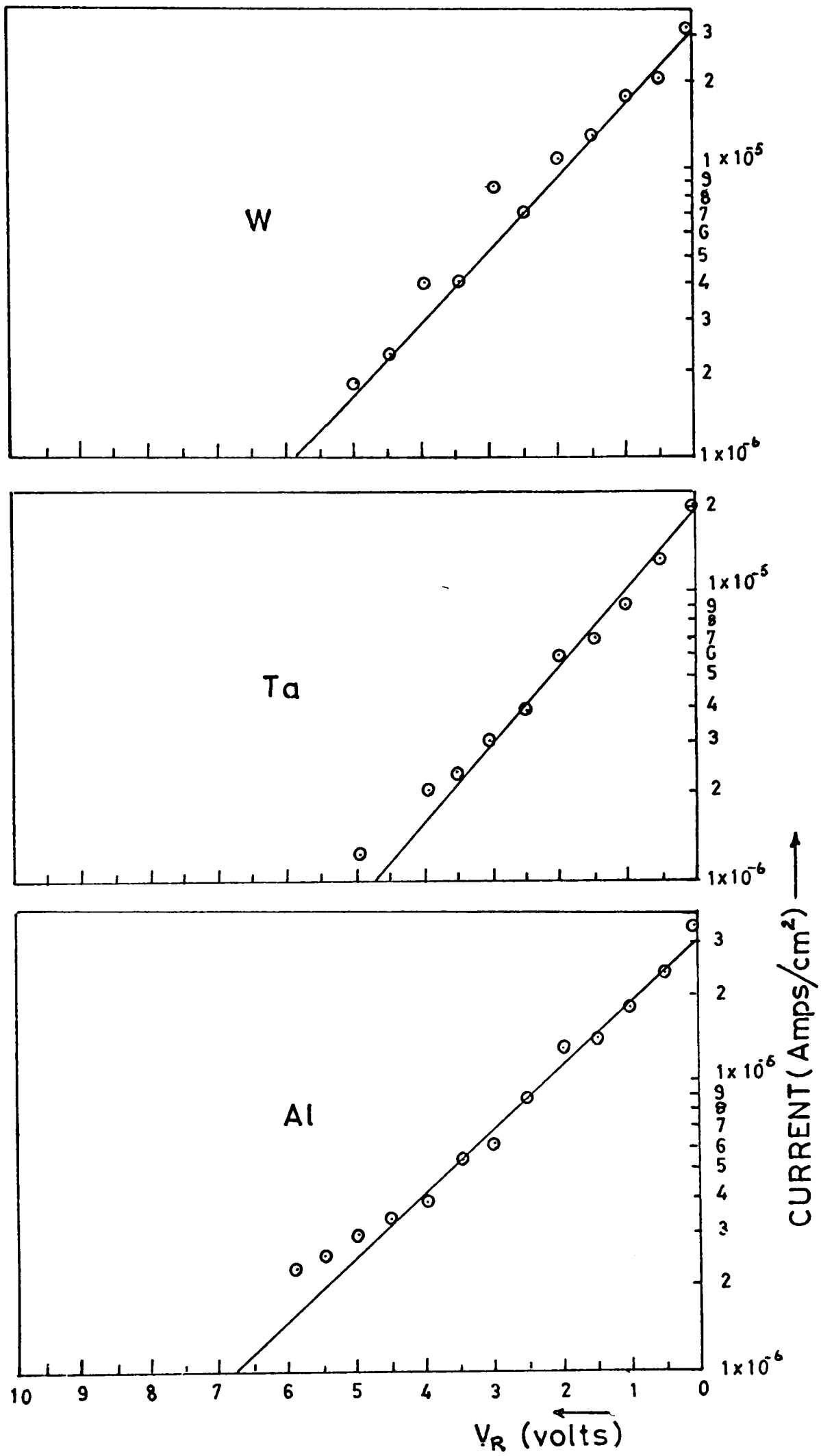

FIG. 5.6. LASER INDUCED CURRENT J VERSUS RETARDED POTENTIAL.

electron emission from metal surfaces under the influence of low intensity laser beam ($\sim$ 1 to 10 MW/cm^2) can be explained by a field-emission-like mechanism. The electric field associated with the laser beam of power ranging between 1 to 10 MW/cm^2 will not exceed 10^5 volts/cm. Such an electric field will be too small to produce any electron current from metal surfaces. In the present experiment the electric field of the laser beam was perpendicular to the normal to the surface. Any electron emission by this field from a metal surface can only arise from the surface inhomogeneities. Even though surface inhomogeneities were taken into consideration, the periodic change of the direction of the electric field ($\sim 10^{14}$ c/sec) will not allow sufficient time for the electrons to be emitted.

A double photon process was further ascertained from the shape of the electron current pulse. The shape of the current pulse will depend on the nature of the process that results in the emission. Following the treatment of Logothetis et al. (13) the order of photoeffect n can be estimated from the relation

$$n = \sqrt{\frac{\Delta}{\Delta'}} \qquad \ldots. \; 5\text{-}5$$

where Δ = width of the laser pulse

and Δ' = width of the current pulse.

The above relation was obtained by assuming the laser pulse to be Gaussian, given by $I = I_p \exp(-t^2/\Delta^2)$ and introducing this in Eqn. 5-2.

From the measurements of the widths of the current pulses and the initiating laser pulses (Fig. 5.7), n was found to be $\sim$ 2 for all the metals studied in the present

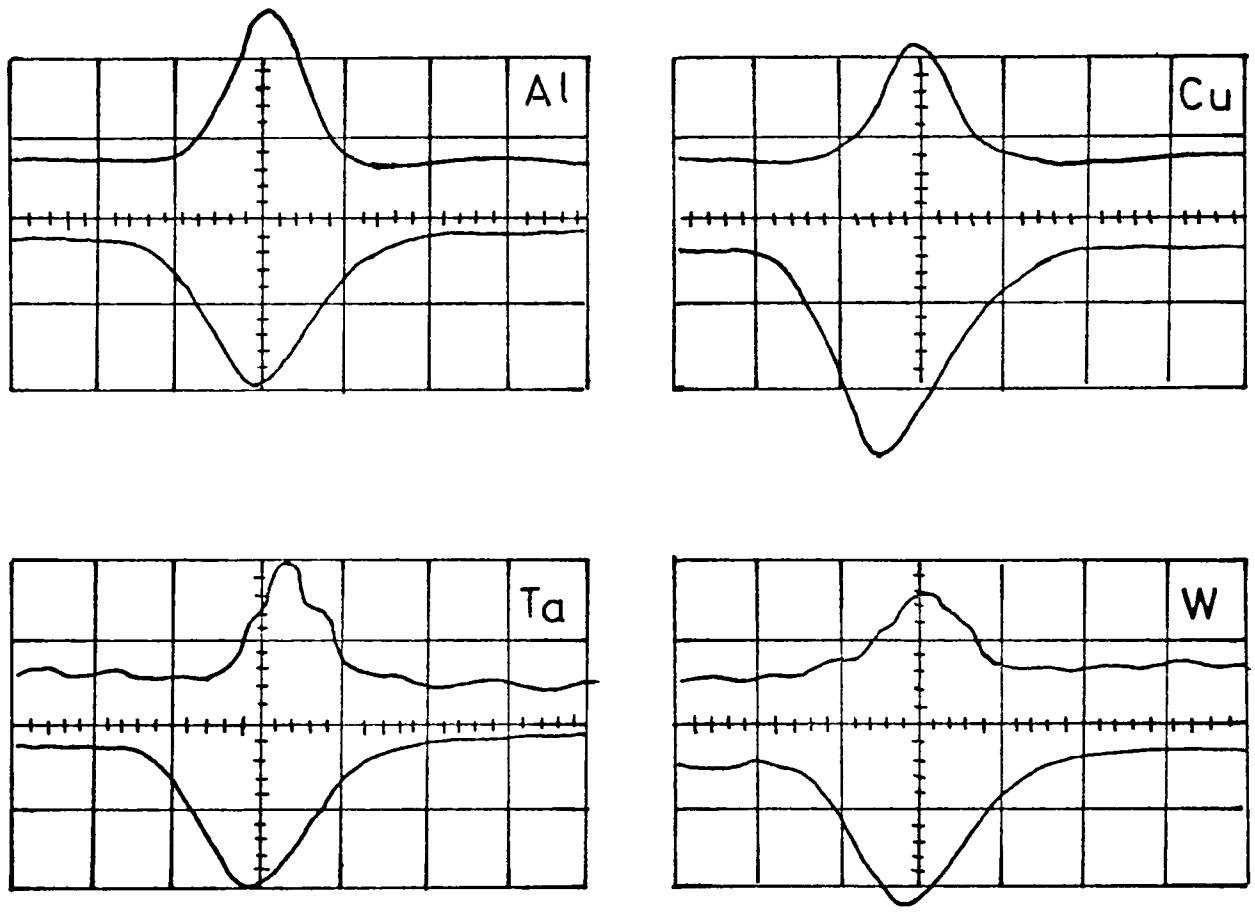

UPPER TRACE - Current signal (upward motion indicates electron emission) - Amplitude scales = Al & Cu - 10^{-3} amps/cm, Ta & W - 5×10^{-4} amps/cm.

LOWER TRACE - Laser pulse - 44 KW/cm. Cross-sectional area of the beam = 0.13 cm^2. Time scale - 40 nsec/cm.

FIG. 5.7. OSCILLOGRAM OF THE CURRENT SIGNALS FROM DIFFERENT TARGETS.

experiments.

Further observation on the laser induced current was made with higher laser power. From the temperature calculation for a Ta surface it was shown that the metal is expected to boil-off for incident intensity above $\sim$ 30 MW/cm^2. The current signals recorded for incident intensity below this value was found to be different in shape and amplitude than the signals induced by laser light of intensity below $\sim$ 2 MW/cm^2. The current pulse, instead of producing a sharp peak corresponding to the laser peak, increased further to produce a second peak after a considerable time from the laser peak, as shown in Fig. 5.8. It appears that the second pulse started just after the photoelectric current pulse reached its maximum value. The initial rise of the current had a steeper slope than that of the final increase. The observation clearly indicated that at high laser intensity (> 2 MW/cm^2) a slower process of electron emission is associated with the instantaneous photoelectric emission. As stated in the introduction, such a delayed emission appears to be characteristic of a thermionic process. But unfortunately no systematic experiment was possible to investigate the nature of the electrons pertaining to the second peak, because the shape and the amplitude of the second pulse was found to be highly irreproducible from shot to shot (different laser burst). The second peak (slope) was found to disappear at a retarded potential of $\sim$ 0.5 to 0.6 volts, indicating a smaller value of the maximum energy pertaining to the second current pulse compared to the maximum initial energy of the photoelectrons. Very similar current signals were also observed by Knecht (7)

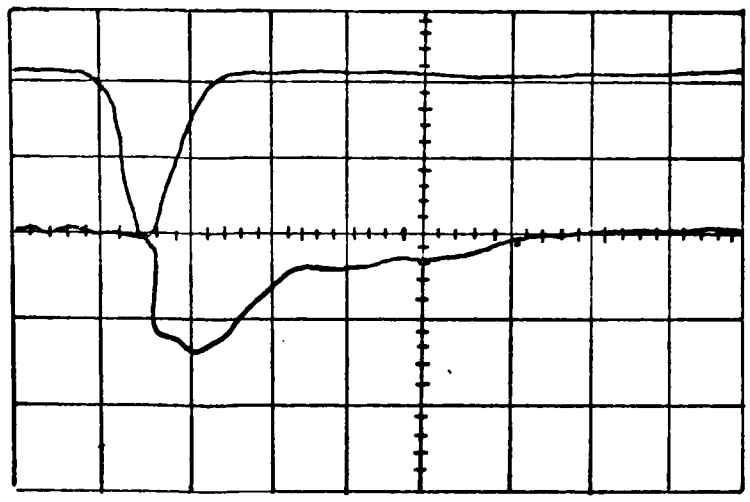

LASER INTENSITY $\sim$
2.6 MW/cm^2

CURRENT SCALE
1 mA/cm

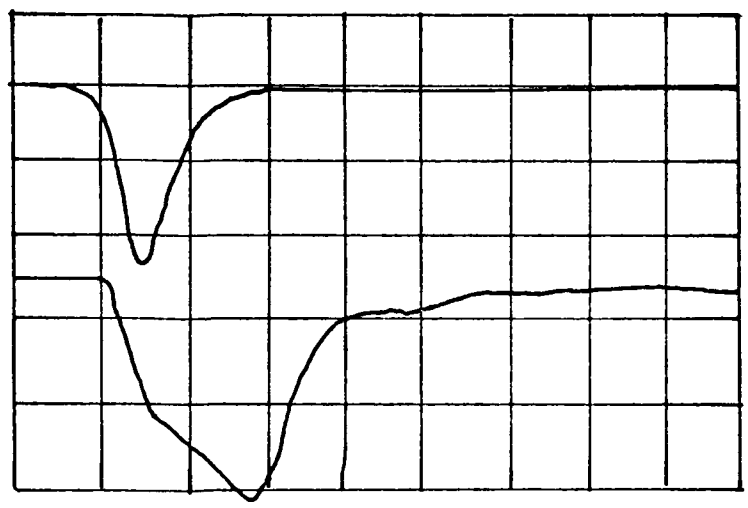

LASER INTENSITY $\sim$
4.3 MW/cm^2

CURRENT SCALE
1 mA/cm

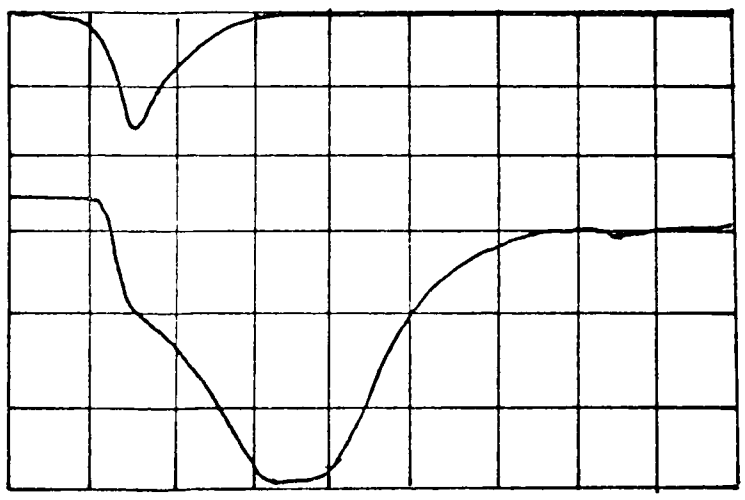

LASER INTENSITY $\sim$
10 MW/cm^2

CURRENT SCALE
10 mA/cm

TIME SCALE 100 nsec/cm.

(Target - Ta)

FIG. 5.8. CHANGE OF THE SHAPE OF THE CURRENT PULSE WITH INCIDENT INTENSITY OF THE LASER PULSE.

for laser intensities near the threshold for thermionic process from W. He observed a change in the shape of the current signal with the orientation of the target with respect to the direction of the laser beam (Fig. 5.9). The second peak of Knecht's observation and the second stage of increase in the current signal in the present observation can both be attributed to a thermionic process. A well-defined initial (photoelectric) peak was not observed in the present experiment because of the much larger electrode separation distance (1.2 cm.) compared to 0.1 cm. for Knecht's observation (transit time effect). The reason for the disappearance of the second peak and higher current of the initial current at 80° orientation of the target with the direction of the laser beam can easily be explained by the fact that, at this angle, the area of the irradiated surface was larger. Though the same magnitude of laser power was incident onto the surface for each orientation, the intensity (watts/cm^2) was less in the case of 80° orientation, thus the temperature rise will be less in this case than the temperature rise for the normal incidence. Most probably the Richardson effect was below the measurable limit for this case and caused the disappearance of the second peak. On the other hand, a larger area was activated for the same power, causing an emission of more photoelectrons. This may account for slightly higher values of amplitude of the photo-electric current pulse at this angle of incidence.

It was also observed that the slope of the second current pulse increased with the increasing laser intensity, as shown in Fig. 5.8. As the intensity is increased near the threshold value at which the boiling-off of the spot is

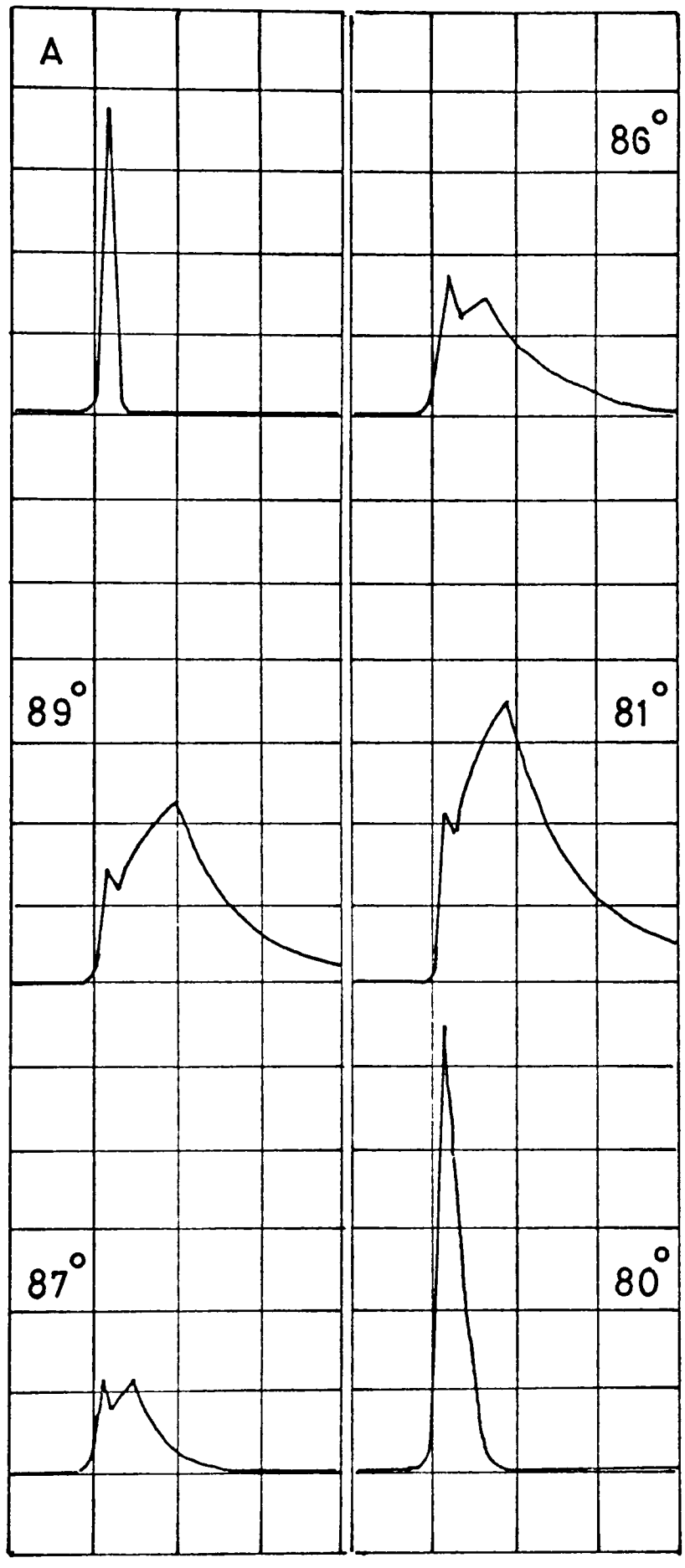

Amplitude scale for emission patterns is 4×10^{-4} amps/div.
Time scale is 100 nsec/div. Laser power = 74 KW.
Illuminated area $\sim 10^{-2}$ cm^2.

FIG. 5.9. ELECTRON EMISSION PATTERNS FOR SPECIFIED ANGLES OF INCIDENT LASER PULSE A (AFTER REF. 7).

likely to take place, the slopes of the initial (photo-electric pulse and the second pulse become comparable and a single pulse was observed. The result can be understood from the fact that as the intensity is increased the rate of temperature rise increases, consequently the threshold for thermionic emission is reached more rapidly. Thus the thermionic emission becomes comparable with the instantaneous photoemission as far as the relative emission time is concerned.

The thermionic concept mentioned above has also been successfully employed by Verber et al. (3, 42) to explain their results. Since a thermionic current is strongly dependent on the temperature of the emitter, a precise knowledge of the absolute value of the temperature is required to calculate the current. In the present case a ± 20% error in the absolute value of the calculated temperature was expected, so a meaningful prediction of the thermionic current for a particular intensity of the incident beam was not possible.

Finally, it can be suggested that with an appropriate time-resolved energy analyzer the photoelectrons and the normal thermoelectrons can possibly be distinguished and the states of the electrons can be known. It appears that for the accurate analysis of the interaction of low and moderate power laser beam with metal surfaces, much more sophisticated experimental techniques must be employed. It is further suggested that for the detection of photoeffects which involve more than two photons, highly pure metals must be used and the observation should be carried out at very low temperatures, apart from employing very sensitive detection systems.

CHAPTER SIX

I. INVESTIGATION OF THE LASER-PRODUCED PLASMA FROM METAL SURFACES

6.1 Introduction

The previous chapter was devoted to the investigation of the initial fast pulse of the laser-induced electron current signal at low laser intensity. Mention has, however, been made earlier of the major current peaks following the initial fast peak of lower amplitude when highly intense beams ($> 10^7$ MW/cm^2) were used. In Refs. 8 and 9 the occurrence of two peaks in the electron current signal has been mentioned. The broader peak, occurring two to three hundred nanoseconds after the laser peak, has been considered by the authors as due to thermionically-emitted electrons. In the present work the so-called laser-induced ion current has revealed two well-defined peaks separated by $\sim$ 1.6 μseconds (Fig. 6.1, a & b) in accordance with the results of the previously mentioned works. The initial peak occurred during the laser pulse and had lower amplitude than the following broader peak. The current signal was obtained by biasing the collector negative with respect to the target (accelerating the ions only). The initial peak could not be identified as due to ions, as it required ion energies of a few thousand electron volts, which is very unlikely. This has been considered to be due to a different process which will be discussed later in this chapter.

When a collector is biased positive with respect to the target so as to accelerate electrons from the laser produced plasma, the current signal obtained had three well-defined peaks as shown in Fig. 6.1, c & ad. The nature of

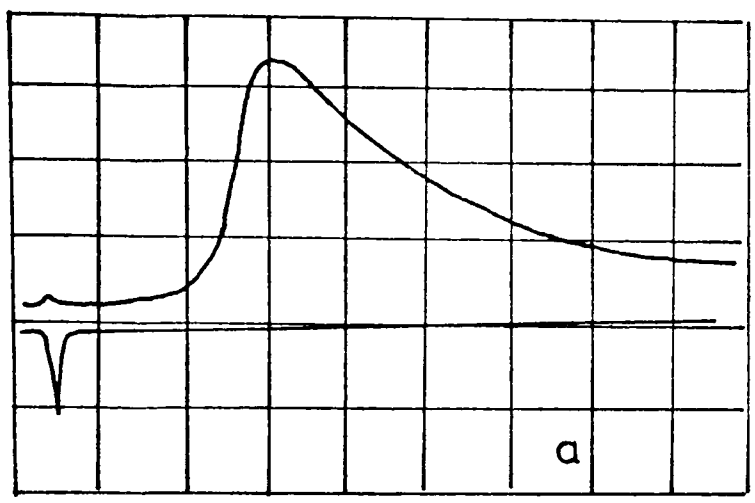

UPPER-Current signal-0.75 amps/cm.
LOWER-Laser signal
TIME SCALE-500 nsec/cm.

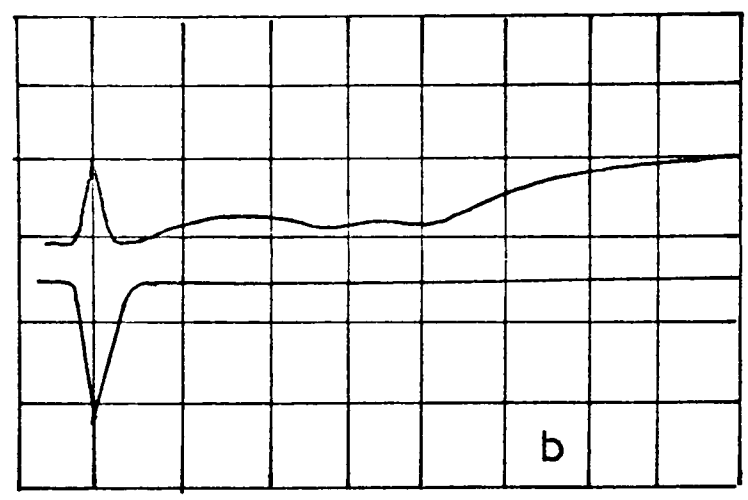

UPPER-Current signal-20 mA/cm
LOWER-Laser pulse
TIME SCALE-200 nsec/cm.

a & b - Current signals with the collector at a -ve voltage w.r.t. the target.

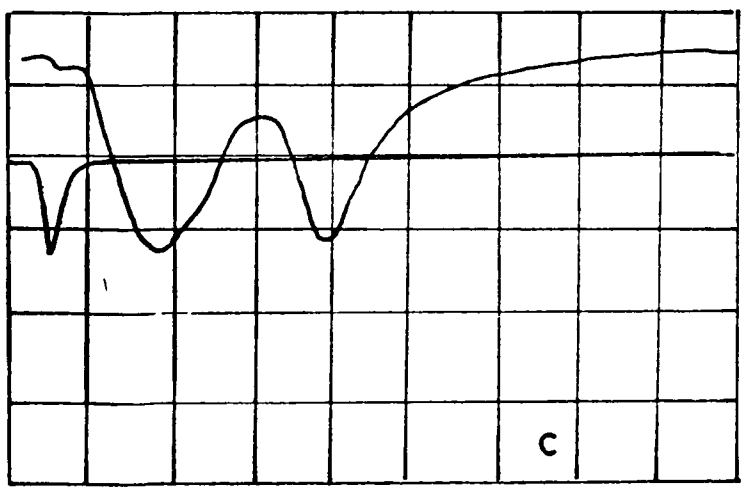

UPPER-Current signal-0.4 amps/cm
LOWER-Laser pulse
TIME SCALE-200 nsec/cm

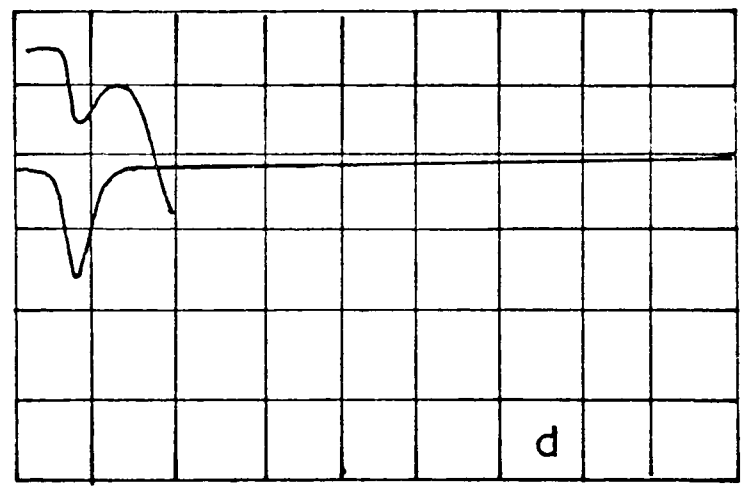

UPPER-Current signal-5 mA/cm
LOWER-Laser pulse
TIME SCALE-200 nsec/cm

c & d - Current signals with the collector at a +ve voltage w.r.t. the target.

FIG. 6.1. CURRENT SIGNALS AT DIFFERENT BIASING CONDITIONS.

the initial peak has been investigated in the previous chapter. In the present work it is considered that the major peak of Fig. 6.1 (ion acceleration towards the collector) and the two so-called thermionic peaks of Fig. 6.1c (electron acceleration towards the collector) are not produced by the motion of any single species of charges. When any current is detected from the laser-produced plasma, the conventional concept of electron current or ion current has to be modified. Because, in an applied field, current will be given by the combined motion of the two different species of charges in their preferred directions. It is expected that this concept will give an insight into the nature of origin of the peaks. It is also believed that without a proper concept of the mechanism of production of the current signals, any measurement of the parameters like electron or ion current, temperature, density, etc. will not be meaningful. In the present chapter, a brief qualitative account of the production of the plasma by the laser pulse is presented first. Later, a phenomenological model of the propagation of the plasma in an applied electric field and the generation of the current signal is given. A justification for the concept of a 'plasma' is also presented and the different parameters associated with it are estimated.

6.2 Production of the Plasma

It was mentioned in the previous chapter that a fraction of the energy of an incident bean of light on a metal surface is carried away by the photoelectrons. The quantum efficiency of such a process was found to be very small. Thus most of the energy absorbed by the surface electrons will be dissipated inside the metal. From the

spectroscopic studies of the light emitted from a metal when irradiated with an intense beam of laser, a very high temperature of the spot was predicted (9). Study of the laser-activated spot (Fig. 3.3) under a microscope showed a crater and burning of the spot. Calculation of the surface temperature presented in Chapter Three also indicated a very high temperature of the laser-irradiated spot.

Thus, assuming the validity of the equivalence between the laser flux and the flux of heat introduced in Chapter Three, a temperature of the laser-irradiated spot can be defined after the thermalization time (> 10 nsec.). The rate of increase of the temperature will depend on the rate at which the power is delivered to the surface. For a triangular-shaped laser pulse of $\sim$ 100 nsec. duration and peak intensity below 50 MW/cm^2, the boiling temperature of a metal (e.g. Ta boils at about 5.7×10^3 ^oK) will be attained at least 70 nsec. after the onset of the laser pulse. Whereas it can be seen (Fig. 3.2) for laser intensity above 10^2 MW/cm^2, such a temperature will be reached within $\sim$ 40 nanoseconds (assuming a 10 nsec. thermalization time). Thus, for very high intensity laser pulse, the initial temperature is expected to be very rapid and the metal will start evaporating and subsequently boil off within a few tens of nanoseconds.

The problem of how the laser light further interacts with the surface which had already reached the boiling point is very complicated. The ordinary heat transfer equation used earlier cannot be applied here as the constants of the material at such a high temperature become strongly dependent on the temperature. Moreover, the absorption process takes place in different phases (already augmented vapour cloud, densely

ionized solid and undisturbed solid underneath). In view of the complexity of the problem, only a brief outline of the interaction model proposed by other workers is presented here. Experimental results are then fitted to this model to obtain further information.

At this stage of laser-surface interaction three different phases are considered to exist simultaneously. Following the approach by Caruso and Gratton (43), the three phases are (Fig. 6.2):

Phase 0: The undisturbed solid (mass density ρ_o),

Phase 1: This phase consists of densely-ionized matter completely opaque to the laser light. Initially, when the evaporated material leaves the target surface, it recoils against the underlying surface, thus producing a high pressure pulse (6, and the ref. therein). According to Caruso and Gratton, this pressure pulse propagates as a shock wave along the thickness of the solid and produces this ionized phase.

Phase 2: This phase consists of the vaporized material which has been sublimated and proceeded away from the surface.

In this situation, the absorption of laser light by the dense phase will be strongly regulated by the vapour of phase 2. A self-regulating property of the continuously augmenting phase 2 has been introduced in ref. 2. Whatever be the absorption law of the laser light in phase 2, a part of it will always reach the surface of the dense phase 1. The fraction of the light absorbed by the vapour cloud will cause further ionization of the ions and neutral particles. However, as the pressure increases, the boiling point of the material rises above the normal value and the underlying

layer thus becomes superheated. Eventually as the temperature rises high enough, the heat of vaporization falls to zero. At this point the superheated solid becomes a condensed gas of ions, electrons and neutral particles. Because of the high pressure gradient the gas is ejected away from the solid. Ready's results (6) indicate that almost all the energy of the laser pulse is utilized to supplying the heat of vaporization. However, at the end of the laser pulse a plume of plasma emerges out of the surface.

Various papers have been published to elucidate a theoretical account of the laser-produced plasma and its expansion (35, 44, 45, 46). In some cases, experimental justification of the intuitive models have been tried. The most popular technique was to employ gas-dynamic equations to study the heating, vaporization and expansion of the substance due to the absorption of laser radiation. In the present work a theoretical account of the quasi-neutral property of the plasma is presented from a phenomenological point followed by an experimental justification of the concept of the 'plasma'. The experimental results were interpreted in terms of the ordinary concept of the dynamics of a cloud of charged particles in an applied field. The results were then compared with other works.

6.3 Characteristics of the Laser-Produced Plasma

Quasi-neutral property of the laser-produced plasma has been reported by many workers. In their final report on laser-surface interaction, Ready et al. (47) concluded that for a laser flux density of approximately 50 MW/cm^2, the blow-off material contains roughly equal numbers of electrons and

ions, along with neutral atoms and molecules. They also predicted that the initial plasma density is very high. When this high-density plasma starts moving away from the surface of the metal, it tends to expand because of the thermal motion of the charges. Also, it can be expected that because of the higher mobility, the electrons will start moving ahead of the cloud containing ions and neutral particles. In an elementary area inside the plasma, if there exists a departure from the condition $n_i \tilde{\nu} n_e$, an internal electric field will be developed. This internal microfield will depend on the density of the charged particles. The potential energy of the microfield W can be calculated from the following consideration.

Let n_e be the number of electrons per cm^3 in a singly-ionized plasma. The total particle density will be $2n_e(n_e \tilde{\nu} n_i)$. The average volume occupied by a single particle will be $\frac{1}{2}n_e$ cm^3, and the mean distance between the neighbouring particles will be of the order of $(\frac{1}{2}n_e)^{1/3}$ cm. The field at a point halfway between the particles, i.e. at a distance of $\frac{1}{2}(\frac{1}{2}n_e)^{1/3}$ cm from the electrons or ions can be taken as a measure of the intensity of the microfield. The potential energy of the mean electric field W will be given by

$$W = \ell/\gamma^2 \tilde{\nu} 6\ell n_e^{2/3} \qquad \ldots\ (6\text{-}1)$$

If the electronic charge e is expressed in e.s.u., it can be shown that for a plasma density of the order of 10^{20} to 10^{21} particles/cm^3, the potential energy of the microfield W will be greater than 10^4 ergs. This energy is much higher than the average thermal energy of the electrons in the plasma (typically $\sim 10^{-10}$ to 10^{-11} ergs.). Since in a plasma

each charged particle will experience the Coloumb field of the remaining particles, the potential field will prevent the escape of electrons from the ions from their neighbourhood.

Thus, when the charged-particle concentration in a sufficiently large volume is very high, any difference between n_e and n_i will give rise to the appearance of an electric field which may be sufficiently high to maintain the quasi-neutral property of the plasma as a whole. In the final analysis the extent of quasi-neutrality of the plasma will depend on the ratio of the potential energy of an individual ion or electron in the electric field produced as a result of the departure from the quasi-neutrality to the mean kinetic energy associated with its thermal motion. A detailed analysis of the relationship between W and the electron temperature T_e is very complicated. But it is generally considered that an ionized gas contained in a volume of radius γ_c (characteristic length of the density variation in the plasma) is quasi-neutral if (48):

$$\gamma_c >> \gamma_D \tilde{\sim} 7\sqrt{\frac{T_e}{n}} \qquad \ldots\ (6\text{-}2)$$

where γ_D = the Debye radius

and n = the no. of charged particles per unit volume.

Thus at a given charged-particle concentration the potential due to these particles and therefore the potential energy of an individual particle, will depend on the size of the region occupied by the plasma.

From the results of Ready's experiments (6), for a laser flux density of $\sim 10^9$ W/cm^2, focussed onto an area of

$\sim 10^{-3}$ cm^2, the volume of material ionized from a metal like stainless steel was estimated to be $\sim 2 \times 10^{-9}$ cm^3. At the initial stage of expansion, a particle density in the plasma of the order of 10^{20} per cm^3 can be expected. Assuming the boundary of the heated zone as the dimension of the region occupied by the plasma and considering a typical value of the electron temperature of the plasma (at the initial stage of expansion) $T_e \tilde{\sim} 10^5$ ^oK (35, 44), a value of the Debye radius $\gamma_D \tilde{\sim} 2 \times 10^{-6}$ can be obtained, whereas the characteristic radius of the region occupied by the plasma, $\gamma_c \leq 10^{-3}$ cm. Thus it can be concluded that the condition of quasi-neutrality of the plasma stated by the inequality equation (5-2) will be valid at the initial stage of the expansion of the laser-produced plasma. Now, as the plasma expands, the characteristic radius γ_c increases with time. The total plasma energy goes into radial expansion kinetic energy, consequently the electron temperature T_e decreases with time. Since the particle density n will also decrease as a result of the expansion, the temperature and the density are expected to decrease with time by the same ratio. Thus maintaining the Debye radius more or less constant with time, whereas the radius γ_c increases with time. It can thus be inferred that the laser-produced 'plasma drop' will expand in the vacuum region set for the experimental investigation as a quasi-neutral cloud of ionized gas.

The motion of such a 'plasma drop' as a whole will not give rise to any electric current. In the laser-produced plasma there may exist a high concentration of neutral atoms and molecules. If the distribution of these atoms and molecules is not uniform a pressure gradient will be developed

and a diffusion of electrons and ions will take place through the neutral components. Since the plasma is quasi-neutral, the rate of diffusion will be the same for both electrons and ions. But since the electrons have a greater mobility, they will leave the ions behind, giving rise to an internal electric field which will decelerate them very rapidly while slightly accelerating the heavy ions. As a result the velocities tend to become equal and the current due to such diffusion (ambipolar diffusion) will be negligibly small.

The diffusion process described above is a result of the collisions of electrons and ions with the neutral atoms. In a collision-dominated plasma, the external electric field will have very little effect on the motion of individual charges. Usually, the total velocity acquired by an electron or ion in one free path is quite small compared to the thermal velocity. Also the energy gained by the field will be repeatedly lost by collision process. Thus the influence of the external field on the motion of the charges in the plasma can be neglected. A current will appear only if the charges have a directed motion.

6.4 Experiment to Investigate the Quasi-Neutral Property of the Plasma

If the laser-produced plasma is neutral as a whole, the applied electric field will have very little effect on the motion of the plasma drop. Near a biased electric conductor, however, the constituent-charged particles of the plasma will be influenced and the collection of charges will give rise to current signals. Before the charges separate near the surface of a collector, the motion of the cloud of

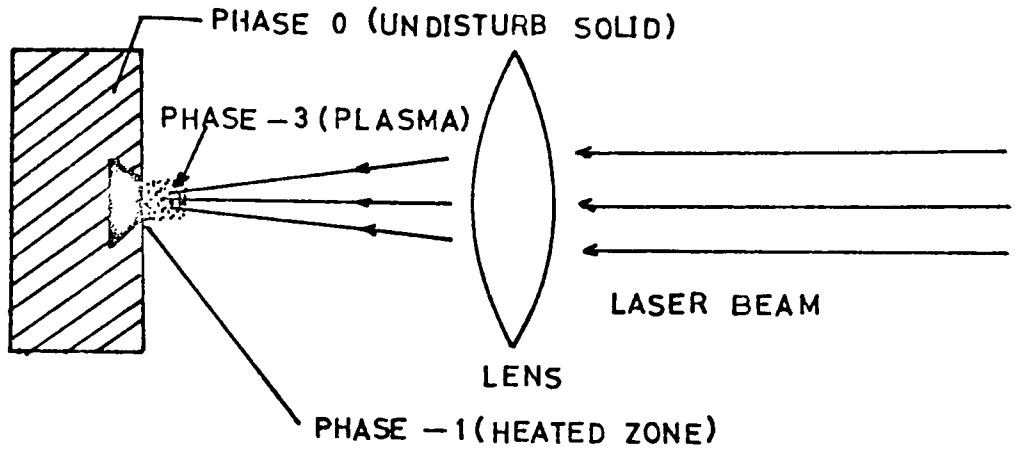

FIG. 6.2. DIFFERENT PHASES IN A METAL IRRADIATED WITH A LASER BEAM.

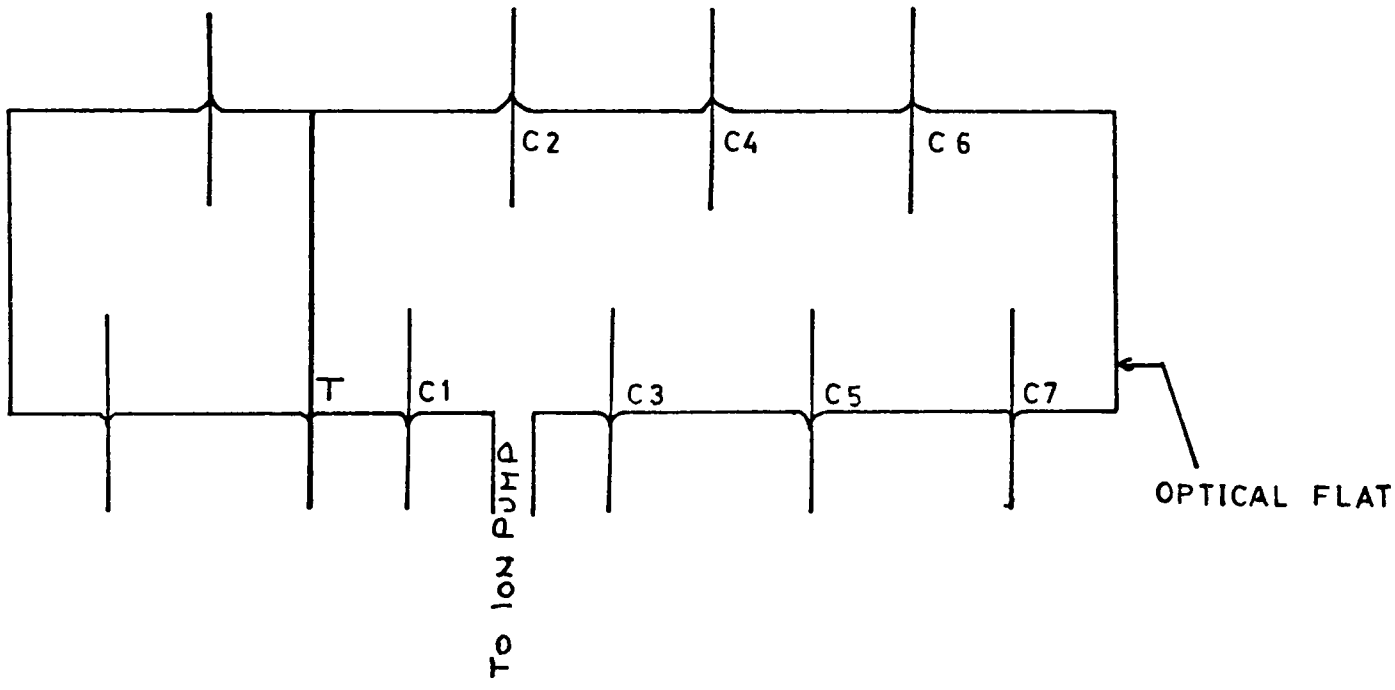

FIG. 6.3. SCHEMATIC DIAGRAM OF THE EXPERIMENTAL TUBE TO COLLECT CURRENT AT DIFFERENT DISTANCES.

particles will not constitute any net current if the cloud can be considered to be in a quasi-neutral state. To verify this, an experimental tube was designed to collect charges from the plasma at different distances away from the target. A schematic diagram of the tube is shown in Fig. 6.3.

The tube contained a tantalum target in the form of a disc of diameter 3.5 cm. Seven tungsten pins were used as collectors at different distances from the target. The pins were inserted through the wall of the glass envelope in such a way that all the pins were directly exposed to the target surface without being overshadowed by the others. The glass envelope had a diameter of 4 cm and the inside ends of the pins left a clearance of diameter 2 cm for irradiating the laser beam onto the target. A photograph of the cross-sectional view of the tube is shown in Fig. 6.4. Some collector pins were also introduced at the rear side of the target to investigate any possible 'rear-side' effect which will be discussed in the next chapter. Current signals were monitored at different collectors across a 50Ω resistor and with a positive bias at the collector. Some typical current signals detected at different distances from the target are shown in Fig. 6.5. The following observations were made from the experimental data:

i) The delay between the laser peak and the second current peak increased with the increasing target-collector separation length, whereas the initial kink remained co-incident with the laser peak.

ii) The applied field had negligible effect on the delay between the laser peak and the second current peak

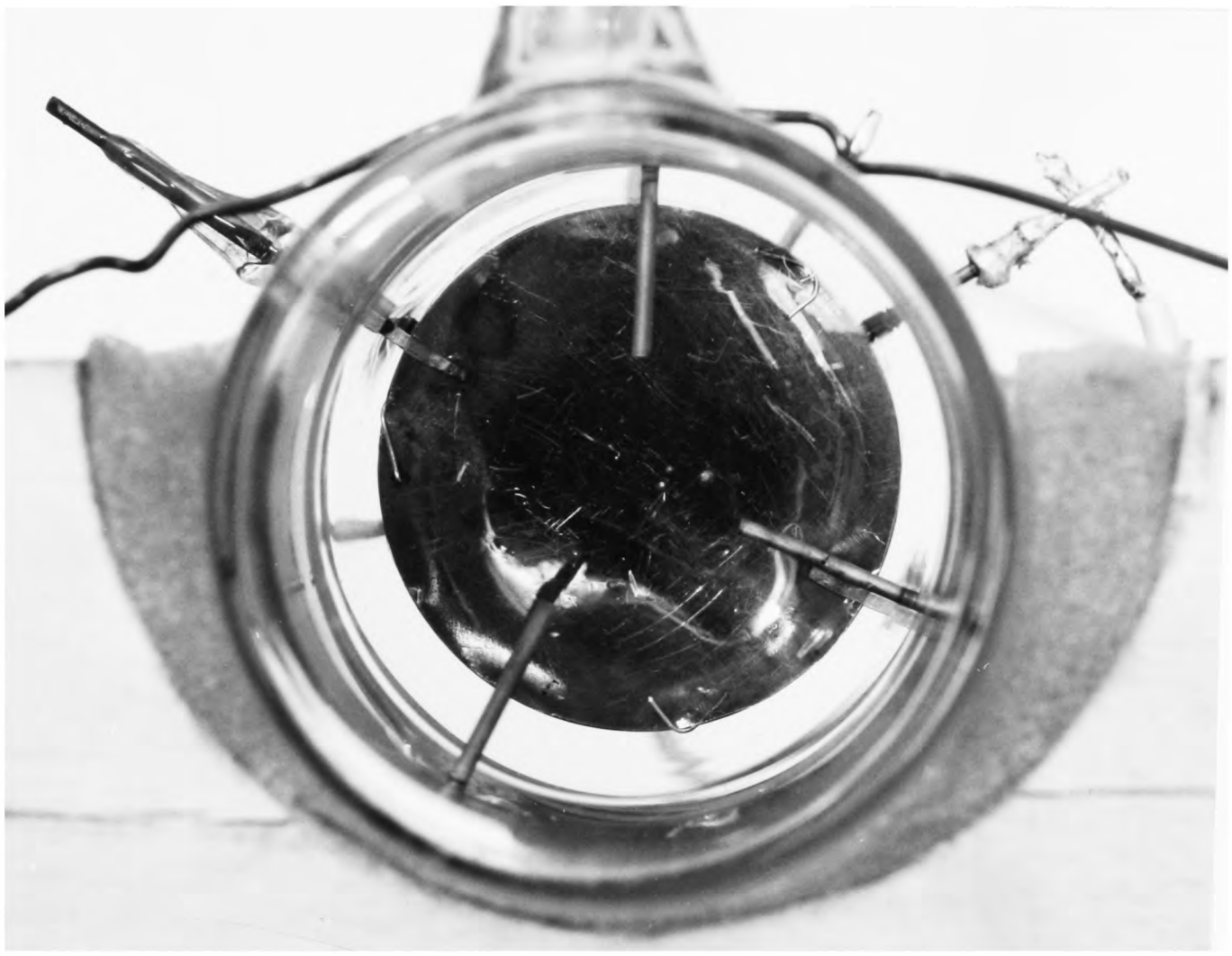

FIG. 6.4. CROSS-SECTIONAL VIEW OF THE EXPERIMENTAL TUBE.

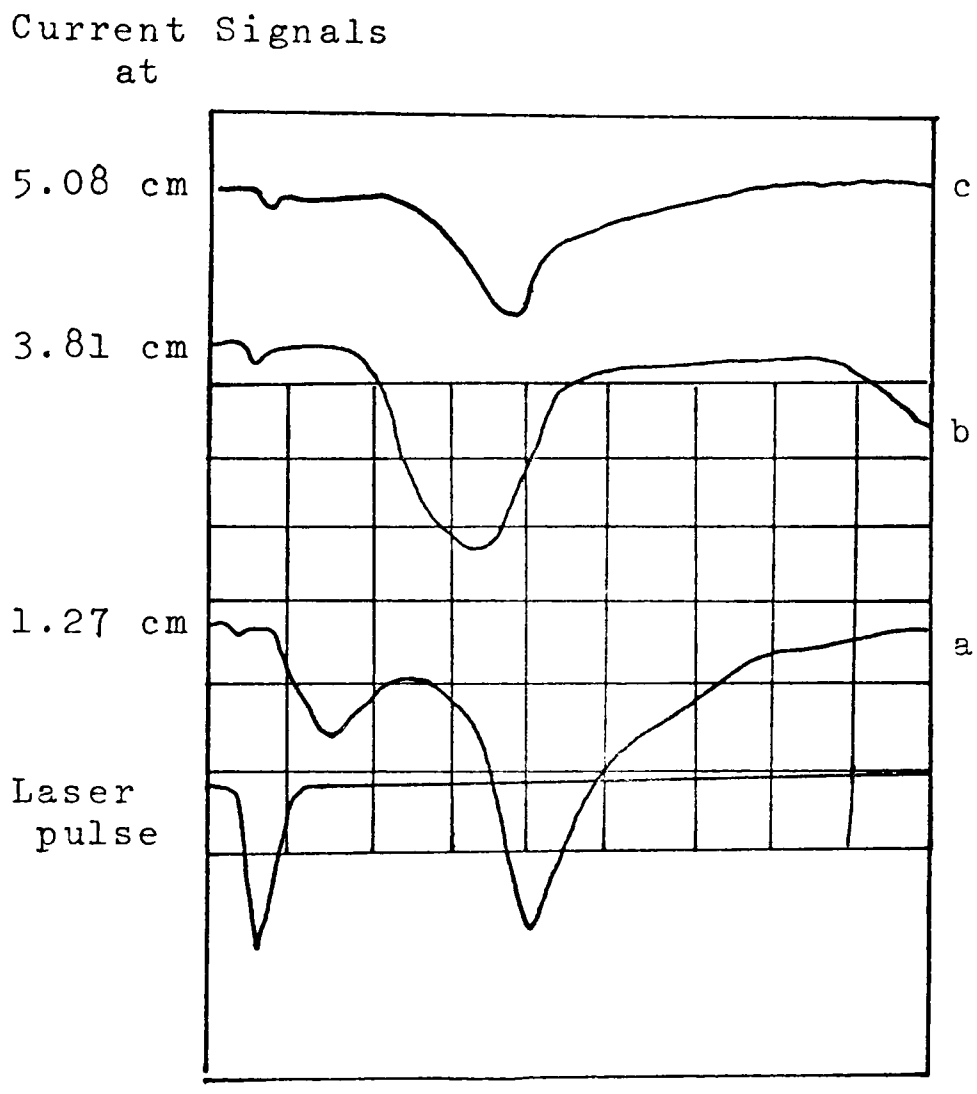

Current scale - a) 0.2 amps/cm; b) 0.04 amps/cm.
c) 0.02 amps/cm.

Time Scale - 200 nsec/cm.

FIG. 6.5. CURRENT SIGNAL AT DIFFERENT DIATANCES FROM THE TARGET.

though the amplitudes of the peaks were dependent on the applied field and the electrode separation length.

The second observation suggested that the plume of material reached the collector surface in a 'plasma' state and the signal appeared when the electrons were rapidly collected from the outer edge of the 'plasma drop' while at close proximity with the collector surface. If it is assumed that the plasma was produced immediately after the initial peak and started to move away at the same time then the delay between the trailing edge of the initial peak and the leading edge of the second peak will correspond to the time of flight of the plasma. Measurement of time of flight from the oscilloscope traces will not be accurate as the edges were not sharply defined. Since the initial peak was always coincident with the laser peak irrespective of the target-collector separation distance and the rise time of the second peak is expected to be the same for signals collected at different collectors and with a similar biasing condition, the delay between the initial peak and the second peak can be taken as the relative time of flight. The relative time of flight for different target-collector separation length was measured and plotted against the separation distance. The plot, as shown in Fig. 6.6, fitted a straight line. This indicated a linear motion of the plasma and also suggested that the concept of the motion of the cloud of material in a 'plasma' state, before a biased collector is encountered, is a valid concept. Whatever be the actual magnitude of the time of flight of the plasma from the target to the collector, from the slope of the straight line of Fig. 6.6 an accurate value of the absolute velocity of the

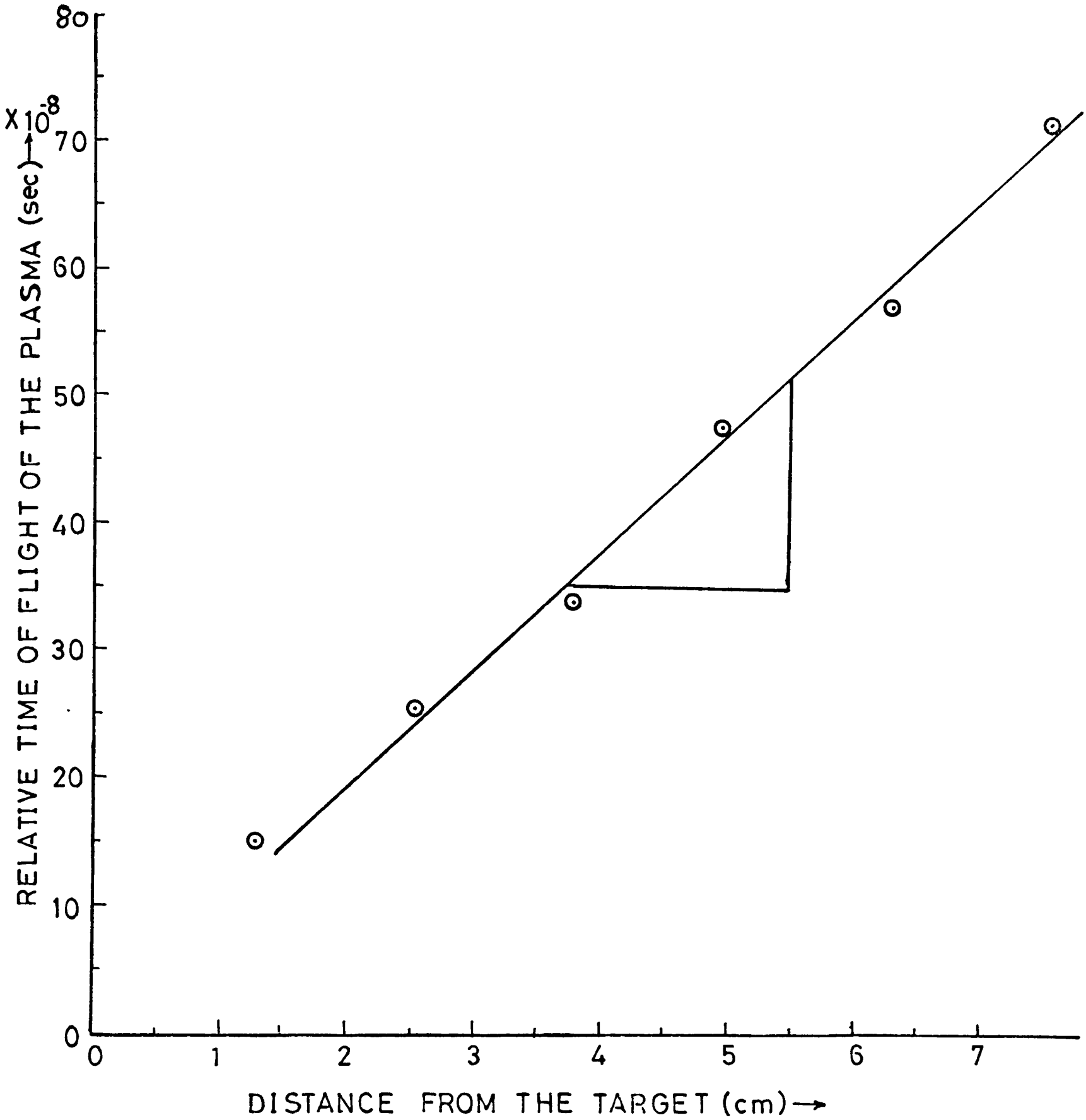

FIG. 6.6. DISTANCE VERSUS TIME OF FLIGHT.

'plasma drop' can be obtained. The observed velocity was 3.1×10^7 cm/sec. This is in good agreement with the predicted value of 2.2×10^7 cm/sec. for the velocity of the plasma boundary by Fader (35) with a hydrodynamic model of a spherical plasma.

The results strongly suggest that the laser-produced blow-off material maintains a quasi-neutral property and a directed motion of the charges takes place only near a biased collector.

II. DIAGNOSIS OF THE PLASMA AND INVESTIGATION OF THE MULTIPLE PEAKS

6.5 Introduction

It has been mentioned earlier that the current signals obtained by focussing laser light onto metal targets consists of different peaks. The shape and the amplitude of the different peaks depend on various parameters like laser power, applied voltage, target-collector separation distance, etc. However, before any attempt to investigate the state of charged particles in the plasma from the observed current signal, the essential requirement will be to specify the nature of the origin of the different peaks. A phenomenological model of the production of two different current peaks due to the motion of charges from the plasma after being influenced by the applied field is presented below. Two different conditions for the production of current signal are being considered here.

a) When the collector is biased positive with respect to the target the electrons will be collected and the ions will be repelled. The situation, however, is not as simple as it appears. In the plasma region there exists an internal potential field. Since the electrons are more mobile they will

move ahead of the ion cloud, but will always experience the long range attractive potential of the ion cloud. For an idealized case of a singly-ionized plasma, the internal field will be given by Eqn. 6.1, as stated before.

At low applied field only electrons with high temperature will be collected by a collector. To draw a maximum current from the plasma the applied field should be higher than the plasma potential near the boundary of the collector. The electrons are usually collected at a potential at the collector roughly equal to or greater than the plasma potential (commonly called space potential). The space potential can be estimated from the I-V characteristic of the plasma. At this potential of the probe with respect to the target, the bulk of the plasma is at the same potential as the probe and the electrons will be collected only with their thermal energy. Collection of such electrons will give rise to an electron collection signal. During the time of the collection of the electrons, the ions will be accelerated in the opposite direction and will be collected by the target itself. The motion of the ions in the reverse direction will constitute the third peak in observed current signal. If it is assumed that in the plasma $n_i = n_e$ and the ions are singly charged, then the current corresponding to the two peaks will depend upon the velocity acquired by them. At an applied electric field of 120 volts, the tantalum ions will acquire a velocity of $\sim 10^6$ cm/sec, whereas the typical thermal velocity of the electrons are some two orders of magnitude higher than this. Thus it appears, in an idealized situation, the current constituted by the reverse motion of the ions (third peak) will be considerably less than the

electron current caused by the collection of electrons. When the target-collector separation distance is long and the applied field is not very high, the process of the complete collection of the electrons will be over, long before the ions are retarded and accelerated back to the target. For a shorter separation distance, the ions will start constituting a current signal before the electrons are completely collected away. In this case, the observed ion signal (third peak) will be a result of the combined current produced by the electrons of the decaying edge of the second peak and the ions. The amplitude of the two peaks will depend on the reaction time of the applied field on the ions and the amplitude of the current signals if obtained independently. This will be discussed later in this chapter.

b) When the collector is biased negative with respect to the target, the situation of the dynamics of the charges are reversed. Electrons experience a repulsive force and are retarded to zero velocity before being accelerated back towards the target. At the same time the ions are collected by the collector. At larger electrode separation distance, the collection of ions and the rapid acceleration of the electrons towards the target will be a comparable process in time. The current signal obtained will be given by the combined motion of the electrons and ions shown in Fig. 6.1a. If, however, the two processes are not synchronized in time the two peaks may be observable.

6.6 Experiments

To verify the phenomenological model described above

the following experimental observations were made. The experimental tube of Fig. 6.3 was employed to detect the current signals at different distances away from the target. The current was recorded with a positive bias at the collector. The tube was in high vacuum. Several readings (laser bursts) were taken for the current signal observed at a particular position and the mean value was taken into consideration. The following results were obtained from the observations:

a) For target-collector separation distance greater than 1.3 cm, three well-defined peaks in the current signal were observed. For the same laser intensity and the applied voltage the recorded current signals at different collectors are shown in Fig. 6.7. It can be seen that at short distance ($\sim$ 1.3 cm) the current corresponding to the second peak dropped approximately 30% of its peak value before the third peak started to appear. At larger distance the peak current of the electron collection signal (second peak) dropped down to the initial value (zero) and there was a considerable delay before the occurrence of the third peak. If it is assumed that the model described earlier is the actual mechanism of the creation of such peaks, it must be concluded that the observed current produced by the motion of the ions in the opposite direction (third peak in Fig. 1.6c) has an amplitude which is comparable in magnitude to the second peak. The result is in contradiction to the proposed model.

b) The amplitude of the pulses corresponding to the second and third peaks were plotted against the target collector separation distance, d. The experiment was done with a laser beam of peak power of $\sim$ 166 KW and focussed onto an

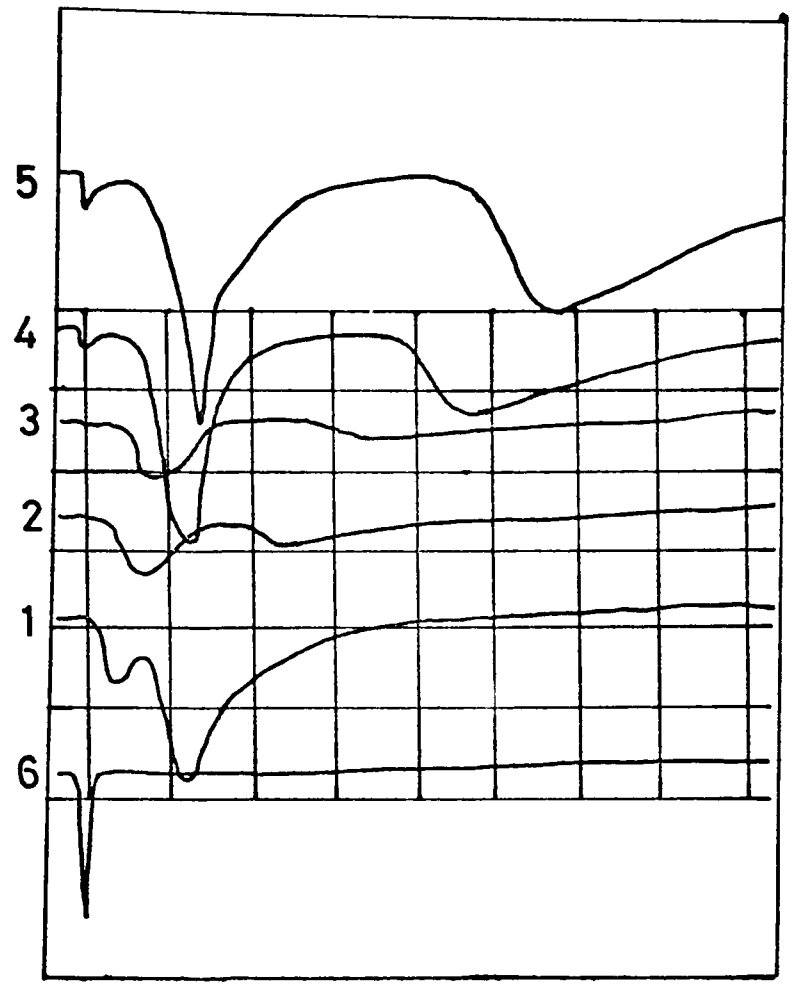

FIG. 6.7.

CURRENT SIGNALS RECORDED AT DIFFERENT DISTANCES

	Distance from the Target cm.	Scale amps/cm.		Distance from the Target cm.	Scale amps/cm.
1	1.27	0.45	4	5.08	0.021
2	2.54	0.210	5	6.35	0.012
3	3.81	0.117	6	Laser pulse	1 V/cm

Bias Voltage = 110 v.

Time Scale = 500 nsec/cm.

estimated area of $\sim 10^{-3}$ cm^2. Throughout the experiment the collectors were maintained at a positive potential of 120 volts with respect to the target. The results are shown in the graph of Fig. 6.8. The results clearly indicate two different processes of the generation of the current signals. The third peak shows an inverse-square law dependence with the distance which is a characteristic of the current flow by a single species of particles (49). Since the second peak is considered to be due to electron collection from the collector, the current will decrease with distance as a result of the loss of electron-thermal energy due to the expansion of the plasma and also probably due to the loss of electrons by recombination process. An exact nature of the variation of the electron current produced from such a transient plasma with the distance of electron collection could not be predicted because of the lack of available theory.

6.7 Discussion of the Results

The experimental results of the previous section can qualitatively be explained by the proposed model of the generation of the current pulses from the laser-produced plasma. But the magnitude of the third peak which has been considered to be due to the reverse motion of the ions appears to be too large to fit the intuitive model, if n_i was taken roughly equal to n_e. A plausible answer to the observed high ion current can be obtained if the contribution of the secondary ions are taken into consideration. The possibility of secondary emission by the high energy primary ions from the collector surface has been reported (47) to be of considerable importance. Such a possibility of

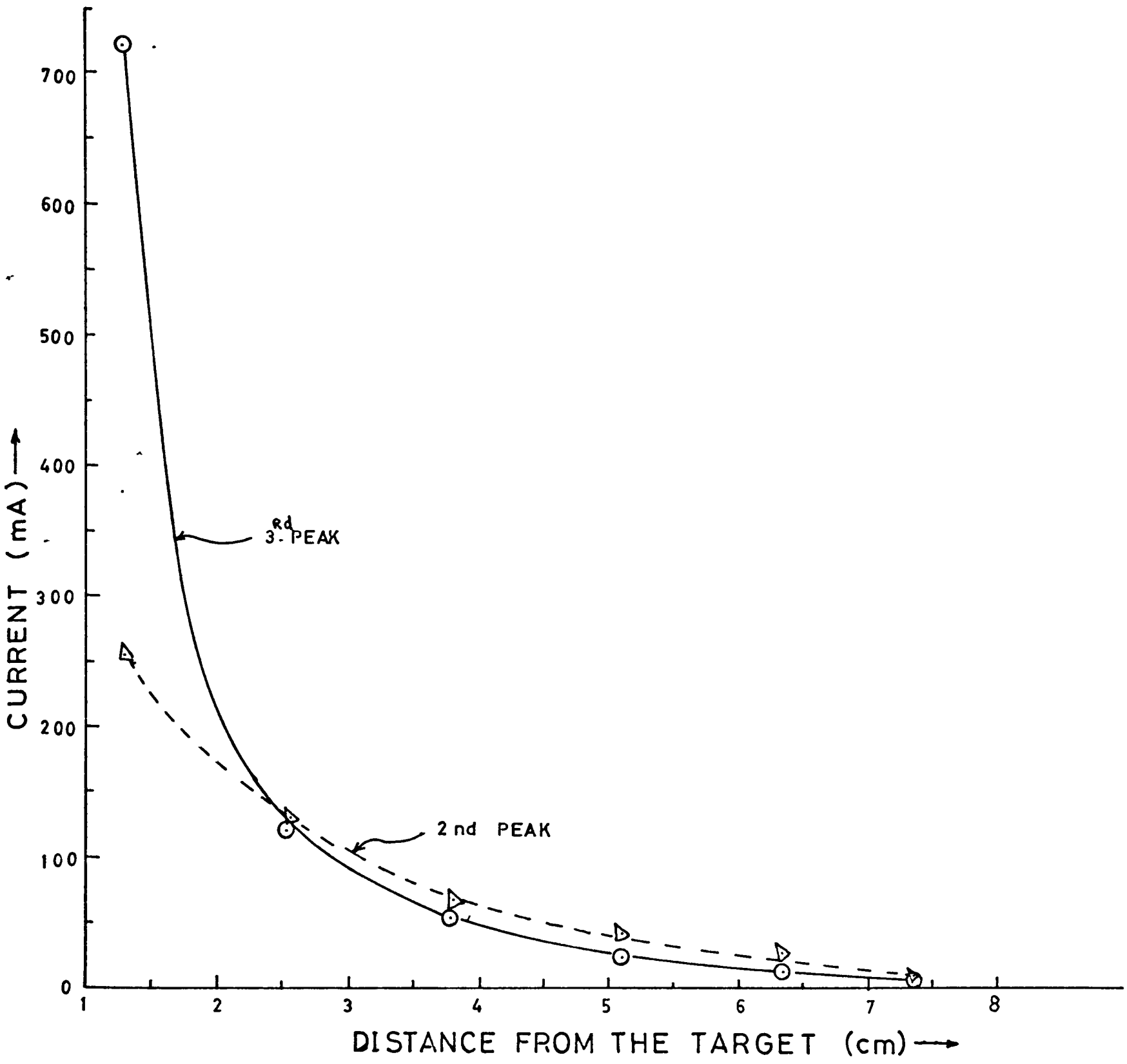

FIG. 6.8. CURRENT VERSUS DISTANCE.

secondary emission by high energy ions in the expanding plasma has also been suggested by Haught et al. (44). The radiation from the laser-produced metal plasma can also produce significant amounts of electron current from the collector (discussed later in this chapter). Though a secondary ion emission coefficient is more than an order of magnitude lower than that for electrons, a considerable contribution to the ion current can be expected by the secondary ions.

Thus, considering the ion current to be comparable to the electron current, a phenomenological picture has been drawn (Fig. 6.9) to illustrate the mechanism of the production of different current peaks at different biasing conditions. This is, however, a general picture, the actual shape of the signals will depend on other experimental conditions. The reason for the sharp increase of the third peak with decreasing distance can easily be understood from this picture. At target-collector separation distance less than approximately 2 cm, for the present experimental conditions, the second peak is expected to be smoothly added up with the third peak and a single pulse will be observed. This is because the ions are much more rapidly accelerated so that the current due to electron collection and the ion collection by the target peak more or less at the same time. With a different tube, current signal obtained at 0.2 cm away from the target has a single peak, as shown in Fig. 6.10.

The third peak can be further identified as due to the motion and collection of ions from their time of flight. Assuming that the delay between the second peak and the third

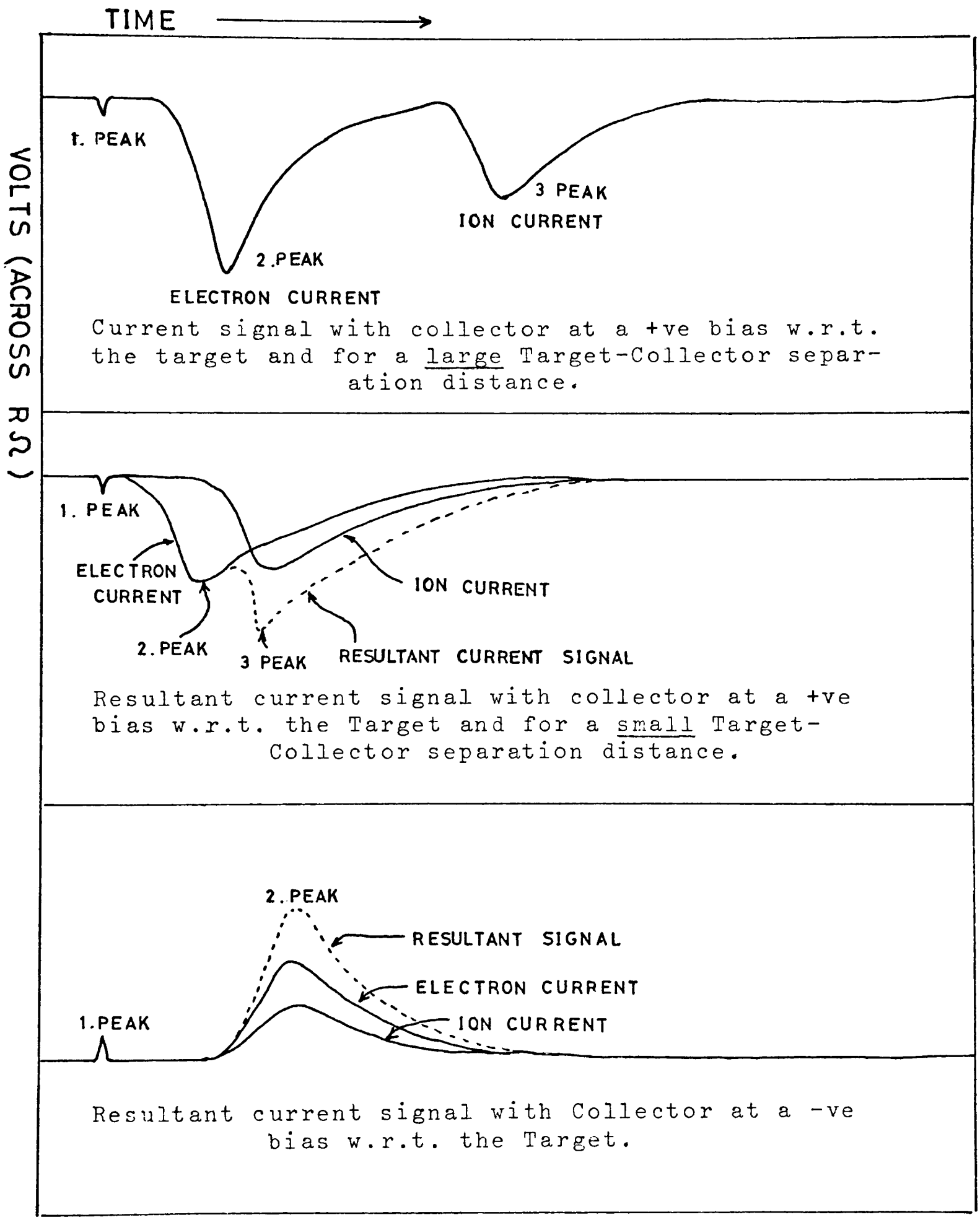

FIG. 6.9. A MODEL OF THE GENERATION OF THE CURRENT SIGNALS.

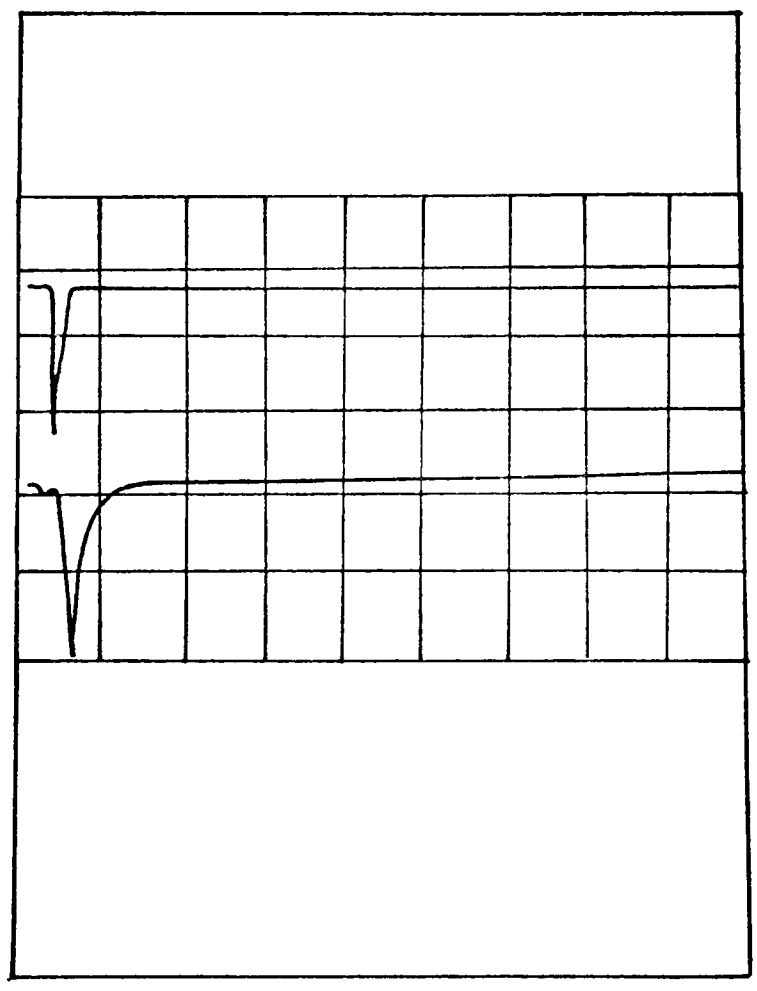

UPPER TRACE - Laser pulse
LOWER TRACE - Current pulse - 2 amps/cm
TIME SCALE - 1000 nsec/cm
TARGET-COLLECTOR SEPARATION = 0.3 cm

FIG. 6.10. CURRENT SIGNAL AT A CLOSE DISTANCE FROM THE TARGET.

peak is the relative time the ions take to reach the target being accelerated from the zero initial velocity from near the collector, the time of flight can be plotted against the distance. The graph is shown in Fig. 6.11. The points fit a straight line. From this straight line the peak ion velocity attained was estimated to be $\sim 3.4 \times 10^6$ cm/sec. If a Ta ion of mass $\sim 1.2 \times 10^{-22}$ gm with zero initial velocity is accelerated with a potential of 120 volts, the maximum velocity acquired will be $\sim 1.8 \times 10^6$ cm/sec. The agreement between the observed value of the ion velocity and the calculated value is considered to be excellent. This puts more weight to the idea that the third peak is originated from the reverse motion of the ions.

Since the second peak has been identified as due to the diffusion of electrons to the positively-biased collector, an estimate of the electron temperature can be made from the current-voltage characteristics of this peak. The experiment was done with a tube having a tantalum target and a circular disc collector held at a distance of 2.54 cm. The intensity of the laser beam was estimated to be $\sim 1.5 \times 10^8$ watt/cm^2. The amplitudes of the second peak were plotted against the various values of the applied voltage in a semi-log graph. The curve obtained is shown in Fig. 6.12. It can be observed that the current increases linearly from a retarded potential of $\sim$ 9 volts (V_R = -9 volts) to an accelerating potential of $\sim$ 25 volts. Above 40 volts the current has been found to saturate. The form of the curve is typical of a Langmuir probe characteristic.

To calculate the temperature from the above results, the particles in the plasma must be considered in thermo-

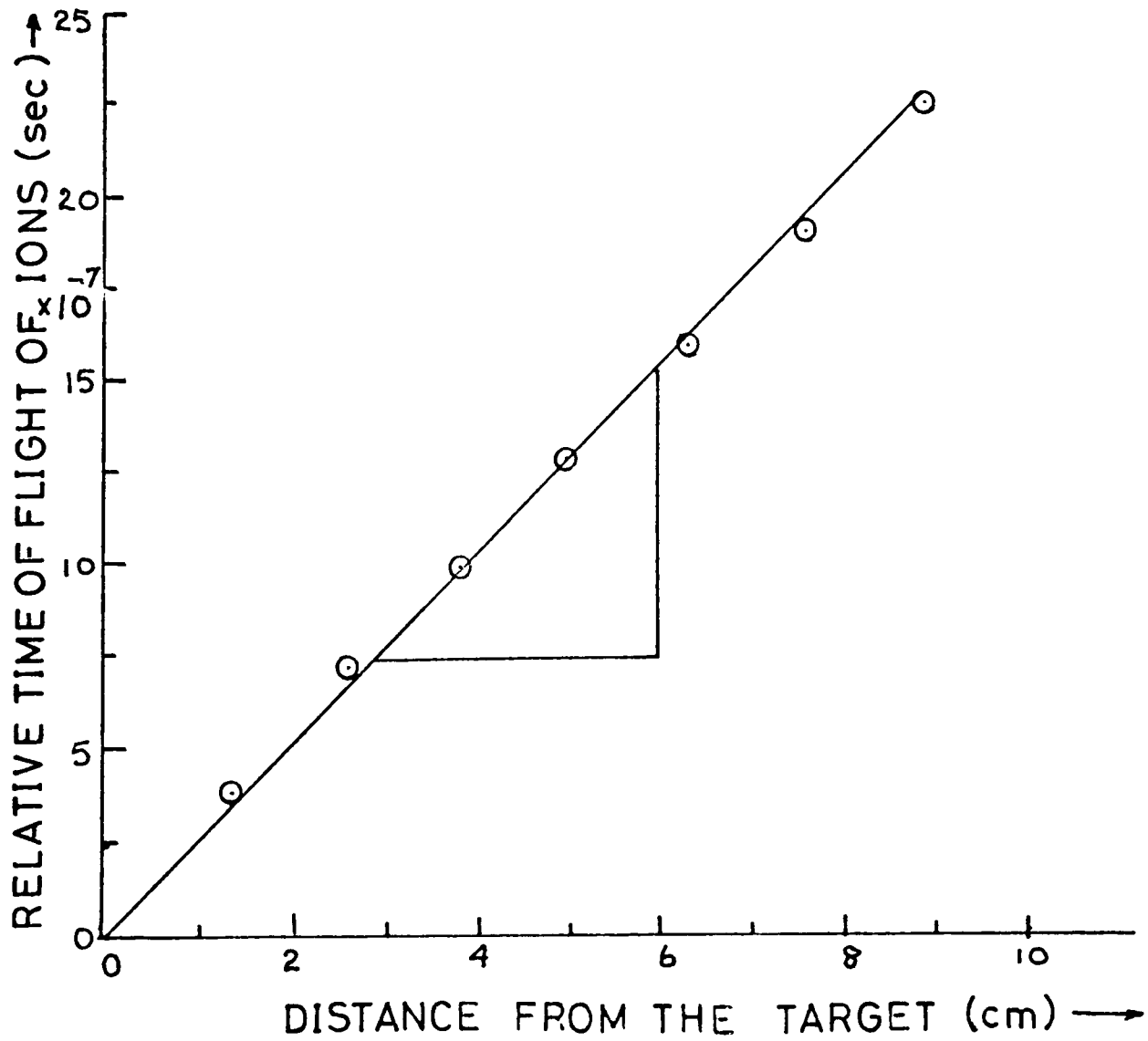

FIG. 6.11. DISTANCE VERSUS ION-TIME OF FLIGHT.

dynamic equilibrium. For such particles the energy distribution will be Maxwellian and the electron current at the surface of the probe will be given by,

$$i_e = i_o \exp\left(-\frac{eV_s}{kT_e}\right) \qquad \ldots\ (6\text{-}3)$$

where i_o = saturation electron current,

k = Boltzman Constant,

T_e = electron temperature,

and V_s is the potential of the probe negative with respect to the bulk of the plasma. If the plasma potential is denoted by V_P (the potential of the probe with respect to the target at which the current saturates) and the applied potential by V, then the current in terms of the applied probe potential, given by Eqn. 6-3, will be:

$$\ln i_e = \ln i_o - \frac{eV_P}{kT_e} + \frac{eV}{kT_e}$$

$$= \text{const.} + \frac{eV}{kT_e} \qquad \ldots\ (6\text{-}4)$$

Thus, from the straight line of $\ln i_e$ vs. V plot (Fig. 6.12), the slope was found and the electron temperature T_e was calculated from Eqn. 6-4. The electron temperature estimated by this method was $\sim 0.7 \times 10^5$ °K. In Ref. 35 the temperature of a LiH particle when irradiated by high power laser pulse has been calculated from the hydrodynamical model of the expansion of the plasma. Maximum temperature of the order of 10^5 °K has been predicted from such a calculation.

Temperature calculated by Richards (9) for a metal plasma from the I-V characteristic was $\sim 1.5 \times 10^5$ °K. The value is slightly higher than the temperature calculated here. The anomaly can be attributed to the fact that in the

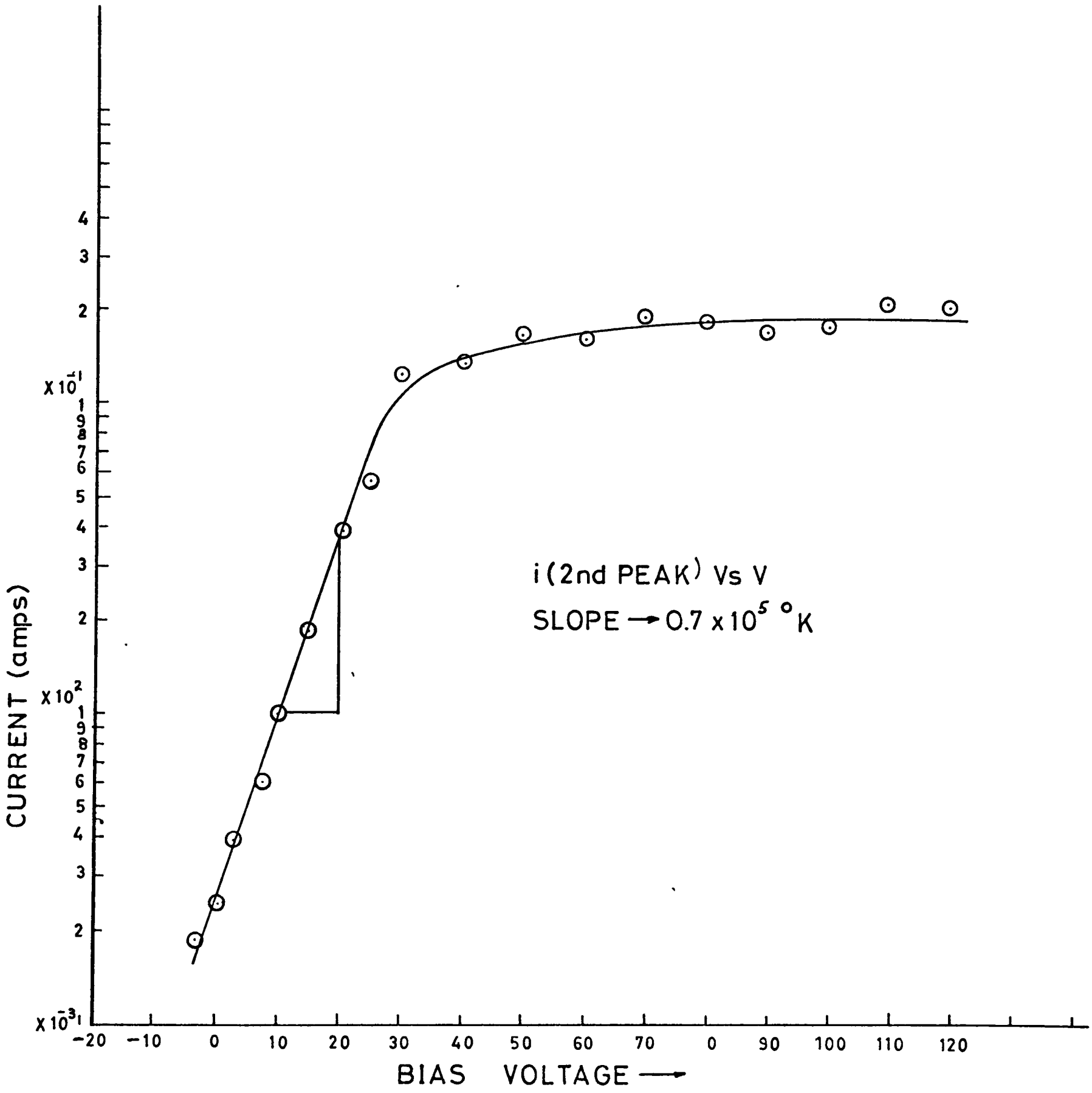

FIG. 6.12. I-V PLOT FOR THE ELECTRON CURRENT (2nd PEAK).

experiment of Ref. 9 the target-collector separation length was only 3 mm, so that the contribution of the ion current due to their reverse motion was not eliminated.

For the calculation of the temperature by the above method the following conditions must be satisfied:

a) The hotter component of the plasma (usually electrons) should be collected, so that the distribution at the sheath edge is approximately Maxwellian.

b) The pressure inside the tube should be low enough so that the mean free path is much larger than the probe or sheath dimensions.

c) The perturbation of the plasma produced by the presence of the probe should be negligible.

The conditions are roughly applicable to the present investigation and the method of temperature calculation is expected to be valid.

It must be considered that original Langmuir probe theory was developed for a steady plasma where the probe current was small compared to the conduction current through the plasma. In such a transient plasma, the concept of temperature will be of little significance if the bulk of the plasma has a directional velocity comparable to the thermal velocity of the electrons. From observed results the directional velocity of the plasma was found to be $\sim 3 \times 10^7$ cm/sec, whereas for an electron temperature of $\sim 10^5$ ^oK the thermal velocity is found to be roughly an order of magnitude higher than the plasma jet velocity. Thus it is thought the estimation of temperature of the electrons in the laser-produced plasma give a valid information of the state of the electrons.

III. SECONDARY ELECTRON EMISSION

6.8 Introduction

It has been mentioned earlier that when the collector is biased negative with respect to the target to draw the ions from the plasma, the current signal shows a fast initial peak appearing during the laser pulse (Fig. 6.1b) and has an amplitude of several tens of miliampheres. For ions to constitute such a current signal, they would require energies of a few thousand electron volts, which is very unlikely. A possible process for the appearance of such a current peak could be a secondary electron emission from the collector and possibly the surrounding glass envelope. Such electrons will be accelerated towards the target and give rise to an ion-collection signal at the collector side. There are two possible mechanisms of such emission, e.g. (a) the emission of electrons by the interaction of the fast moving primary particles with the collector and the glass surrounding, and (b) the photoelectric emission of electrons from the collector and the glass wall by the high energy photons produced by the plasma.

Ready et al. (47) has reported that secondary electron emission from collector surfaces bombarded by the incident heavy particles is important in producing the observed signals. In that case the current signal would appear a few microseconds after the laser pulse. The only possibility of the process (a) to account for the initial peak in the so-called ion collection current is the bombardment of the collector by the initial electrons pertaining to the fast initial peak of the electron collector signal.

The possibility of such a process giving rise to current of such high magnitude is quite remote, because even the high energy electrons will lose most of their energy in traversing against the retarded field. The only other possible process is the photoelectric emission (b). An experimental tube was designed to investigate this phenomenon.

6.9 Experiments

The target was a tantalum disc spot welded to one end of an aluminium cylinder of 2.5 cm diameter and 5 cm length. The other end of the cylinder was tightly covered with a quartz window. A tantalum sheet was held in front of the quartz window so that the metal was partially exposed to the radiation emitted from the laser irradiated spot. Since quartz has low absorption coefficient at higher frequencies, most of the light emanating radially from the target will be transmitted out. Another tantalum sheet was held parallel to the previous one, so that it was not exposed to any light emerging from the target. A schematic diagram of the whole arrangement is shown in Fig. 6.13. The two tantalum sheets formed the electrodes of a vacuum diode and the target covered with the window was the source of radiation. Laser light of peak power $\sim$ 400 KW was focussed onto the target slightly obliquely. The focussed area was estimated to be of the order of magnitude of 10^{-3} cm^2. At such power density a visual damage to the target was expected and the light from the spot was observeable. The electrode c_1 (exposed to the laser-induced light) was biased negative w.r. to the collector c_2. The current was recorded across a 100Ω resistor. For the sake of comparison

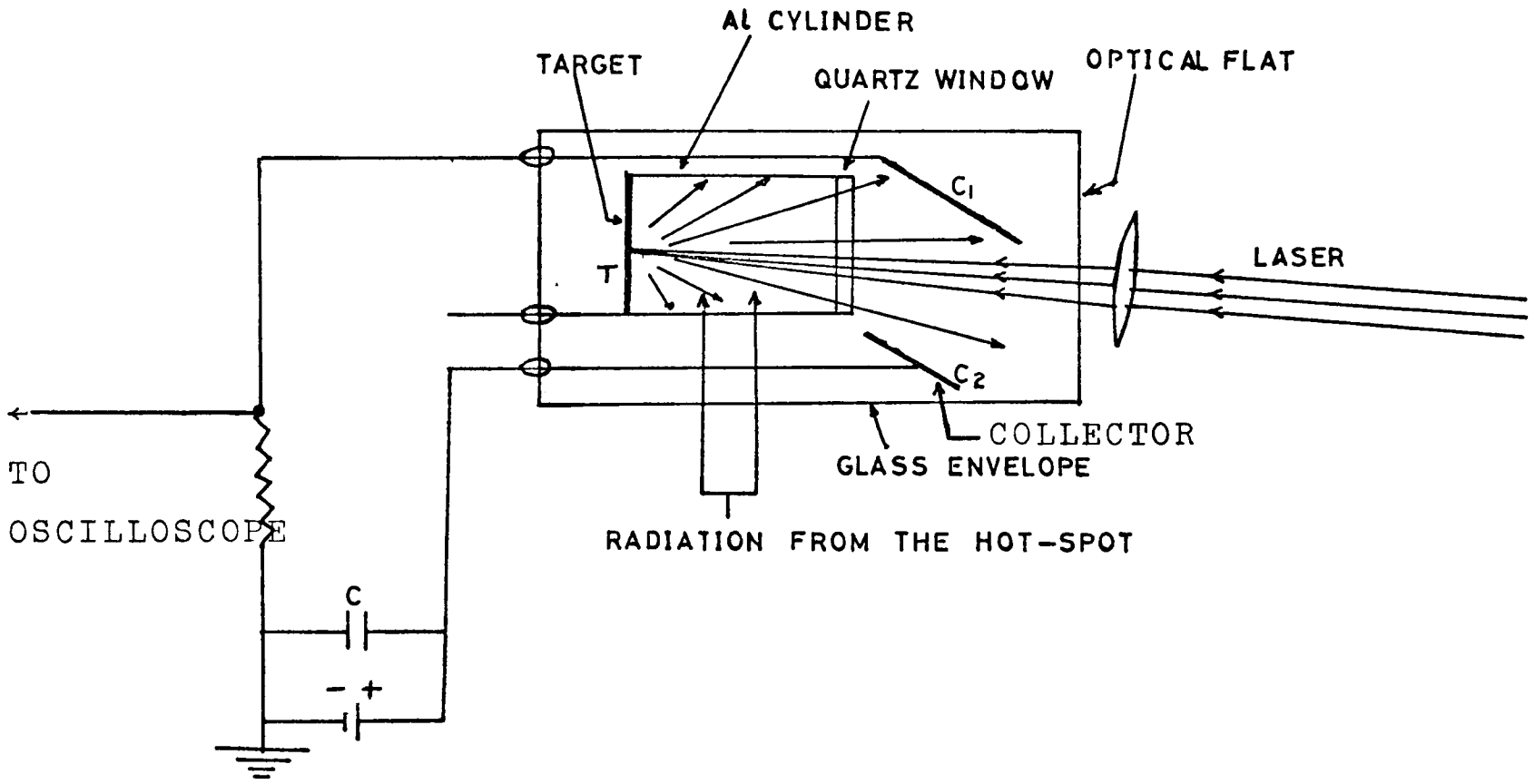

FIG. 6.13. EXPERIMENTAL ARRANGEMENT FOR THE DETECTION OF THE REVERSE PHOTOELECTRIC EFFECT.

the observation was made in two stages:

a) The current was recorded without the quartz window. Thus the light and the plasma produced by the interaction of laser light with the target flew radially and current signal was produced by the separation and flow of charges across c_1 and c_2.

b) A similar observation was made with the quartz window fixed on the near end of the cylinder. It is expected that introducing such a shielding will eliminate any current pulse produced by the charges originating at the target, even though any effect by a 'reverse photo-electric' effect will still be observable.

6.10 Results and Discussions

The results of observations a) and b) are shown in Fig. 6.14a,b,c & d. It can be seen from the oscillograms of the current pulses that when no shielding was introduced to stop the charged particles being influenced by the applied electric field the shape of the current pulse consists of the initial peak of amplitude $\sim$ 4 mA and the broad major peaks due to the motion of the charges from the plasma (as described earlier). In the case b), all the plasma effect was eliminated but the initial peak still persisted. The amplitude of this solitary peak was found to be a factor of 4 less than that obtained in the observation a). The fact strongly indicates that the charges causing the initial peak of the current caused by applying an ion-accelerating bias are not originated from the target. Since the particles produced at the target are shielded to reach any external metal parts, secondary emission by particle bombardment of the external metal parts cannot be held responsible for the

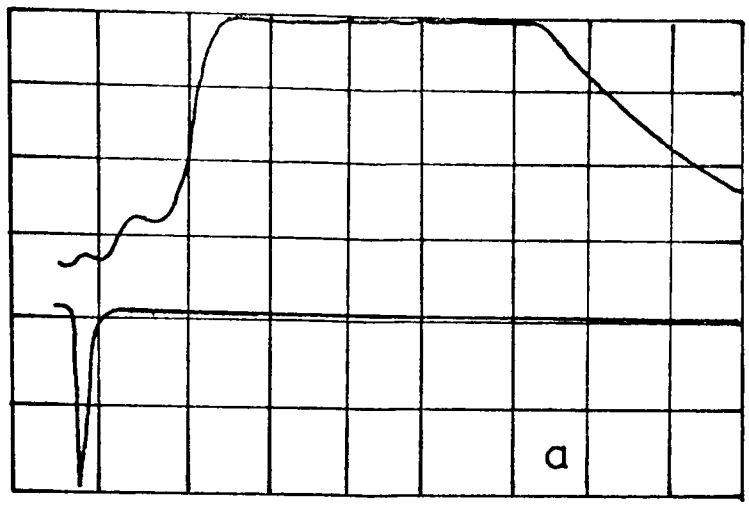

UPPER-Current signal-0.1 amps/cm.
LOWER-Laser Signal-5.0 mA/cm.
TIME-500 nsec/cm.
BIAS-+120V.

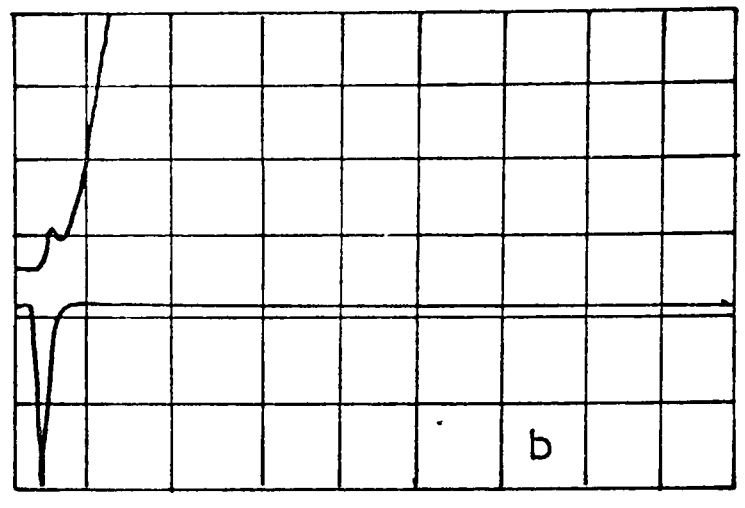

UPPER-Current Signal-10 mA/cm.
LOWER-Laser Signal-5.0 mA/cm.
TIME-500 nsec/cm.
BIAS-+120V.

CURRENT SIGNALS WITHOUT SHIELDING.

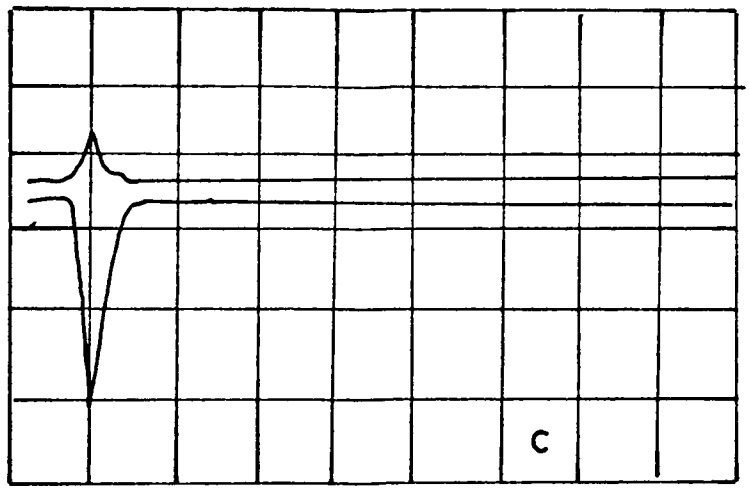

UPPER-Current Signal-2.0 mA/cm.
LOWER-Laser Signal-5.0 mA/cm.
TIME-200 nsec/cm.
BIAS-+120V.

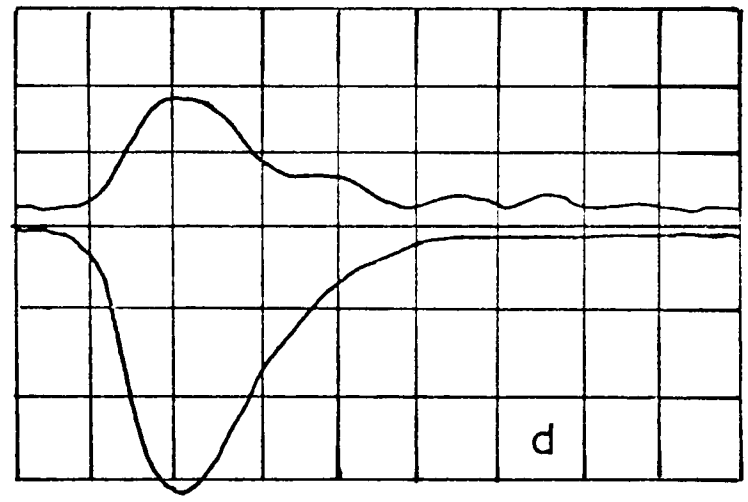

UPPER-Current Signal-1.0 mA/cm
LOWER-Laser Signal-5.0 mA/cm.
TIME-40 nsec/cm.
BIAS-+120V.

CURRENT SIGNALS WITH SHIELDING.

FIG. 6.14. VERIFICATION OF THE REVERSE-PHOTOELECTRIC EFFECT.

observed peak in the case b). The only possible explanation of the occurrence of such a peak will be the 'reverse photoelectric process' described in Chapter Three. Though the concept of such a 'reverse photoelectric effect' was originally suggested by Linlor (33) and Lichtman et al. (2), the author of Ref. 9 failed to observe such effect.

To verify the existence of such an effect the following supplementary observations were made:

i) A 'reverse photoelectric current' will depend upon the surface area of the metal collector exposed to the radiation from the hot spot. To verify this fact current signals were recorded from two different tubes with the same target material (Ta), electrode separation distance, bias voltage and vacuum condition but different collector configurations. The collector configurations are as shown in Fig. 6.15a & b. In the case a), the collector was a pin with an approximate area exposed to the radiation of 1.6 x 10^{-2} cm^2. In the second case, b), the collector was a circular disc with a hole in the middle. The area exposed to the radiation was $\sim$ 4 cm^2. The current signal shows (Fig. 6.14) that the amplitude of the initial peak in the case b) was roughly seven times higher than that of the case a). This adds weight to the idea that the observed 'ion peak' is due to a reverse photoelectric effect.

ii) The intensity dependence of the amplitude of the initial peak is quite significant. The laser beam was focussed to an approximate area of 10^{-3} cm^2 of a W target and the intensity of the incident laser beam was monitored with a calibrated photodiode simultaneously with the current signal. The collector was kept at a negative potential with

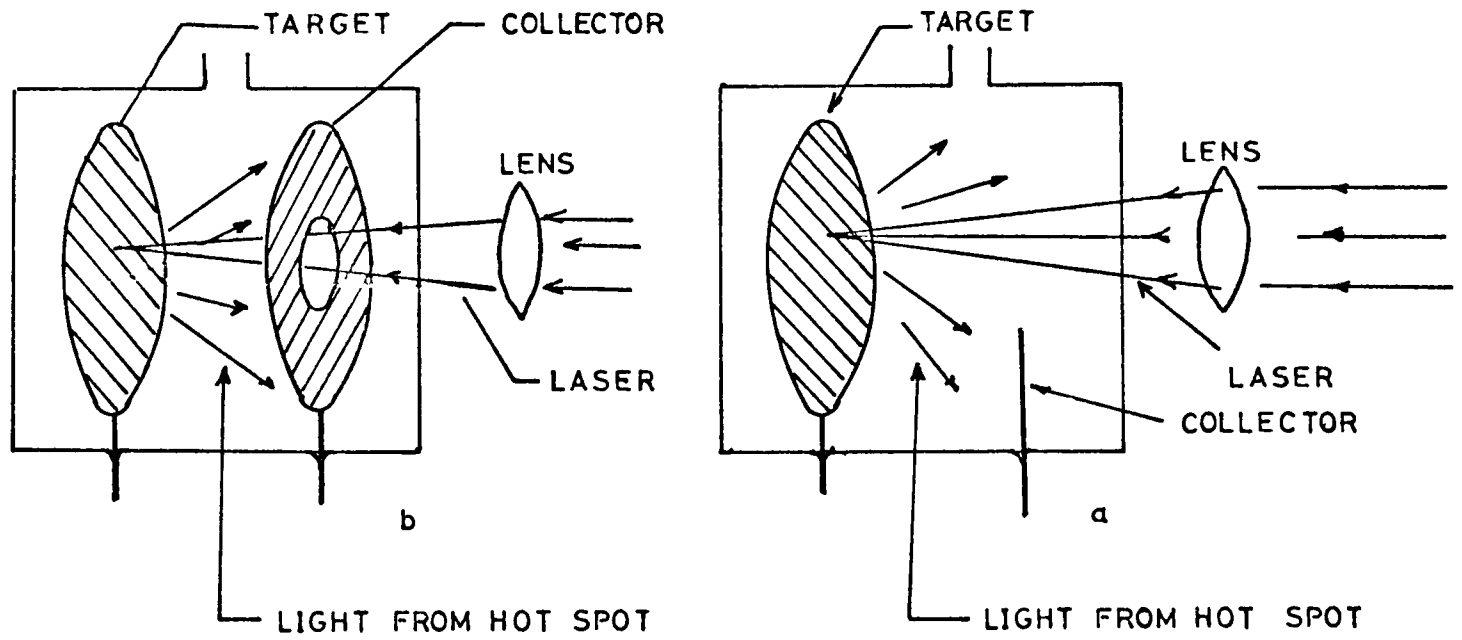

FIG. 6.15. SCHEMATIC DIAGRAM OF THE ARRANGEMENT FOR RECORDING REVERSE PHOTOELECTRIC CURRENT FROM TWO DIFFERENT ELECTRODE CONFIGURATIONS.

respect to the target. The intensity dependence of the amplitude is shown in Fig. 6.16. It is observed that the amplitude has a sharp cut-off power density at about 50 MW/cm^2. Below this value the emission of blue radiation from the irradiated spot ceased. A tungsten target is estimated to attain a temperature below six thousand degrees at this incident power. For such a temperature region the incandescent spot will emit radiation with maximum energy below $\sim$ 2.5 eV. This radiation is not expected to cause any detectable photoemission from the kovar collector. As the power is increased the metal plasma radiates with increasing photon energy and thus causes reverse photoemission

It can be concluded that a current peak which is almost coincident with the laser peak can only be attributed to a photoelectric effect. The laser pulse and the light pulse emitted from the irradiated spot were monitored simultaneously by two photodiodes, as shown in Fig. 6.17. It can be seen that the most copiously emitted radiation signal has a maxima almost coincident with the laser light maxima. Most of the photoelectrons are expected to be produced by the high energy part of the radiation continuum which will have a very short duration compared to the laser pulse. The observed shape of the initial peak (Fig. 6.1.b) contributes to such a hypothesis.

Though a quantitative theoretical analysis of this process was not possible, the results give definite evidence of the photoelectric nature of emission of the initial peak of the laser-induced current signal when recorded with a negative bias at the collector.

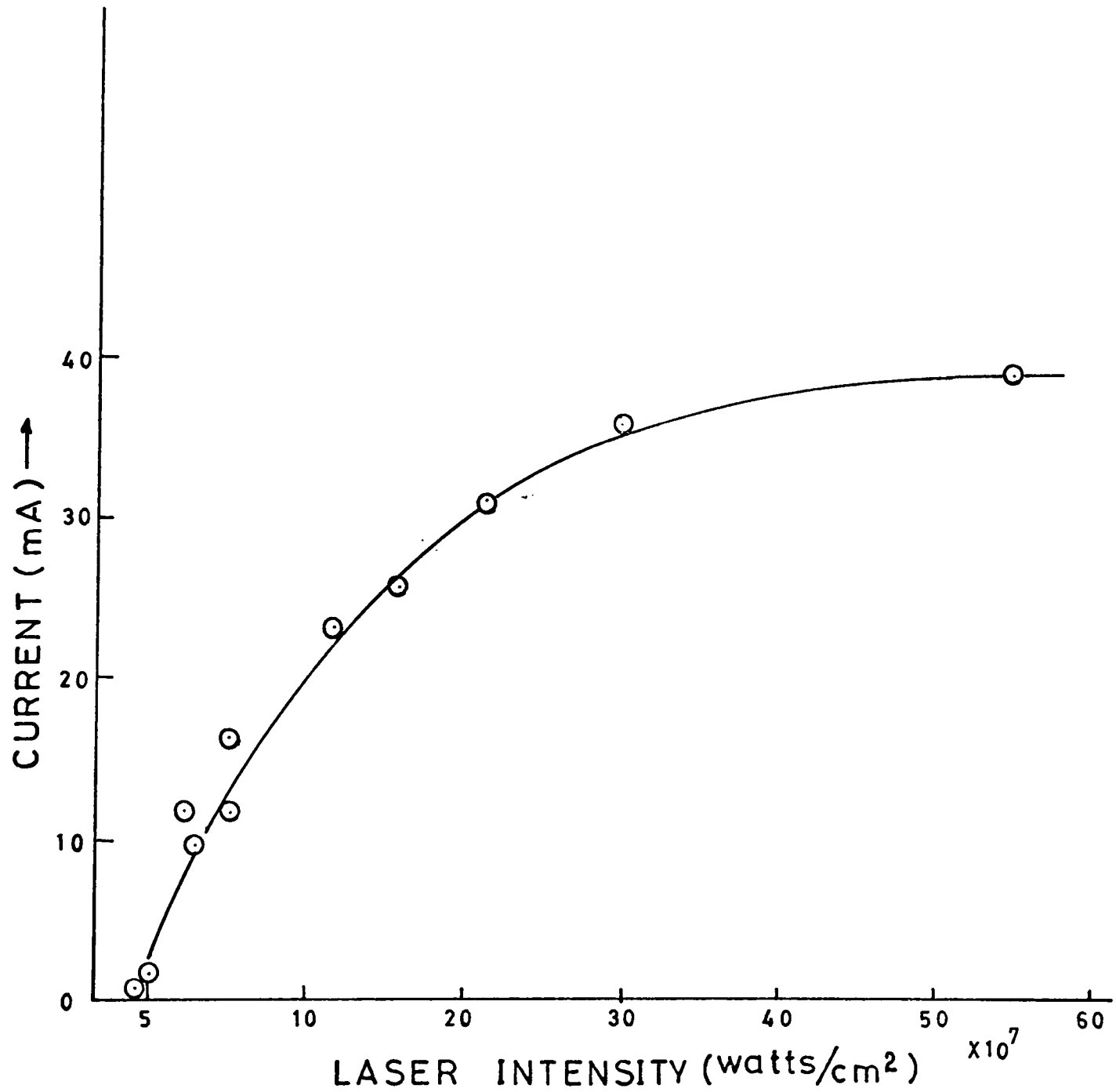

FIG. 6.16. REVERSE PHOTOELECTRIC CURRENT VERSUS LASER INTENSITY.

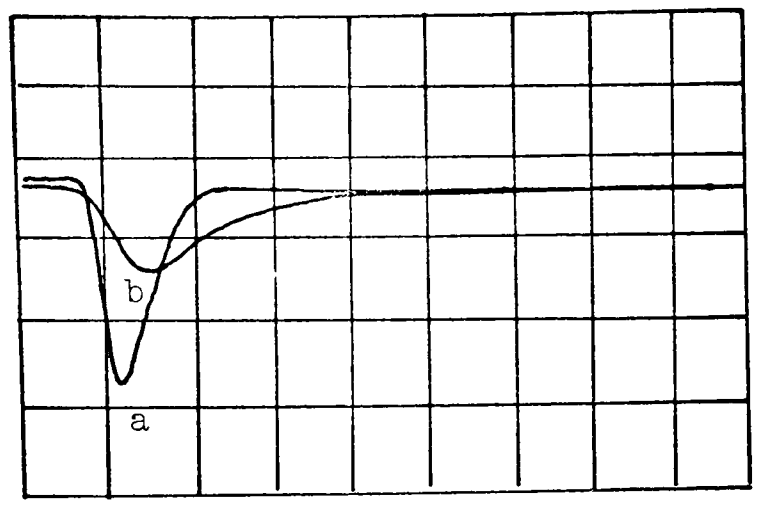

a - Laser pulse

b - Light pulse

Time Scale -
100 nsec/cm.

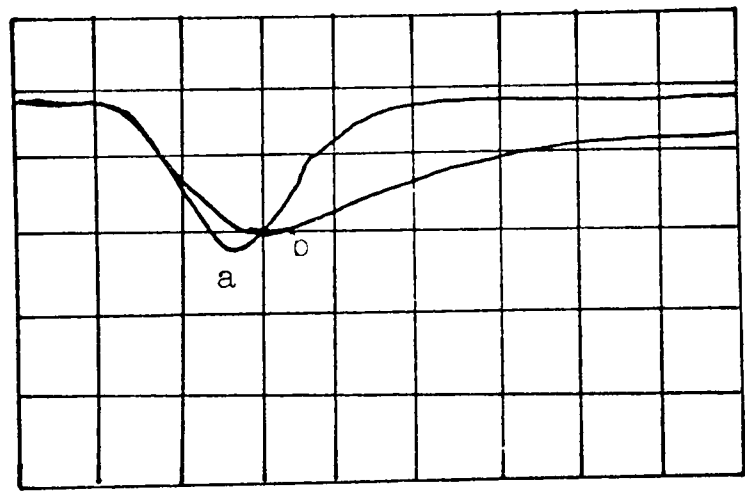

a - Laser pulse

b - Light pulse

Time Scale -
40 nsec/cm.

FIG. 6.17. OSCILLOGRAMS OF LASER SIGNAL AND THE SIGNAL PRODUCED BY LIGHT FROM THE PLASMA.

CHAPTER SEVEN

REAR-SIDE PHENOMENA

7.1 Introduction

Emission of electrons from the rear side of metal foils when the front surface was irradiated with a focussed Q-spoiled laser beam was reported by Knecht (27). He observed two well-defined peaks in the current signal (Fig. 7.1) across a resistor connected to a concealed collector at the rear side of the metal foils. No explanation was given as to the mechanism of emission of such electrons. The author, however, suggested an internal photon-assisted tunnelling effect as a plausible explanation of this electron emission.

During the course of investigating this suggestion Li et al. (28) published a letter reporting evidence against laser-induced spontaneous electron emission from the rear side of metal foils. With inadequate provision of light-shielding of the collector region, current signals very similar to those reported by Knecht were observed. When observation of current signal was made, with the rear collector carefully shielded by a metal tube (Fig. 7.2), Li et al. found that the initial sharp peak disappeared, though the second peak (broad) persisted. They suggested that the results of Knecht can be explained by a photoelectric process. The electrons are being produced from the surrounding metal parts by the ultraviolet photons generated from the laser-produced metal plasma at the front surface. The proposed explanation does not appear to take account of either Knecht's results or their own observations for a variety of

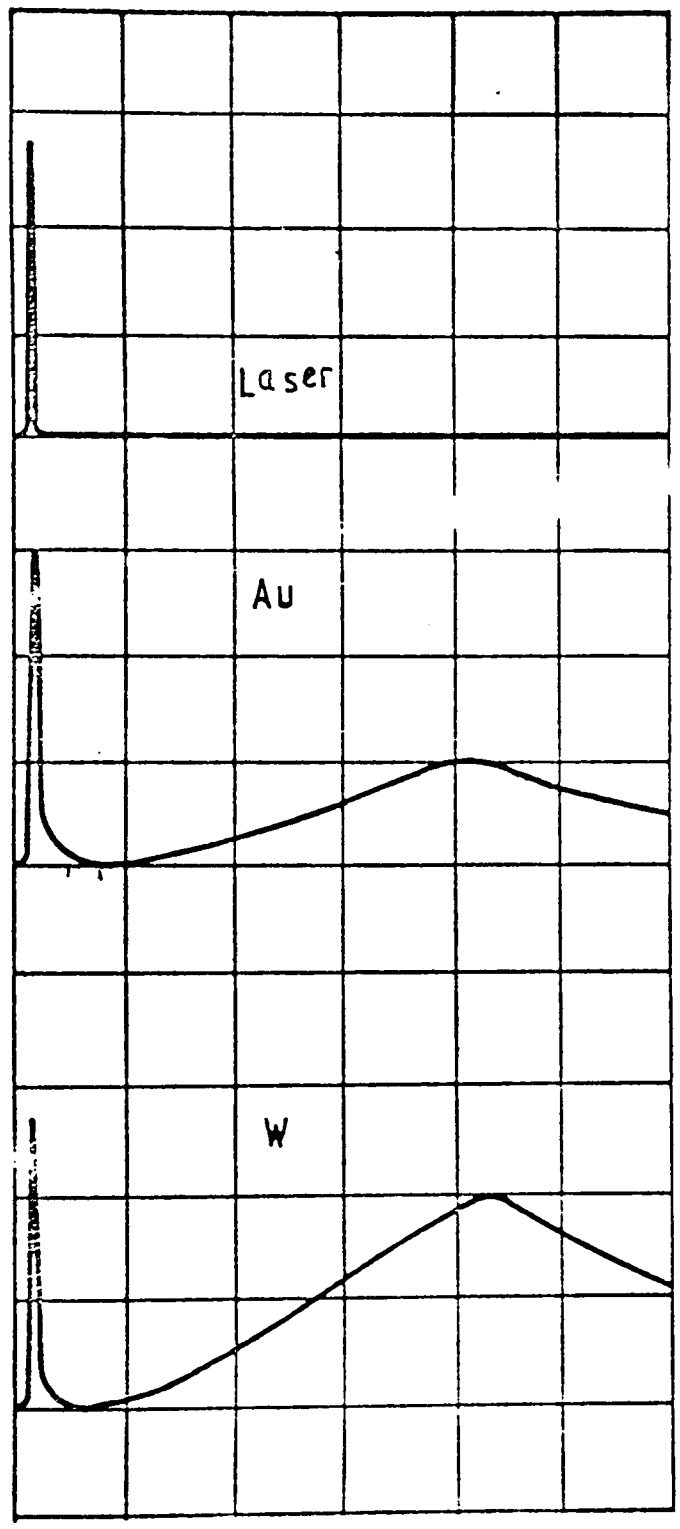

FIG. 7.1. SCOPE TRACE SHOWING, IN THIS ORDER FROM TOP, LASER PULSE AND LASER-INDUCED ELECTRON EMISSION FROM THE REAR SIDE OF FOILS CONSISTING OF GOLD, TUNGSTEN. TIME SCALE IS 1000 NSEC/DIV. AMPLITUDE SCALE FOR ELECTRON EMISSION TRACES IS 1×10^{-1} V/DIV. (AFTER REF. 27).

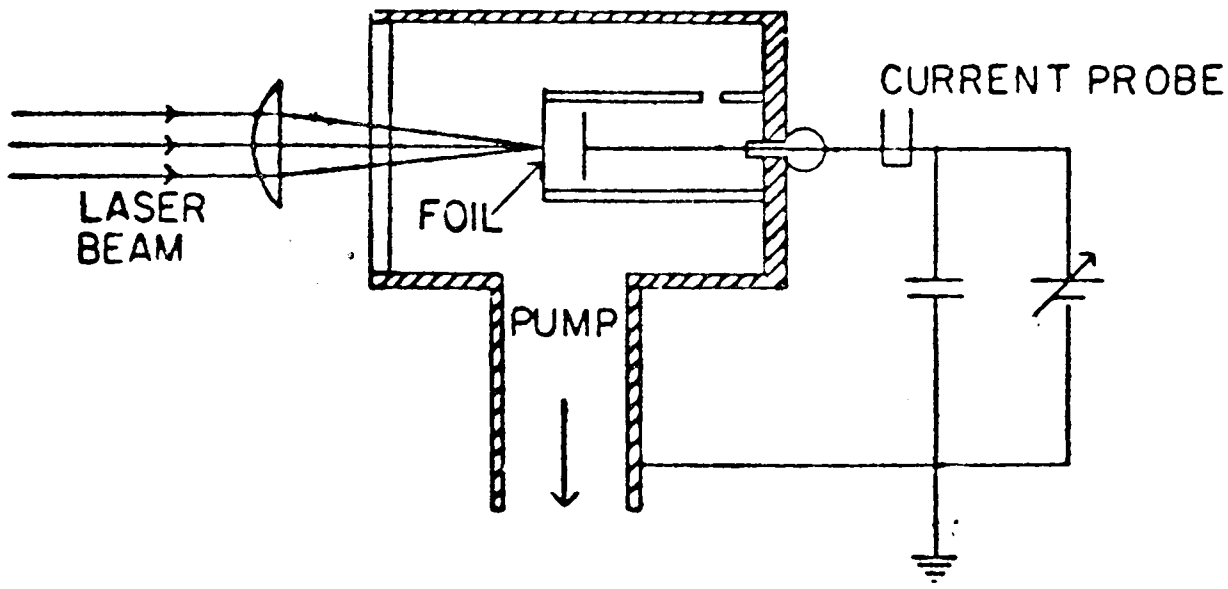

FIG. 7.2. APPARATUS USED TO LOOK FOR LASER-INDUCED SPONTANEOUS EMISSION FROM THE REAR SIDE OF FOILS (AFTER REF. 28).

reasons.

a) The radiation from the laser-produced plasma has been found to take place in a single pulse more or less coincident with the initiating laser pulse (Chapter Six). Thus, even if such a photoelectric process could account for the initial peak, it cannot be held responsible for the broad peak occurring two to three microseconds later.

b) Though a considerable number of high energy secondary photoelectrons may be produced from the surrounding metal parts or from the atoms and molecules occluded in the glass envelope, the possibility of their leaking to the concealed space between the target and the rear collector in Knecht's experimental arrangement will be very small. In the case of Li's arrangement (Fig. 7.2), firstly, no front collector was employed so that the photons could strike out electrons and, secondly, any stray electrons will have a negligible chance of being collected by the highly shielded collector at the rear side.

c) There may be a possibility that the high energy photons produced at the laser illuminated part of the foil will penetrate through the thickness of the target and produce photoelectrons from the interior or near the rear surface of the foil (volume photoelectric effect). These electrons may emerge from the rear side to cause the observed current. Any such effect can easily be detected by varying the thickness of the foil. Li et al. had experimented with varying thicknesses of foil, but no comment on the effect of the target thickness on the current at the rear side was made. Moreover, the occurrence of the second peak after a few microseconds from the laser peak cannot be justified.

Thus it is considered necessary to further investigate this interesting effect to seek a plausible explanation of such observed current. Different possibilities are considered below and experiments were performed to verify them.

Since the temperature of the laser-irradiated spot is very high, the effect of this temperature at the rear side of a thin metal foil must be considered. The surface temperature along the thickness of a metal foil with the front surface at x = 0 has been calculated by Ready (6) with the one-dimensional heat flow equation given by:

$$\frac{\partial^2 T(x,t)}{\partial x^2} - \frac{1}{k}\frac{\partial T(x,t)}{\partial t} = -\frac{A(x,t)}{K} \qquad \ldots\ (7\text{-}1)$$

where T = the temperature,

k = thermal diffusivity,

K = thermal conductivity,

and A = heat production/volume/time.

With the appropriate boundary conditions and for a laser pulse of power density 1.5×10^7 watts/cm^2, he calculated temperature rise at different depths. Some of his results are shown in Fig. 7.3. The results indicate that for depth larger than 10^{-4} cm the temperature will fall rapidly. For targets with thickness larger than 10^{-3} cm the increase in temperature very close to the rear surface will be zero for all practical purposes though in his calculation he neglected any loss of surface heat due to radiation or convection. In the case of higher surface temperature, the ejection of plasma will cause subsequent cooling of the surface before much heat is conducted away along the thickness. If, however, the conducted heat at the rear side is responsible

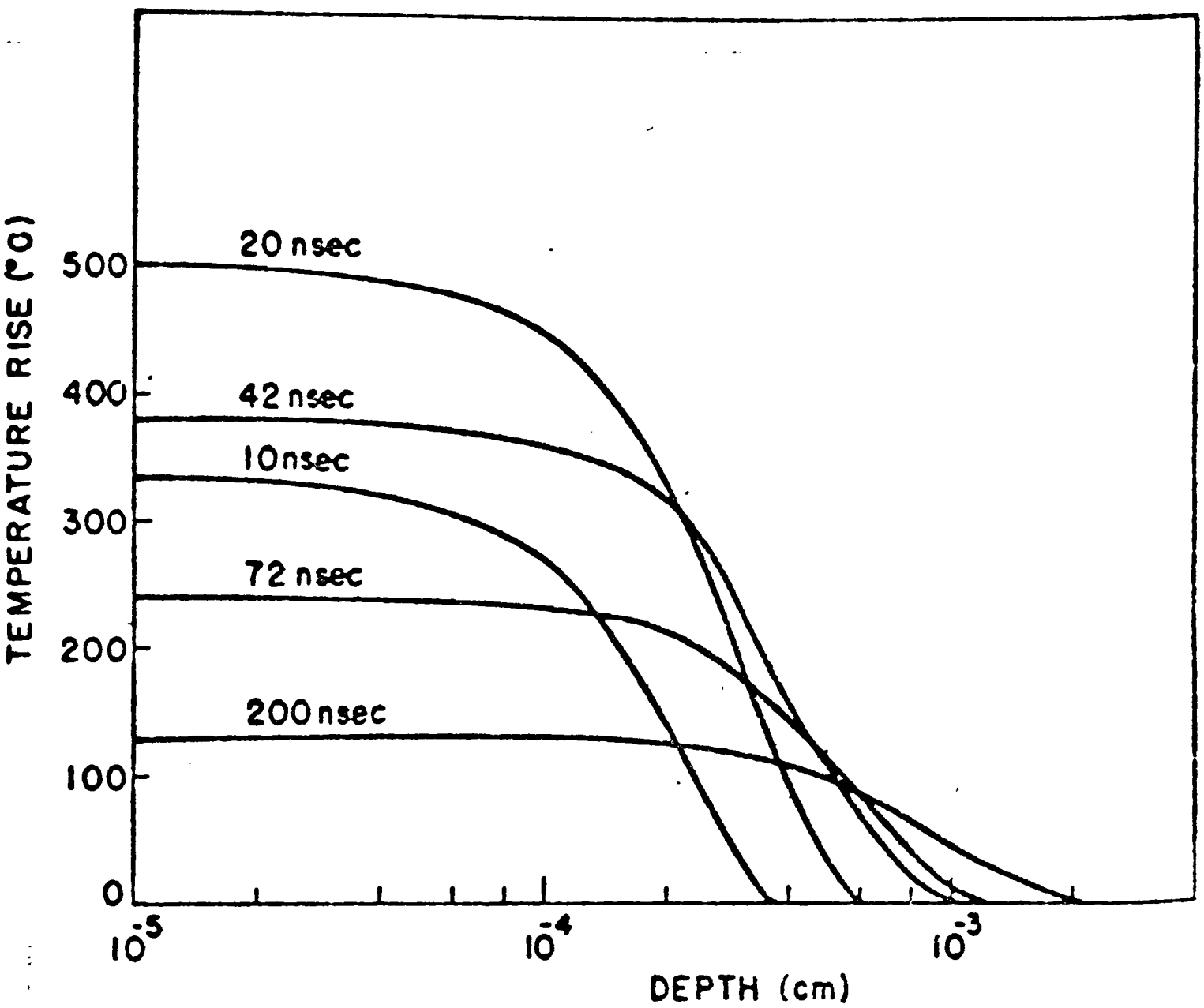

FIG. 7.3. CALCULATED TEMPERATURE RISE AS A FUNCTION OF DEPTH, WITH TIME AS A PARAMETER, IN A COPPER SAMPLE INITIALLY AT 0°C, WHEN A LASER PULSE OF PEAK POWER ~ 1.6×10^7 WATT/CM^2 AND ~ 45 NSEC. DURATION WAS INCIDENT ON IT (AFTER REF. 6).

for the observed rear side emission it can be detected by observing the change of the 'rear-side' current with the variation of the target thickness.

Another possibility is the production and propagation of a shock wave. When the laser-produced pressurized plume of 'plasma' leaves the surface, the recoil energy propagates into the solid as a shock wave. It has been shown by Caruso et al. (43) that if the plasma produced at any interface has a density ρ_p, which is much less than the density ρ_o of the target, then the fraction $1 - (\frac{\rho_p}{\rho_o})^{\frac{1}{2}}$ of the total incoming energy is given to the plasma, whereas the residual fraction is dissipated in the solid by means of a shock wave. For highly intense laser pulse, shock wave of sufficient strength may be produced to transform the solid into a dense plasma. From a phenomenological model of the interaction they have estimated that ionization of the atoms of heavy targets by the shock wave would require laser light of power $P >> 10^9$ watts/cm^2. In the present experiment the laser power used was kept much below this value so that any effect at the rear side due to the propagation of the shock wave can be neglected. Moreover, this effect will also be dependent on the thickness of the targets.

Another possibility which has not so far been considered is the displacement current, produced as a result of the electrostatic coupling of the electrodes. The stray capacitance between any electrode system will be of considerable importance when extremely rapid voltage change is concerned. From the previous experiments it was observed that laser-induced current pulses had very fast rise time

(a few tens of nanoseconds). A typical value of the time rate of change of the voltage at the front collector will be of the order of magnitude of 10^9 volts/sec. If both the front and rear side collectors are earthed through resistors and the target is kept at a negative voltage (as shown in Fig. 7.4), such a fast voltage change at the collector C_F will produce a displacement current flowing between C_R and C_F, if there exists a finite capacitance between them. If C denotes the capacitance between collectors C_R and C_F and V is the voltage at C_F at any instant of time, then the amount of charge induced at C_R will be given by

$$Q = CV.$$

The current flowing across C_F and C_R will be given by the time rate of change of the induced charge, thus we obtain the total current i as:

$$i = \frac{dQ}{dt} = C\frac{dV}{dt} \qquad \ldots\ (7\text{-}2)$$

where the total capacitance C is assumed to be constant with time. From the above equation it can be inferred that even for a stray capacitance of the order of magnitude of a few picofarad, current in the range of milliamps. can be observed.

It can further be suggested that from the results, dV/dt at the collector C_F can be calculated and the corresponding current at C_R can be plotted against the dV/dt. The slope of such a curve is expected to give an estimate of the value of the capacitance C.

If there is no collector held in front of the target as in the case of Li's experiment, there still exists a finite probability of observing a displacement current in

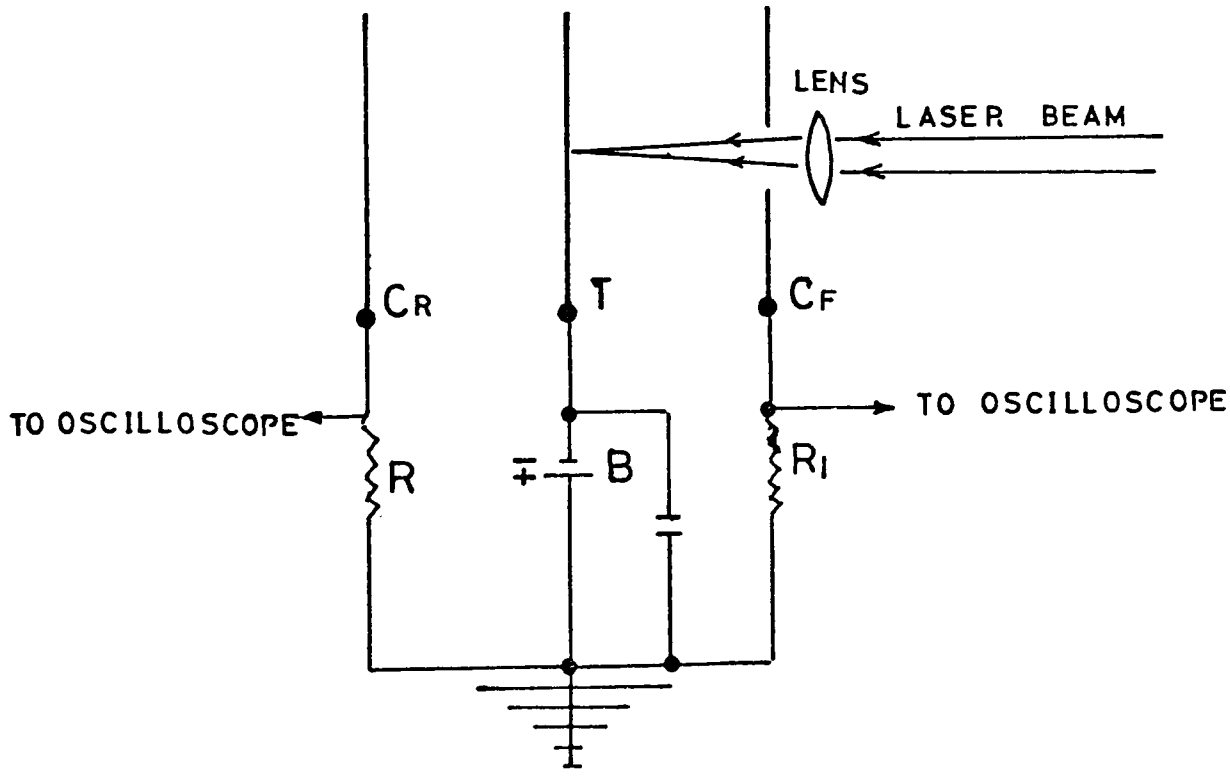

FIG. 7.4. SCHEMATIC VIEW OF THE ARRANGEMENT FOR RECORDING CURRENT SIMULTANEOUSLY FROM THE REAR AND THE FRONT OF THE TARGET.

any conducting collector at the rear side. Because the stray capacitance between the collector C_R and the space in front of the target will still be of considerable importance when laser-induced charges pass through the space so rapidly. With proper screening of the rear collector from the influence of the charges passing along the space in front of the target, such an effect may be minimized.

The experiments performed to investigate the effect and to justify the explanation given above are presented below.

7.2 Experiments

a) Initial experiment

To verify the results obtained by Knecht, an experimental tube was designed and constructed. The target material was a 5.0×10^{-3} thick gold foil which was spot welded to cover one end of a tungsten cylinder of diameter 2 cm and length 1.3 cm. The rear side collector was a tungsten cylinder of 1.2 cm in diameter and 0.7 cm in length. This was held inside the cylinder containing the target at a distance of 0.2 cm away from the rear surface of the target. A photograph of the tube is shown in Fig. 7.5. A cylindrical collector at the front side of the target was also introduced for a comparative study of the front and rear side emissions. The tube containing the electrodes was baked up to a temperature of $450^{\circ}C$ so that most of the adsorbed atoms and molecules in the glass were driven away and finally the tube was evacuated down to a pressure below 10^{-9} torr. The laser flux of $\sim$ 166 kw peak power and lasting

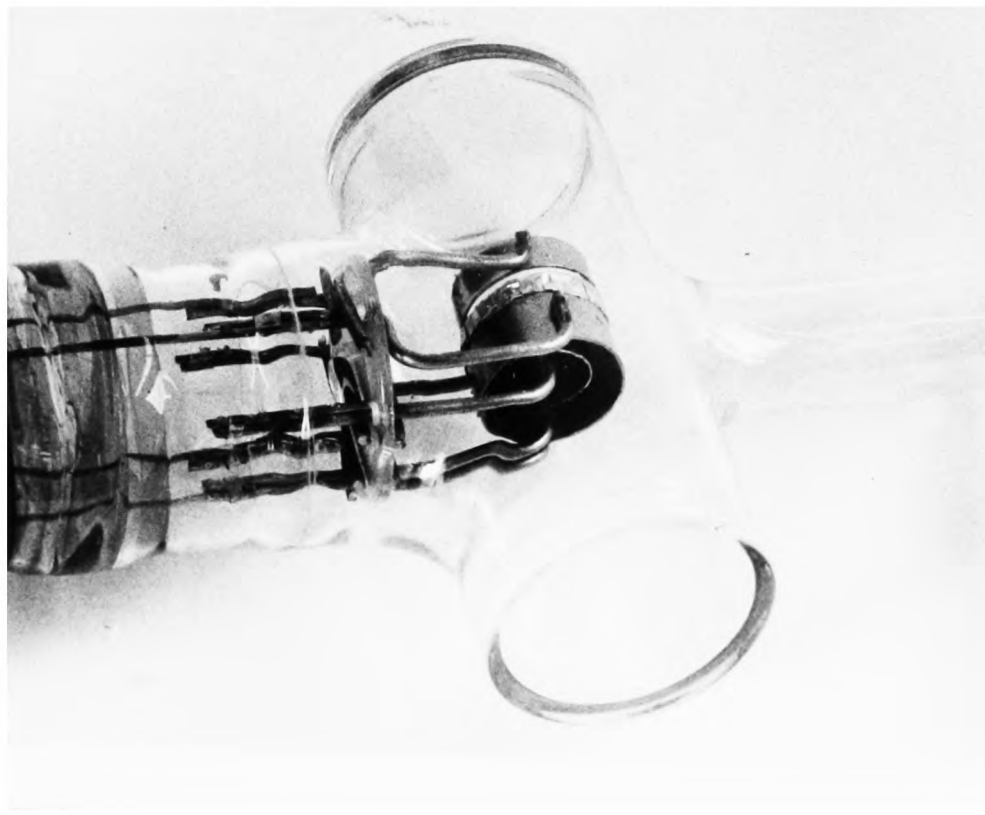

FIG. 7.5. PHOTOGRAPH OF THE TUBE SHOWING REAR AND FRONT COLLECTORS.

for ∿ 90 nanoseconds was focussed onto the front surface of the target by a 2 cm focal length lens. The estimated focussed area was 6×10^{-4} cm^2. Current signals both at the front and rear collectors were monitored across a 100Ω resistor. The following results were obtained.

Results

i) For a positive bias of 125 volts at the collector the current signal obtained had two peaks (Fig. 7.6) very similar to the observation of Knecht. The initial sharp peak occurred during the laser pulse and corresponded to a current of ∿ 35 mA. The second peak appeared slowly after about 2 microseconds from the laser peak.

ii) The current signals were observed at both front and rear side of the target when monitored simultaneously. Both the collectors were earthed through resistors and the target was kept at a negative potential (Fig. 7.7). Both the beams of the oscilloscope were triggered externally by the laser signal. Some typical current signals obtained are shown in Fig. 7.8. The current signals at the rear side showed three peaks corresponding to the three peaks of the front side signals. This fact suggests a correlation of the so-called rear side emission with the voltage signal developed at the front of the target.

b) Effect of target thickness

In this experiment the variation of the magnitudes of the current pertaining to the two peaks with the varying thickness of the target were investigated. The experimental tube was an array of five tubes with Ta targets of different thickness connected together (Fig. 7.9). This arrangement

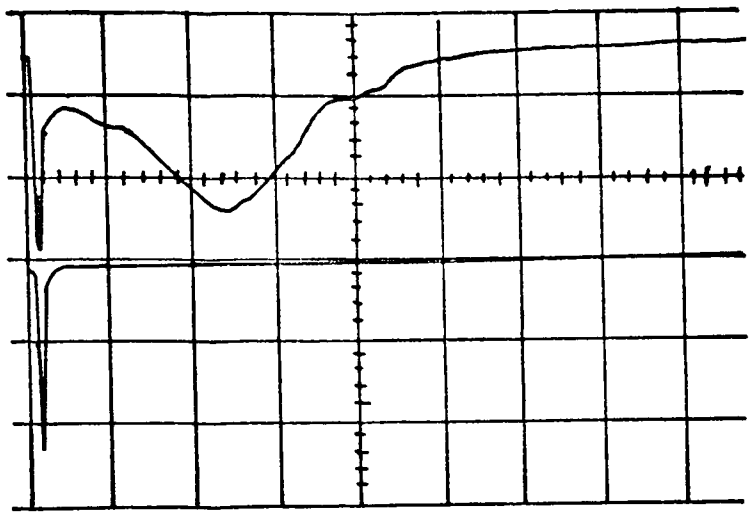

UPPER-Rear Side Current-
20 mA/cm.

LOWER-Laser Pulse

TIME-1000 nsec/cm

FIG. 7.6. OSCILLOGRAM SHOWING THE CURRENT SIGNAL OBTAINED AT THE REAR COLLECTOR.

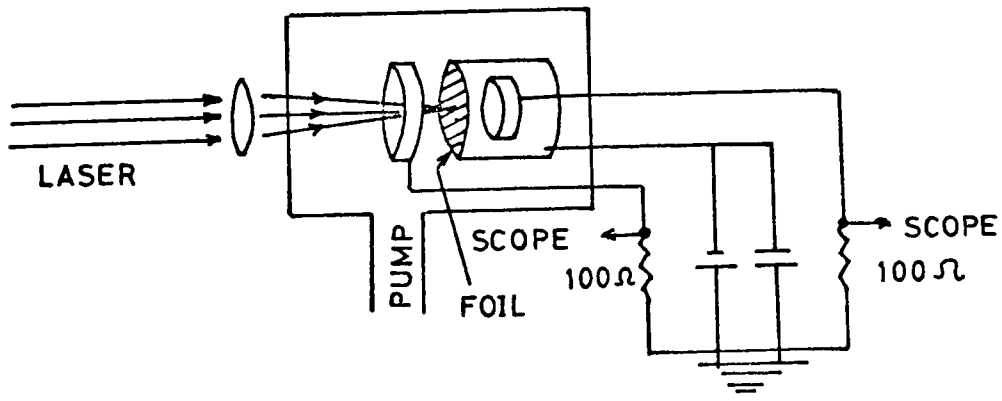

FIG. 7.7. SCHEMATIC DIAGRAM OF THE EXPERIMENTAL TUBE FOR THE PRELIMINARY INVESTIGATION OF THE REAR-SIDE CURRENT.

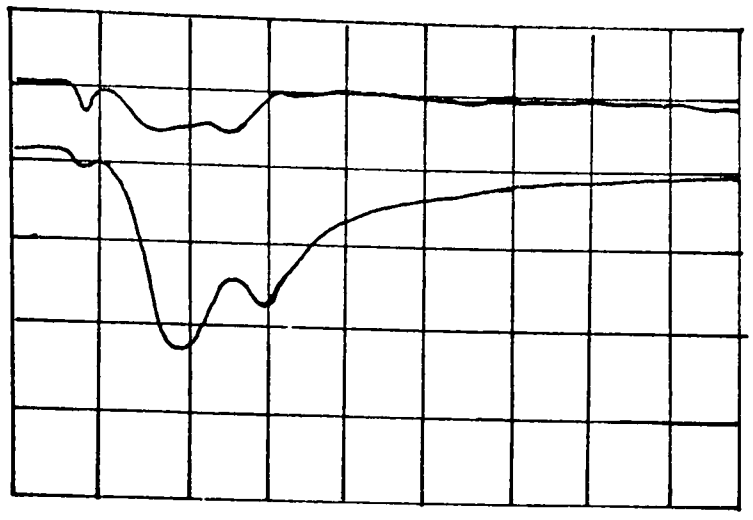

UPPER-Rear Side Current Signal
LOWER-Front Side Current Signal

TIME-200 nsec/cm.

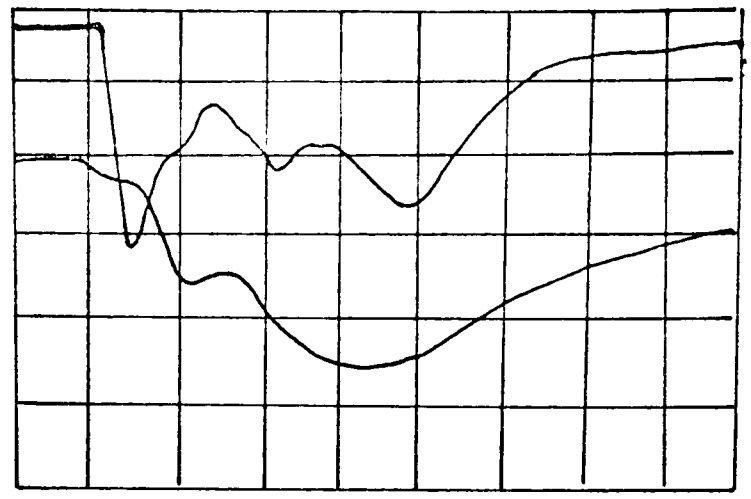

UPPER-Rear Side Current Signal
LOWER-Front Side Current Signal

TIME-100 nsec/cm.

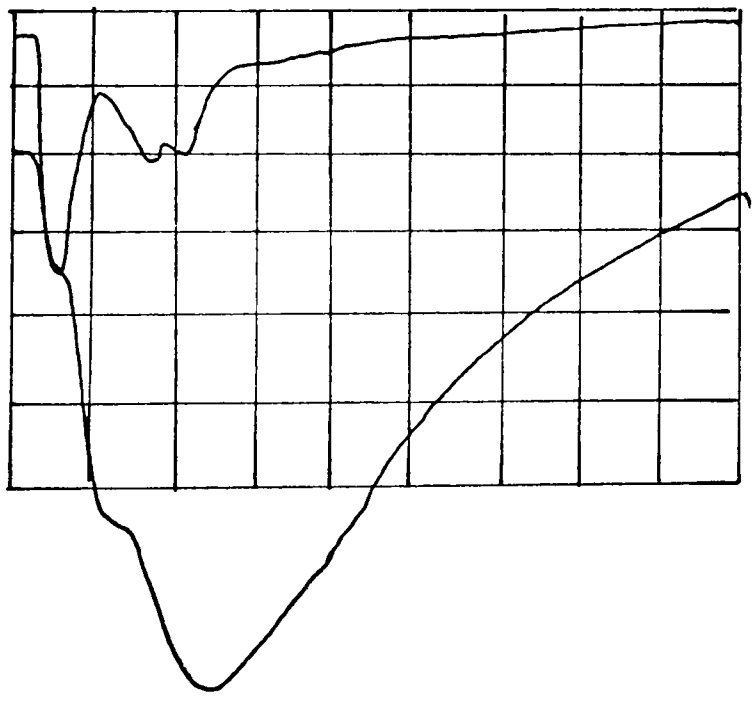

UPPER-Rear Side Current Signal
LOWER-Front Side Current Signal

TIME-100 nsec/cm.

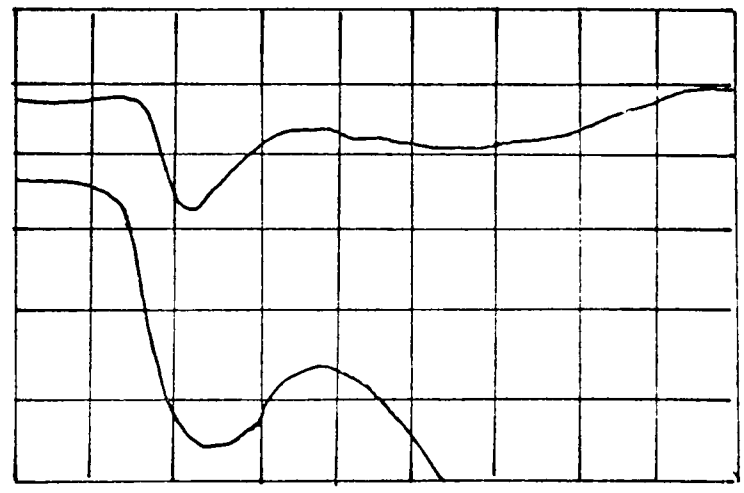

UPPER-Rear Side Current Signal
LOWER-Front Side Current Signal

TIME-40 nsec/cm.

FIG. 7.8. SOME TYPICAL OSCILLOGRAMS SHOWING PEAK-TO-PEAK TIME CORRELATION BETWEEN THE FRONT AND THE REAR SIDE CURRENT SIGNALS.

FIG. 7.9. VACUUM TUBES WITH Ta TARGETS OF FIVE DIFFERENT THICKNESSES CONNECTED TOGETHER.

ensured similar atmospheric conditions for all the tubes. The target thickness varied from 5×10^{-3} cm to 9×10^{-2} cm. All the five tubes had similar electrode configuration. The tube was baked and evacuated. The laser light was fired at the front surface of each target and the corresponding current signals at the rear side were recorded photographically from the oscilloscope. Enough care was taken to ensure that the input laser power was the same for all the targets irradiated. For each target at least five different readings were taken and the average value of the current (peak) was considered.

Results

The typical oscillograms of the current signals recorded for each tube are shown in Figs. 7.10a-d. For the same value of the incident laser intensity ($\sim 2 \times 10^{8}$ watts/cm^2) the measured value of the amplitudes of the current of the first and second peaks corresponding to the particular thickness of the targets are quoted below

Laser Intensity = 2×10^{8} watts/cm^2

Bias Voltage = 120 volts (+ve w.r.t. the target).

Thickness (cm)	Current at Rear Side		Delay between 1st & 2nd peak (sec.)
	1st Peak (amps)	2nd Peak (amps)	
5.1×10^{-3}	3.2×10^{-2}	2.6×10^{-2}	2×10^{-6}
12.7×10^{-3}	3.6×10^{-2}	2.9×10^{-2}	1.6×10^{-6}
25.0×10^{-3}	3.0×10^{-2}	1.9×10^{-2}	1.9×10^{-6}
50.8×10^{-3}	3.2×10^{-2}	2.5×10^{-2}	2×10^{-6}
91.6×10^{-3}	3.1×10^{-2}	2.5×10^{-2}	2×10^{-6}

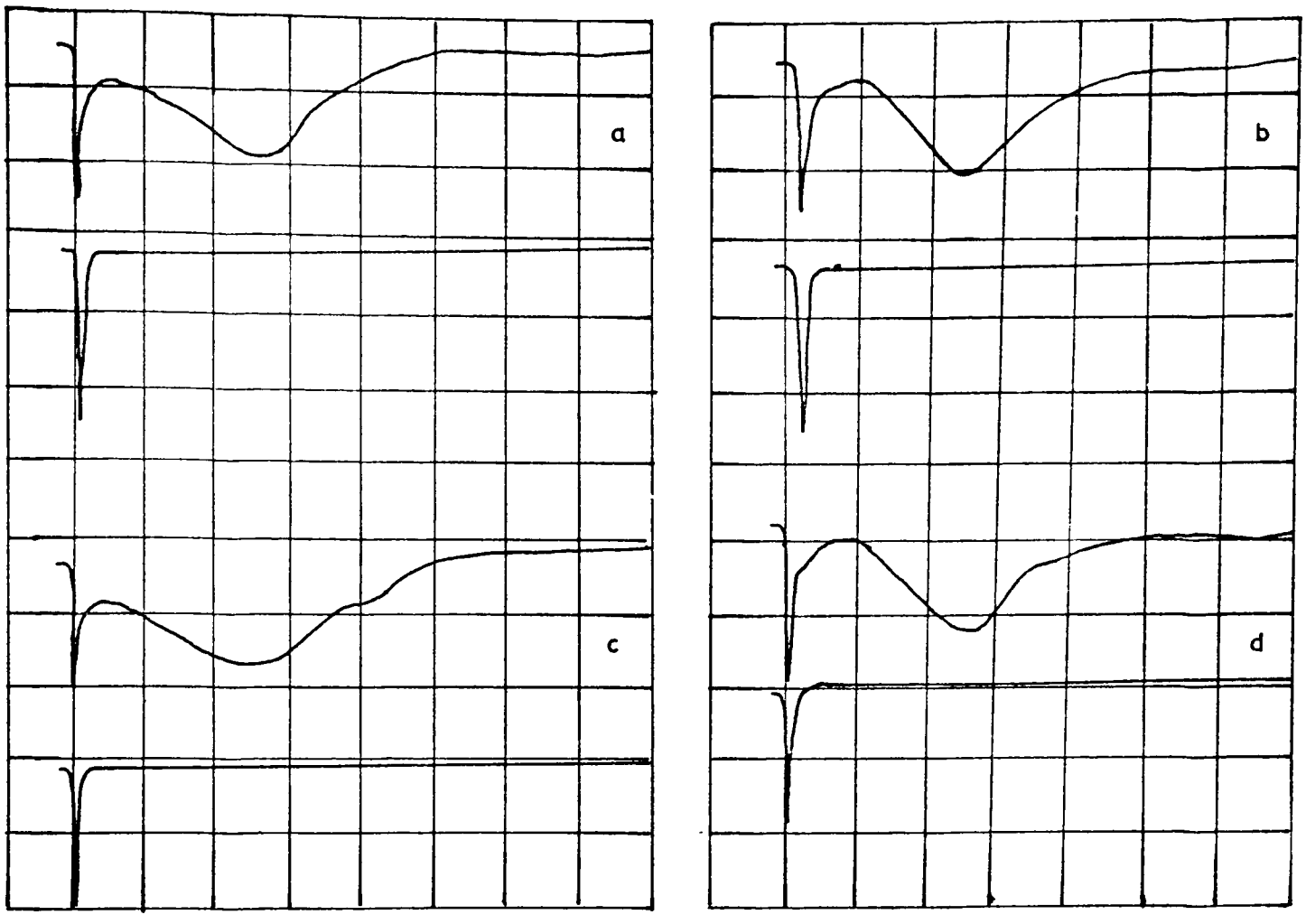

UPPER - Current Signals - Scale 20 mA/cm

LOWER - Laser Pulse - Peak Intensity $\tilde{\sim}$ 2 x 10^{8} watts/cm^{2}

TIME SCALE - 1000 nsec/cm

TARGET THICKNESS - a = 5.1 x 10^{-3} cm., b = 12.7 x 10^{-3} cm.,
c = 25.0 x 10^{-3} cm., d = 50.8 x 10^{-3} cm.

FIG. 7.10. CURRENT SIGNALS RECORDED AT THE REAR SIDE OF TARGETS OF DIFFERENT THICKNESSES.

The results did not show any significant variation in the amplitude of the current with the thickness of the target. Within the accuracy of the observation, the delay between the two peaks was also found to be the same, whatever the target thickness.

When the signals were recorded in the oscilloscope with a faster time scale, a certain delay between the onset of the laser pulse and the current pulses at the front and rear sides were observed (Fig. 7.11a & b). The time lag was estimated to be $\sim$ 20 nsec for both the signals. The signals at the front and rear were found to start simultaneously. No measurable delay between the initial peaks of the rear and front side signals were detected.

The results strongly rule out the suggested tunnelling mechanism. It can only be concluded that the observed current at the rear side of the target is not caused by any disturbance produced at the front surface by laser interaction.

A possible explanation can be an electrostatic coupling effect mentioned earlier.

c) Electrostatic coupling effect

The present experiment is an attempt to explain the 'rear-side phenomena' in terms of the displacement current introduced at the beginning of this chapter. The initial observation of the current signals at the front and rear of the target showed a remarkable peak-to-peak time correlation. This has led to the idea of further investigation of the variation of the amplitude of the current at the rear side with the time rate of increase of the voltage signal at the

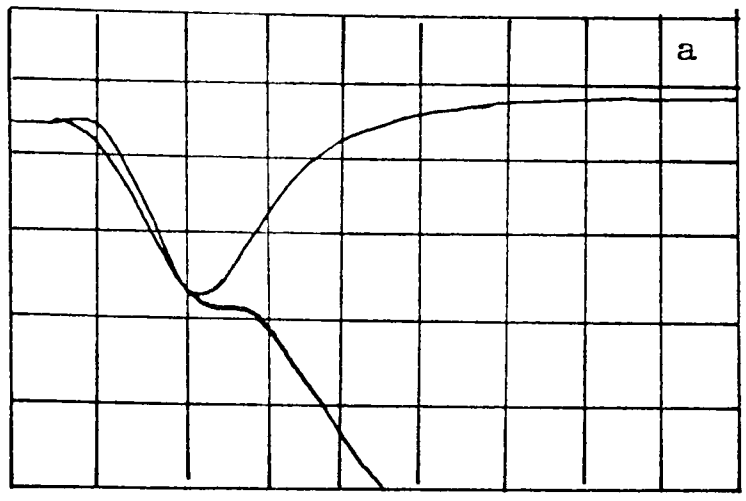

a) CURRENT RECORDED AT THE FRONT COLLECTOR C_F

AMPLITUDE SCALE - 20 mA/cm. TIME - 40 nsec/cm.

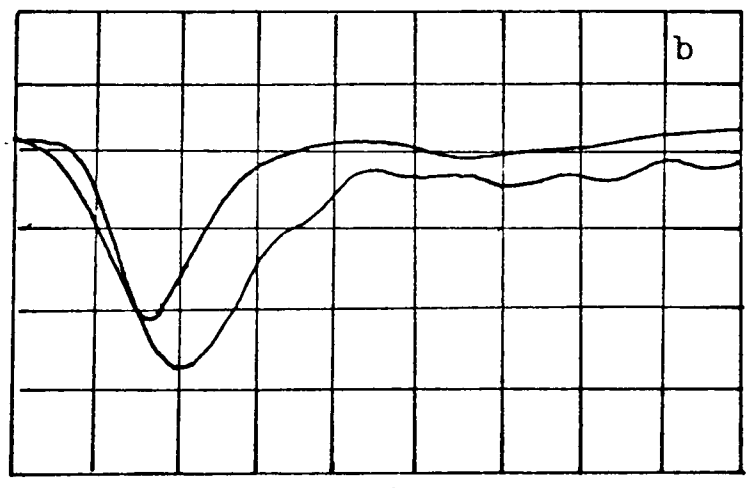

b) CURRENT RECORDED AT THE REAR COLLECTOR C_R

AMPLITUDE SCALE - 15 mA/cm. TIME - 40 nsec/cm.

FIG. 7.11. OSCILLOGRAMS SHOWING CURRENT PULSES RECORDED AT THE REAR AND FRONT COLLECTORS WITH THE CORRESPONDING LASER PULSES.

front collector.

The analysis of the current variation with the dV/dt of the front collector was confined to the initial peaks. The study on the initial peak of the current signal (Chapter Five) has shown that the peak is always coincident with the laser peak irrespective of the amplitude. It has also been observed that the rise time of the initial peak remains constant, while the amplitude increases with the increasing laser intensity. For illustration, some oscillograms, showing the initial part of increase of the front side current signal when laser intensity of varying magnitudes are incident onto the surface, are shown in Fig. 7.12.

Since there exists a finite capacitance between the collectors at the front and at the rear side of the target, any change in the potential of the front collector will induce a displacement current flowing between C_F and C_R. The magnitude of this current will depend on the capacitance C and the rate of change of voltage (Eqn. 7-2).

In the present experiment dV/dt at the front collector C_F was varied by irradiating the target with laser intensity of varying magnitudes. Since the absolute value of the current density was irrelevant, the power density was varied by defocussing the laser light onto the target by a 5.4 cm focal length lens. The laser pulse of peak power of $\sim$ 400 KW and lasting for approximately 100 nanosec. was used. The cross-sectional area of the unfocussed beam was found to be $\sim$ 0.13 cm^2. The current signals at both the front and the rear collectors were recorded with an applied bias voltage of 120 volts positive with respect to the target and through

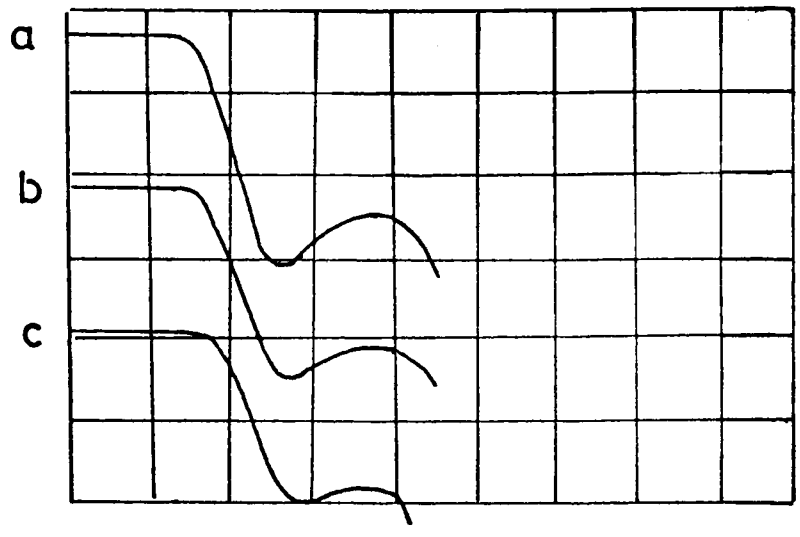

AMPLITUDE SCALES -

a) 5 mA/cm.; b) 10 mA/cm.; c) 15 mA/cm.

TIME SCALE - 40 nsec/cm.

FIG. 7.12. OSCILLOGRAMS SHOWING THE INITIAL INCREASE OF THE FRONT SIDE CURRENT SIGNALS AT DIFFERENT LEVELS OF THE INCIDENT INTENSITY OF THE LASER BEAM.

100Ω resistors (as shown in Fig. 7.3).

Results

From the photographic traces of the current signals the rise time of the initial peak of the current at C_F was estimated to be ∿ 30 nanoseconds. The initial peak of the signal at C_R occurred within ± 5 nanoseconds of the current peak at C_F. For the capacitive origin of the rear side current, the peak will correspond to the maximum dV/dt.

The dV/dt is measured for different values of the voltage signal at the front collector. The values are plotted against the laser intensity (Fig. 7.13). The slope has been found to increase rapidly up to an intensity ∿ 10^8 watts/cm^2. Beyond this value the slope does not increase appreciably. The corresponding rear-side current i_r is also plotted in the same graph. The current i_r has been found to saturate at the same region as dV/dt. The remarkable correlation between these two curves gives strong evidence for the capacitive origin of the rear side current given by Eqn. 7-2.

7.3 Discussion

From the results it can be concluded that the 'emission from the rear side' reported by Knecht and observed in the present investigation is not due to any true emission of electrons from the rear surface of a target. The failure to detect any change in the magnitude or in the time of the onset of the current with the increasing thickness rules out the possibility of any mechanism by which the effect produced at the laser illuminated part of the foil is transmitted through the thickness to cause electron emission from

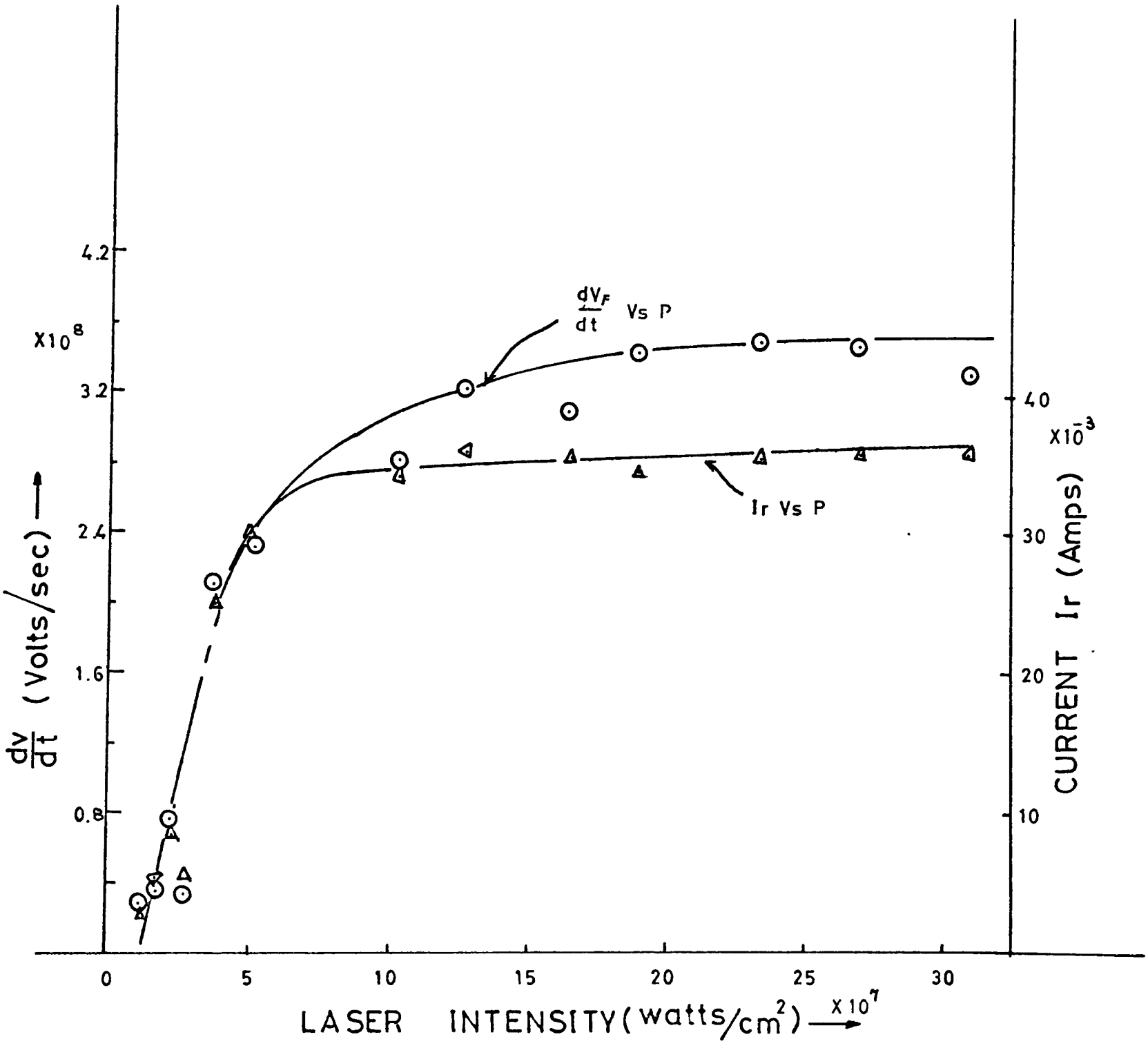
4.2
X10^8
3.2
2.4
1.6
0.8
dV_F/dt Vs P
Ir Vs P
40
X10^-3
30
20
10
CURRENT Ir (Amps)
dv/dt (Volts/sec)
0
5
10
15
20
25
30
LASER INTENSITY (watts/cm^2) X10^7

FIG. 7.13

the rear side of the foil. The observed similarity in the shapes of the current signals recorded from the front and the rear collectors and the correlation between the variation of the slope of the voltage signal at the front collector and the current i_r recorded across the resistor R_2 (rear side) shown in Fig. 7.13 give strong evidence for the capacitive origin of the current proposed in the introduction.

From the Eqn. 7-2, the capacitance between the collectors C_R and C_F can be estimated. From the data of Fig. 7.13, the current i_r is plotted against dV/dt, as shown in Fig. 7.14. The slope was calculated to be $\sim 1.5 \times 10^{-10}$. Thus the capacitance of the effective region will be $\sim 1.5 \times 10^{-10}$ farad.

To compare the estimated values the capacitance C between C_R and C_F plus the distributed capacitance between the connecting leads were measured with a capacitance bridge (Bounton Model 75D). The sensitivity of the instrument was 10^{-3} pf. The effective capacitance was found to be $\sim 0.8 \times 10^{-10}$ farad. The results can be considered to be in good agreement as far as the order of magnitude is concerned. The experimental errors can easily take account of the small discrepancy between the two values of the C.

The applied field between the target and the rear collector was found to have a positive effect on the current. The delay between the two peaks has been found to decrease with the increasing bias voltage. The retarded voltage at which the current ceased to appear corresponded to ~ 14 eV, in agreement with Knecht's results. These facts apparently give evidence against the capacitive origin of the rear-side

current. These observations can easily be accounted for if it is considered that the applied field between the target and the rear collector will slightly influence the charges moving in the space in front of the target.

The way the field will influence the charges in front of the target is illustrated in Fig. 7.15. Unless the rear collector is adequately shielded the lines of force will always extend into the front surface. As the field is increased the electrons emerging from the front surface will be more and more accelerated to give rise to increasing displacement current at the rear collector. Thus, while estimating the maximum electron energy by the retarding field, Knecht only estimated the maximum electron energy of the front side emission. Observed similar values for the maximum electron energies pertaining to the initial peaks of the current at the front and rear adds weight to this idea.

The mechanism of the production of the current peaks by focussed laser beam has been discussed in Chapter Six. It was observed that in a weak field only the initial and the second peak was observed. Thus when a potential of $\sim$ 200 volts is applied between the target and the rear collector of an electrode system, as shown in Fig. 7.4, the field at any point in front of the target will be fairly low. In this field the initial electrons will be accelerated fairly quickly to produce the sharp initial peak, whereas the 'plasma' following the initial electrons will not be much affected. A current will flow across the front side resistor R_1 only when a directed motion of charges is established. In weak field, the formation of a voltage signal will be

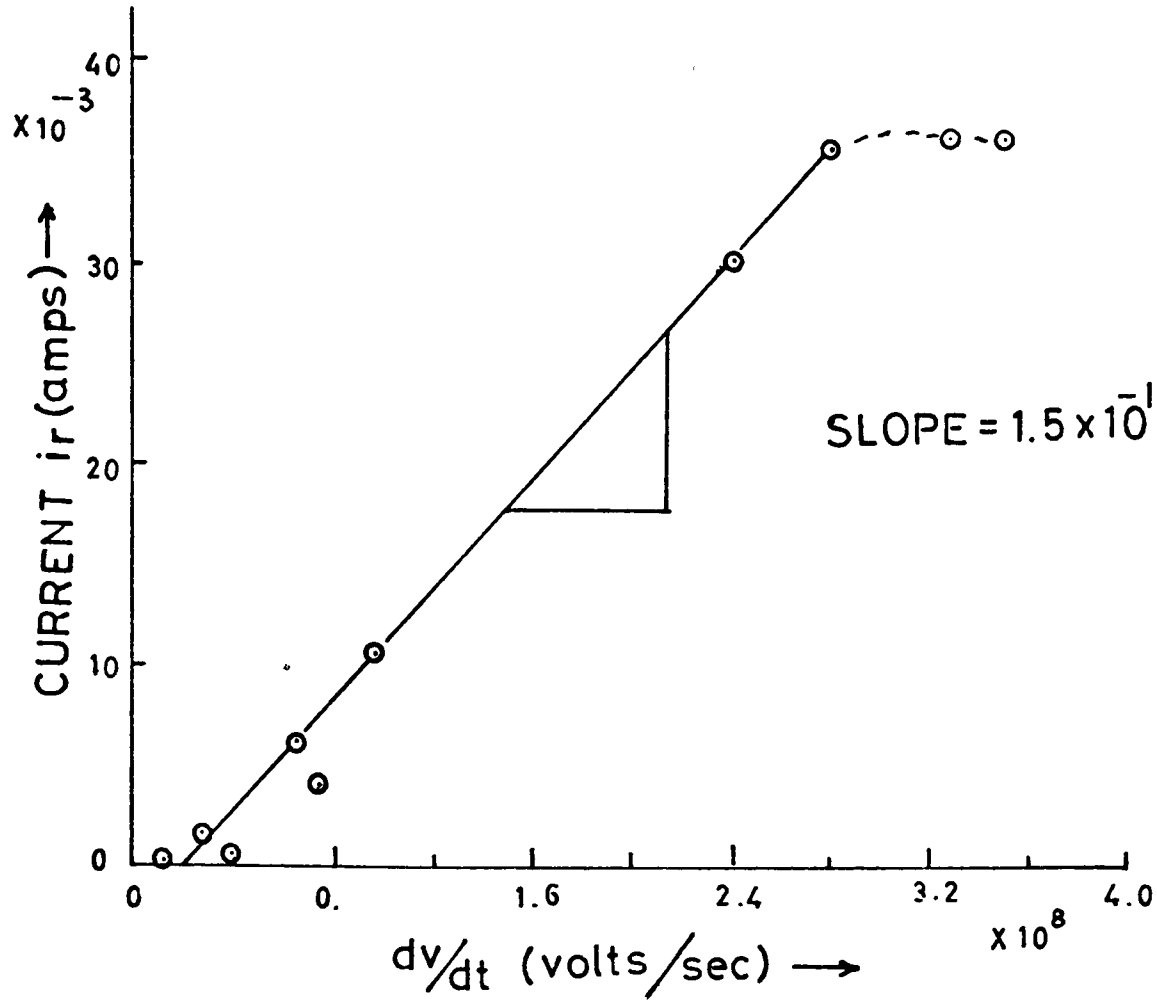

FIG. 7.14. SLOPE OF THE RISE OF THE INITIAL VOLTAGE PULSE VERSUS THE REAR-SIDE CURRENT.

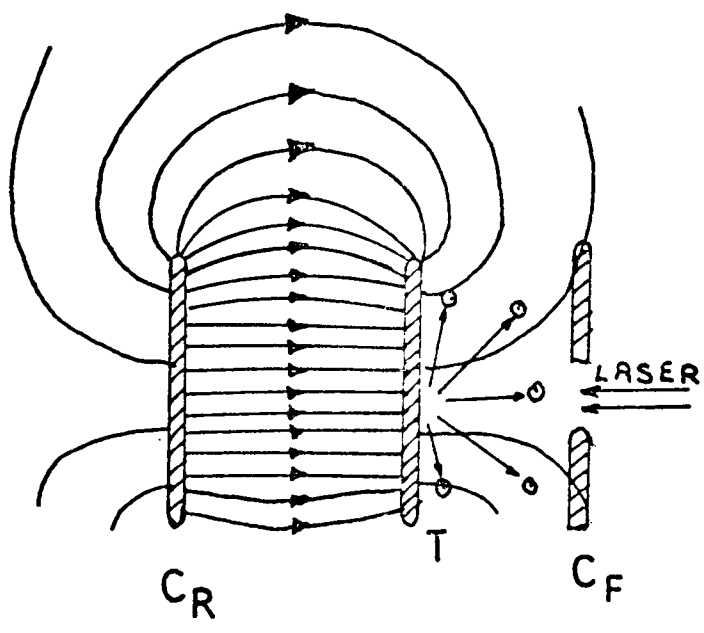

FIG. 7.15. ELECTRIC FIELD NEAR THE EDGES OF TWO PARALLEL CONDUCTORS.

complicated by the space charge and other interactions. The process will be relatively slow and eventually a net current will flow across R_1, thus giving a voltage signal.

At still higher applied field (above 250 volts), the field may be strong enough to influence the plasma to give rise to the splitting in the current signal, as mentioned before. Any such splitting will be observable in the rear side signal if the current is due to the capacitive coupling between C_R and C_F.

The signal recorded at the rear side with applied field above 250 volts shows three peaks, as can be seen from the oscillograms of Fig. 7.16. Li's results obtained with adequate shielding of the rear collector may be explained in terms of the above-mentioned mechanism.

With the electrostatic shielding introduced in his experiment, the field in front of the target can be considered to be nil even though there may exist high field between the target and the rear collector. The initial electrons will experience a retarding image force and only the high energy electrons will reach the front collector to produce a voltage signal. Such a voltage signal will have a very small magnitude (in the range of millivolts). Thus dV/dt at any point in the space will be too small to give rise to any appreciable displacement current. On the other hand, during the motion of the plasma, the mobile electrons in large numbers will move ahead of the ions, thus producing a voltage change in the neighbourhood which eventually gives rise to the second broad peak observed by Li et al.

COLLECTOR BIAS
(Positive w.r.t.
the target).

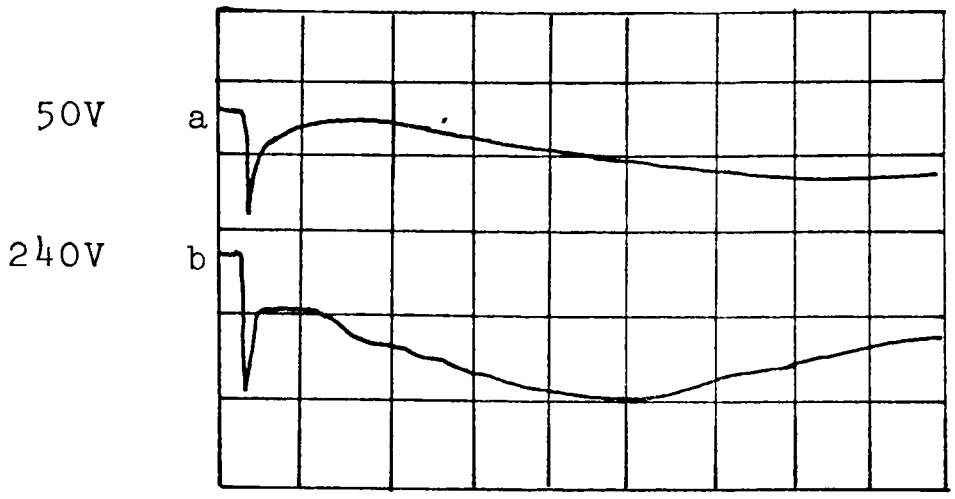

AMPLITUDE SCALE - a) 5 mA/cm; b,c,d) 10 mA/cm;
e) 20 mA/cm.
f) LASER PULSE - Peak Power $\simeq 10^8$ watts/cm^2
TIME SCALE - 500 nsec/cm.

FIG. 7.16. EFFECT OF APPLIED BIAS ON THE SHAPE OF THE LASER INDUCED CURRENT PULSE AT THE REAR SIDE OF A TARGET.

CHAPTER EIGHT

INTERACTION OF A Q-SWITCHED RUBY LASER WITH CADMIUM SULPHIDE

8.1 Introduction

A double photon photoelectric process in metal has been reported in Chapter Five. Intensity dependent laser interactions in metals and semiconductors have also been reported by other workers. The present chapter is devoted to further investigation of such a multi-photon process in a semiconductor.

Cadmium Sulphide (CdS) has been chosen for such studies for a variety of reasons. Single photon absorption process has been extensively studied in this substance. This has been reported to show high quantum yield in the visible region of the spectrum. CdS has a band-gap (Eg $\tilde{\sim}$ 2.4 eV) which is higher than the energy of a single ruby photon ($h\nu$ = 1.78 eV) but lower than the combined energy of two photons. For a band-to-band transition at least a double photon process must take place. Thus it is expected that a double photon process can conveniently be studied in this material. Moreover, the substance can easily and accurately be cut and polished into a thin crystal platelet. Also, it has a high melting point and can be obtained in a considerably pure state (high electrical resistivity). Some properties of the CdS crystal are quoted below. The authenticity of the quoted values will be referred to when such values are used in any context of the present investigation.

TABLE 8.1

Some Properties of CdS Crystals
(II-VI Compound)

1)	Density	4.82 gms/cm^3
2)	Melting point	1480 ± 10°C at 2.7 atm.
3)	Crystal system	Hexagonal
4)	Energy gap	2.4 eV at room temperature
5)	Electron mobility	∿ 200 cm^2/V.sec at room temperature
6)	Lattice constant (25°C)	a_o = 4.1368 A° c_o = 6.7162 A°
7)	Electron lifetime	∿ 10^{-3} sec.
8)	Hole lifetime	∿ 10^{-8} sec.
9)	Refractive index	∿ 2.5 (at ∿ 0.7 μ)

The values of electron mobility and the electron lifetime quoted above are typical. They may vary from crystal to crystal depending upon the concentration of the impurity atoms.

It is considered necessary to give a brief account of the mechanism of the optical absorption and photoconductivity in semiconductors from the existing knowledge of the optical properties of the material.

8.2 Optical Absorption in CdS

In a CdS crystal absorption of ruby photons may take place in a number of ways.

a) Intrinsic exciton absorption

Absorption of a single photon may raise a valence electron into an excited state which remains bound in a hydrogen-like orbit around either the parent atom or the positive

hole from which it came. If it is bound to the atom, the excitation may be passed on from atom to atom through the crystal. In the second case, the bound electron-hole pair may move bodily through the crystal. The concept is known as 'excitons' and the motion of excitons will not give rise to any photoconductivity unless there is separation of the positive and negative charges. Diemer and Hoogenstraaten (50) assumed that such a process occurs in CdS. However, for such absorption process, the transmission of laser light will be linear with the intensity. Excitons can be created by the absorption of a photon ($h\nu < E_{gap}$) almost anywhere in the crystal and since there is a large concentration of valence electrons available for exciton production, absorption of laser light in CdS by such a process can be of considerable importance at low laser intensity.

b) Free carrier absorption

In an electrically resistive medium the free charged particles may absorb photons from the laser light. The extra energy of the charges may be dissipated in the medium as heat or the charges might be energized enough to be ejected from the surface barrier with a finite kinetic energy. In a typical CdS crystal, free carrier density of the order of 10^{15} to 10^{17} per cm^3 can be expected (51). This is considerably lower than the density of atoms ($\sim 10^{22}$ per cm^3) in the substance. So, absorption of laser light by this process will be negligibly small compared to the other processes. For very low resistivity samples, i.e. with high impurity concentration, this absorption process may be of considerable importance.

c) Double photon absorption

Recent work on the laser activation of semiconductors has given birth to the concept of the 'double-photon absorption process'. If the incident photon density is high then the possibility that two photons will strike an atomic area in a time comparable to the formative time of an electron, i.e. the time an electron takes to be excited, may be considerable. Thus the possibility of the simultaneous absorption of two ruby photons of combined energy 3.56 eV by an electron of the valence band and a subsequent transition to the conduction band (across the band-gap of $\sim$ 2.54 eV) may be quite significant in a CdS crystal. A double photon absorption process may also take place in steps. In this case, an electron of the valence band is raised to an excited state in the band-gap and may be trapped in some impurity centre. If, before it is de-excited to the ground state or before it is released from its trapped positions by some mechanism, it encounters another photon, the absorption of the energy will cause it to make a transition to the conduction band. Whatever be the mechanism of such an absorption, it will always be associated with photoconductivity. For a high resistivity material like the sample used in the present experiments, band-to-band transition may be a predominant process as the concentration of the impurity atom is small compared to the density of the atoms.

A double photon process will depend on the square of the incident intensity of the light (as stated in Chapter Five). It can be speculated that such an absorption process has to be considered whenever a solid is irradiated with an intense source of monochromatic light of photon energy greater

than half the band-gap. Braunstein et al. (12) have derived expressions for the absorption coefficient in CdS with a specific band structure model consisting of a valence and two conduction bands. In the derivation of their result they considered a transition probability for an electron to be excited from an initial valence-band state k to a final conduction-band state k by simultaneously absorbing two photons. From their results it can be concluded that if the photons have the same energy $h\nu$ and is slightly less than the band-gap, the double photon absorption coefficient will depend on the density of the incident photons, which may be expressed as:

$$B = GN \qquad \ldots\ (8\text{-}1)$$

where N = density of the photons

and G = the constant which contains all the physical information about the interaction.

Ignoring the complex mechanism of absorption and the actual states involved in the electronic transition, a transmission equation of the following form can be set for an absorbing medium.

$$\frac{dN}{dx} = -\ (AN + BN^2) \qquad \ldots\ (8\text{-}2)$$

where A = linear absorption constant due to a single photon process

and B = nonlinear absorption constant due to a double photon process.

It is assumed that the nonlinear absorption due to a higher order effect (third, fourth, etc.) is negligible. The left hand side of the above equation gives the change of the

photon flux (number of photons per cm^2 per sec.) along the thickness of the crystal. The interpretation of the experimental results on the optical absorption in a CdS crystal will be based on fitting such a specific transmission equation.

The equation 8-2 can be integrated from x = 0 (front surface) to x = ℓ (rear surface). If the incident photon flux at x = 0 is denoted by N_i and the photon flux crossing a unit area at n = ℓ is denoted by N_t, which is the transmitted flux, the result of the integration can be put as

$$\frac{1}{A}\left(\ell n \frac{N_t}{N_i} - \ell_n \frac{A + B N_t}{A + B N_i}\right) = -\ell \qquad \ldots\ (8\text{-}3)$$

where ℓ = thickness of the specimen under observation.

In the deduction of the above equation the reflection from the surface at x = 0 was assumed to be negligible. The surface reflectivity was measured and the validity of the assumption was justified later in this chapter. The photon density along the cross-sectional diameter of the beam was considered to be uniform.

The linear and nonlinear absorption constants A and B respectively can be calculated from Eqn. 8-3 by fitting the equation to an appropriate transmission curve.

8.3 Photoconductivity in CdS

Electrical conductivity in CdS in the dark is due to the impurity carriers. In a very pure semiconductor the number of free carriers will be negligibly small and the crystal will behave as an insulator. The conductivity can be increased by activating the crystal with photons. The incident photons may produce free carrier electrons from

the valence band which is completely full. For such a conductivity (by a transition from valence band to the conduction band), the threshold energy of the photons will be $h\nu \gtrsim Eg$ where Eg is the band-gap (energy difference between the top of the valence and the bottom of the conduction band). For ruby photons with $h\nu = 1.78$ eV such transitions in CdS (Eg = 2.4 eV) are not possible. At low laser intensity the predominant absorption process will be a single photon absorption by intrinsic excitation. Such a process will contribute very little in photoconductivity. But the absorption of a single photon by an impurity atom whose valence electrons lie slightly below the conduction band may give rise to an appreciable photoconductivity in most of the practical semiconductors with energy gap higher than the photon energy. At room temperature lattice vibration may assist such a single photon photoconductivity.

At high laser intensity the probability of a band-to-band transition by the absorption of the energy of two ruby photons may be a comparable process. Photocurrent produced by such a process will have a distinct intensity dependence law and the present work is mainly oriented to investigating such a possibility.

When no electric field is applied across the medium, the electrons and holes produced by the ruby photons will wander about inside the crystal. The electric current will be constituted by the combined motion of both the charge carriers. Recombination and trapping of charges take place inside the crystal, thus attributing definite lifetimes for the charges. Direct recombination of electrons and holes is prohibited by the momentum conservation law. However,

recombination takes place in the presence of a third body which can either furnish or take away the momentum necessary to conserve momentum in the process. Anything which disturbs the periodicity of the crystal lattice may act as a third body.

It has been observed that for CdS the lifetime of electrons and holes is typically $\tau_e \sim 10^{-3}$ and $\tau_h \sim 10^{-8}$ respectively (51, 55). Thus the photocurrent in an applied electric field is determined only by the electron lifetime, as the hole lifetime is very short. In an applied field E the photocurrent density is given by

$$i = ne\mu E \qquad \text{amps./cm}^2 \qquad \ldots\ (8\text{-}4)$$

where e = the electric charge

μ = mobility of the electrons (drift velocity in unit field)

n = the density of photoelectrons at any instant of time.

The number of photoelectrons per unit volume at any time will depend on the generation rate and the lifetime of the electrons. Electron lifetime may be introduced to the above equation from a phenomenological definition as,

$\Delta n = q\tau_e$, which simply states that the equilibrium increase in carrier concentration is equal to the generation rate q times the lifetime τ_e. Thus Eqn. 8-4 can be written as:

$$i \tilde{=} qe\tau_e\mu E \qquad \ldots\ (8\text{-}5)$$

The generation rate of the charge can be related to the incident photon density in the following way:

Let N_a be the number of incident photons per unit

volume of the medium, per unit time. If we assume that at high incident photon density the contribution to the photocurrent is due mainly by a band-to-band transition, then a double photon absorption coefficient must be introduced. Thus for a double photon process the total number of photons absorbed will be BN_a, where B is the double photon absorption coefficient given by Eqn. 8-1. Since B is a linear function of the incident photon flux per unit volume, the total number of photons absorbed will be proportional to N_a^2. If η_2 be the quantum yield (electrons/absorbed photon) of this process, the generation rate of the charge q will be given by,

$$q = G\eta_2 N_a^2$$

where G is the constant which accommodates all the interaction parameters.

The photoconducting current will be given by,

$$i = G\eta_2 N_a^2 e\tau_e \mu E \qquad \text{amps./cm}^2.$$

The above equation can be written as

$$i = bN_a^2 \qquad \ldots\ (8\text{-}6)$$

where b is the constant for a particular value of the photon flux.

The relation can easily be experimentally verified by observing the change in the amplitude of the current with the variation of the incident photon flux density.

The number of electrons produced per incident photon can be calculated from Eqn. 8-6. If,for a specimen of the CdS, the current induced by a flux of photons per unit volume N_a is i amps./cm^2, the quantum yield (which implicitly contains the absorption coefficient) may be written as

$$\eta = \frac{n_e}{N_a} = \frac{bN_a}{1.6 \times 10^{-19}} \qquad \ldots\ (8\text{-}7)$$

where η is defined as the number of free electrons produced per incident photon.

8.4 Experiments

a) Nonlinear absorption in CdS

In this experiment the absorption characteristic of a CdS crystal when the ruby laser light passes through it is investigated. The absorption is then related to the induced conduction current. The Cadmium Sulphide was obtained from the Associated Electrical Industries, Rugby (AEI). The crystal was cut into a rectangular slab of area 1.06 x 0.8 cm and thickness of 0.16 cm. The crystal was cut accurately by employing a slow and continuous mechanical sawing arrangement devised in this laboratory (courtesy - S. Armitage). The crystal plate was mounted on a perspex slab which had a hole so that the rear side of the crystal just covered the hole. This arrangement transmitted the laser light through the crystal unhindered by the perspex. A part of the laser light incident onto the crystal surface was deflected by a beam splitter to a matt surface. The scattered light from the matt surface was monitored by a calibrated photodiode (P.d-1). The transmitted light was also deflected by a beam splitter and allowed to fall on another matt surface. The scattered light was again monitored by another photodiode (P.d-2). Both the photodiodes were shielded against the flash tube light. A filter was introduced in the path of the transmitted light. The purpose was to transmit only the laser light and stop any fluorescent light emitted from the crystal from reaching the photodiode. The photodiodes used were

SGD-100. Linearity of the photodiodes was checked and found to be linear for the range of laser power detected by these. A schematic diagram of the arrangement is shown in Fig. 8.1. An extra photodiode (P.d-0) was used at the front side of the crystal to trigger externally both the beams of a 551 dual beam oscilloscope simultaneously. The photodiode signals monitoring the incident and the transmitted intensity were recorded in the two channels of the oscilloscope. The second photodiode (P.d-2) at the rear side of the crystal was calibrated with respect to the first one. The calibration was done by monitoring laser power by both the photodiodes without putting the CdS crystal in the path of the laser beam. A slit was introduced in the path of the laser beam to illuminate a small area of the crystal uniformly. A photographic plate was illuminated by the laser light and the diameter of the laser spot was found to be 0.6 cm. The energy distribution along the cross-section of the beam was found to be fairly uniform. The laser power was varied by introducing dielectric coated mirrors of different reflectivity in the path of the beam. The experiment was done at room temperature ($300^{\circ}K$) and in atmospheric conditions.

Results

For the incident laser pulses of varying amplitudes the transmitted pulses were recorded photographically from the oscilloscope. The incident laser pulses were also recorded simultaneously so that an accurate relation between the incident intensity and the transmitted intensity can be obtained. Thus the absorption at any value of the incident

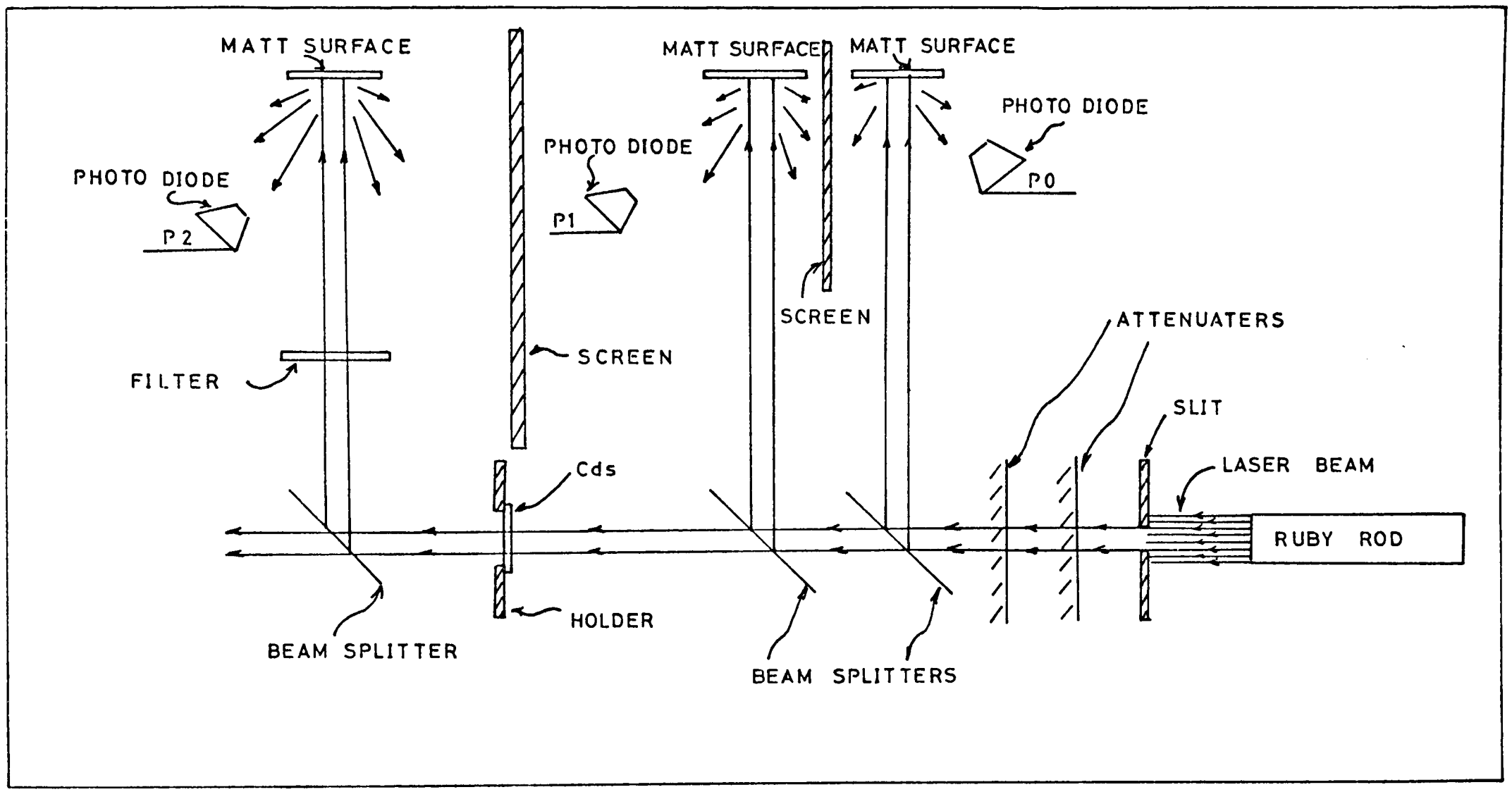

FIG. 8.1. EXPERIMENTAL ARRANGEMENT TO INVESTIGATE OPTICAL ABSORPTION IN CdS.

intensity was estimated within an accuracy of ± 5%. Approximating the laser signal as a triangular pulse of 100 nanosec. duration, the incident and the transmitted photon fluxes (no. of photons per sec.) on the illuminated area of the crystal ($\sim$ 0.3 cm^2) were calculated. The transmitted photon flux (through a thickness of 0.16 cm of the crystal) was plotted against the incident photon flux in a log-log scale. The transmission curve thus obtained is shown in Fig. 8.2. The experimental points show two distinctly different regions of absorption. Initially up to a photon flux of $\sim 10^{21}$ photons sec^{-1}, the transmitted photon flux increases with the incident flux. Above this value the transmission curve is characteristic of an intensity dependent nonlinear absorber and the transmission is found to be limited.

To verify the linearity of the low-level transmission a straight line with slope equal to 1 was drawn to fit the experimental points in Fig. 8.2. It was found that within the experimental error the points fitted the straight line reasonably well. This indicates that the low-level transmission is linearly proportional to the incident photon flux. This is a strong indication of a single photon absorption process.

If such an absorption process is associated with the creation of excitons, the photoconductivity will be negligible. Any photoconducting current due to the linear absorption of incident photons, if observed, must be attributed to a single photon excitation of impurity atoms. If the nonlinear region of absorption is due to a double photon process, an appreciable photocurrent can be expected to flow across the crystal

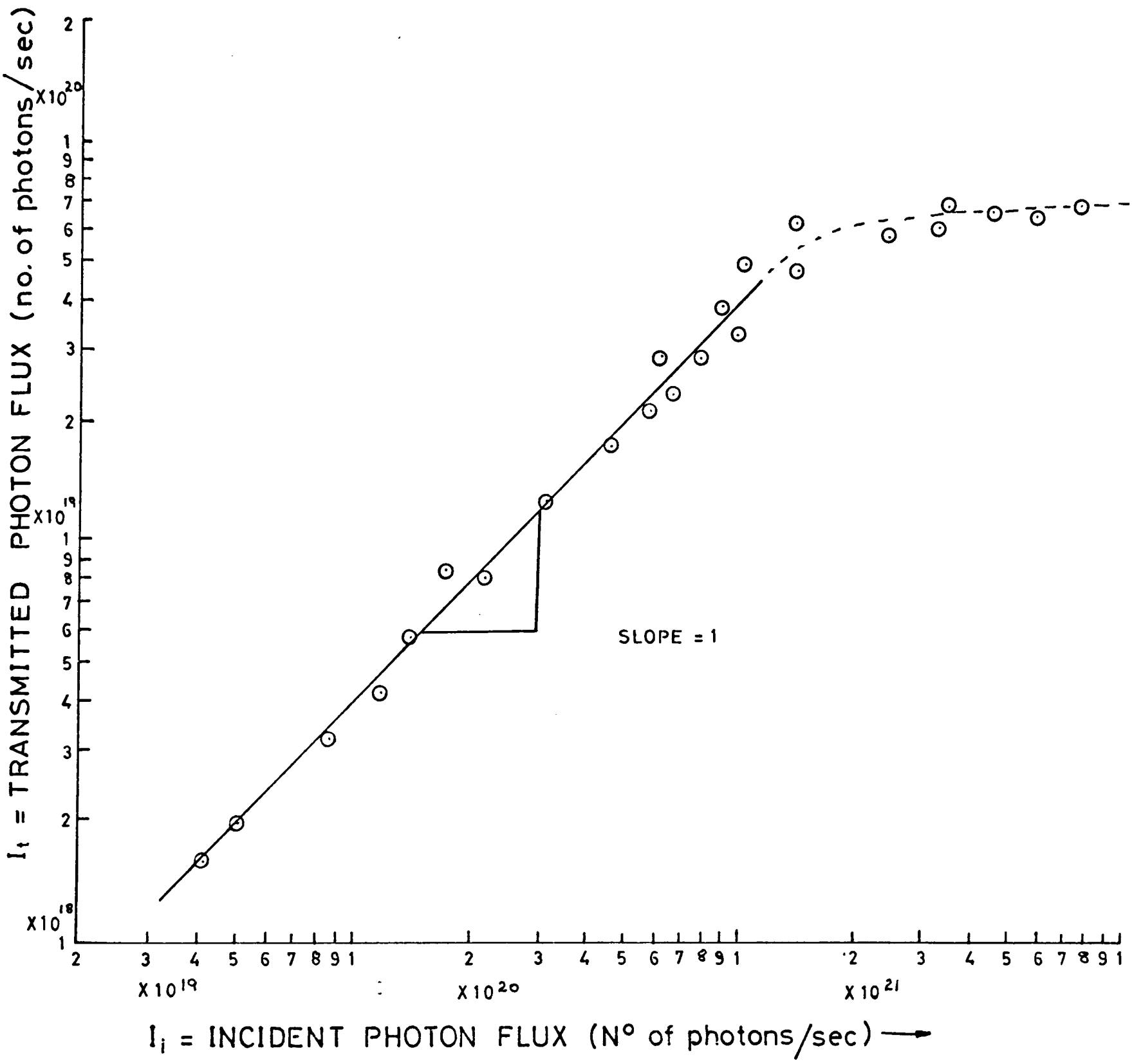
I_t = TRANSMITTED PHOTON FLUX (no. of photons/sec)
X10^20
X10^19
X10^18
SLOPE = 1
X10^19
X10^20
X10^21
I_i = INCIDENT PHOTON FLUX (N° of photons/sec) ⟶

FIG. 8.2.

because of the band-to-band transition of the valence electrons. The photocurrent thus produced will have a quadratic relation with the incident photon density as stated before. To investigate such a double photon process it is considered relevant to investigate the variation of the photoconductivity with the incident photon flux of the laser beam.

b) Photoconductivity in Cadmium Sulphide

The current induced in the CdS crystal by the activation of ruby photons from the Q-switched ruby laser system was drawn by an arrangement as shown in Fig. 8.3. The same crystal plate as was used in the previous experiment was employed to study the photoconductivity. Two sides of the crystal (lengthwise) were connected to a dry cell through a resistor. Electrical contacts between the crystal sides and the connecting wire were made with a silver paste (Dag). The use of such a material for making contact was checked and found to give ohmic contact for all practical purposes. The surface of the crystal was irradiated with the Q-switched ruby laser and the induced current which flew in the crystal was monitored across a 100Ω resistor. The applied voltage between the two sides of the crystal was 60 volts.

Results

The current signals obtained by irradiating the specimen with laser radiation was found to be a single pulse with the peak more or less coincident with the laser peak. At low laser intensity the current signals faithfully follow the laser pulse and the current can be considered to be instantaneous as shown in Fig. 8.4a. The prominent feature of the shape of the current pulse at higher laser power input

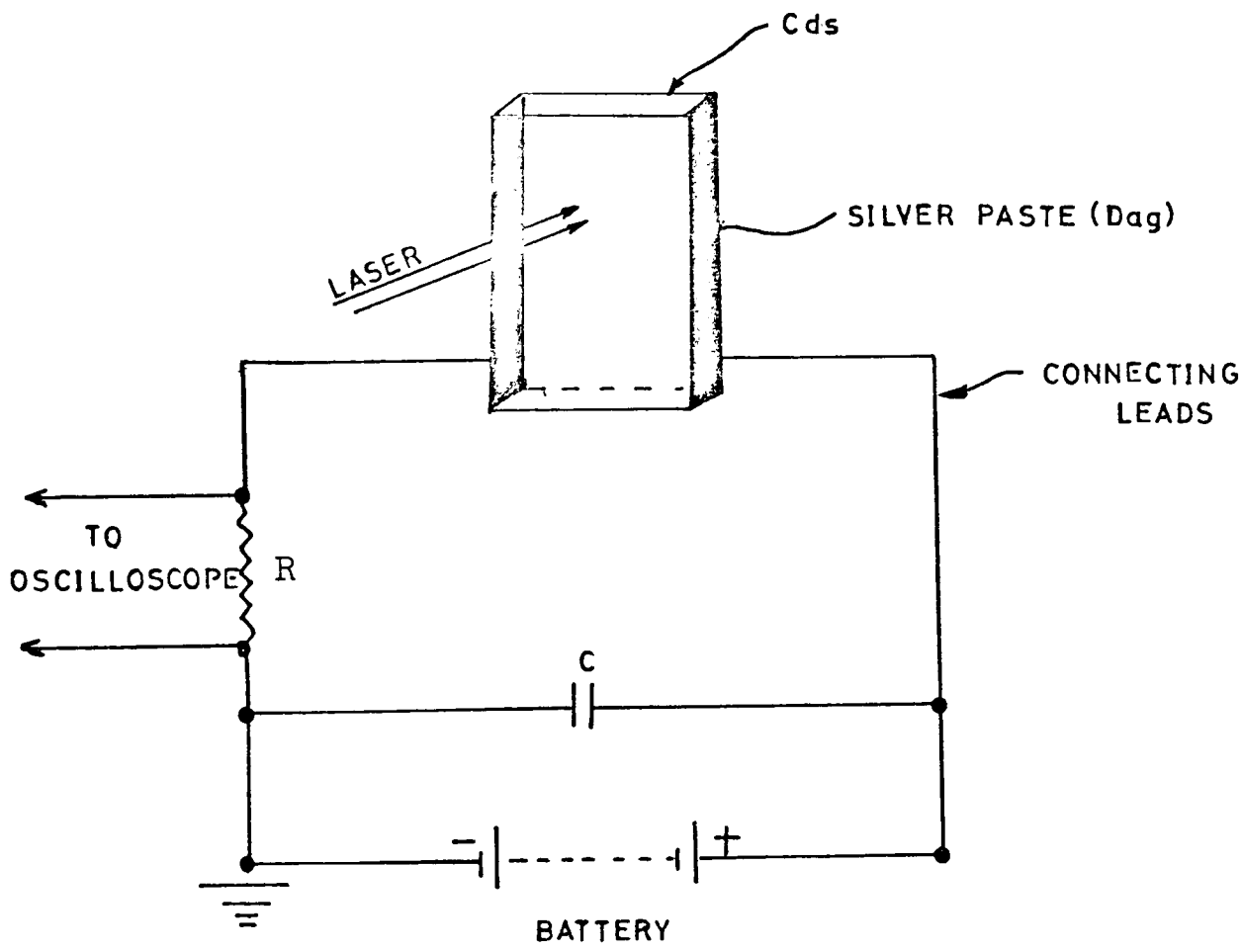

FIG. 8.3. ARRANGEMENT TO DETECT PHOTOCURRENT ACROSS A CdS CRYSTAL.

is the much slower decay of the pulse, as shown in Fig. 8.4b. Although the photocurrent starts to increase at the onset of the laser signal, slow decay remains quite long after the laser pulse has ceased to deliver power to the crystal. A similar observation was made by Katsumi et al. (54) when a CdS crystal was irradiated with ordinary ruby laser (non-Q-switched). It was considered that such a slow decay was probably due to the release of the trapped carriers.

The amplitude of the photocurrent was plotted against the corresponding photon flux on the crystal in a log-log graph (Fig. 8.5). The experimental points for photon flux above approximately 10^{-21} photons sec^{-1} showed a steady increase of the current with the magnitude of the photon flux. Since the absorption was found to be nonlinear above a photon flux of $\sim 10^{21}$ sec^{-1}, a double photon photoconductivity may be expected for such high photon flux. A straight line with a slope 2 was drawn to fit the experimental points. It was found that the straight line fitted the experimental points remarkably well for photon flux above $\sim 7 \times 10^{20}$ sec^{-1}. The results showed that at high photon flux on the crystal the photoconductivity is predominantly due to a valence band-conduction band transition by a double photon absorption process.

For photon flux below $\sim 10^{20}$ sec^{-1}, the photocurrent was found to be very small ($< 10^{-4}$ amps.). An intensity-dependence study for this region was not possible, because the experimental error was found to be comparable with the magnitude of the current detected. The detection of the current was limited by the sensitivity of the system ($\sim 10^{-5}$

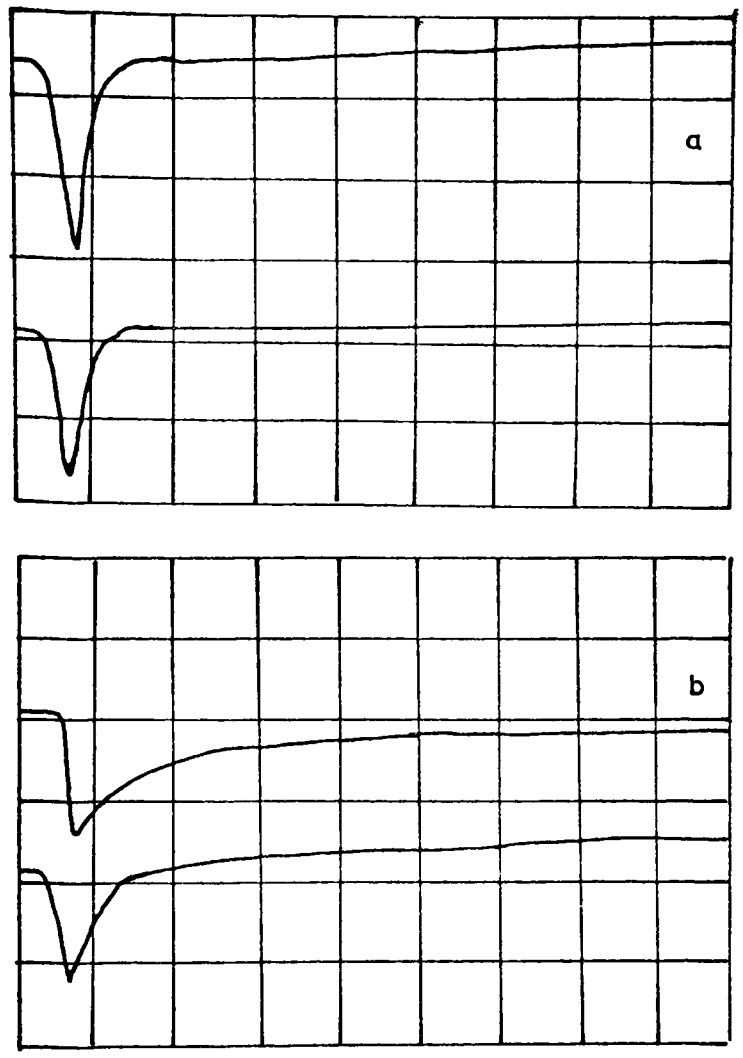

a) UPPER - Current Signal - Scale 0.1 mA/cm
   LOWER - Laser Peak Power $\tilde{\sim}$ 3 x 10^3 watts

b) UPPER - Current Signal - Scale 2.0 mA/cm
   LOWER - Laser Peak Power $\tilde{\sim}$ 2.5 x 10^4 watts

TIME SCALE - 100 nsec/cm

FIG. 8.4. OSCILLOGRAMS OF PHOTOCURRENT ACROSS THE CdS AT DIFFERENT LEVELS OF INCIDENT INTENSITY.

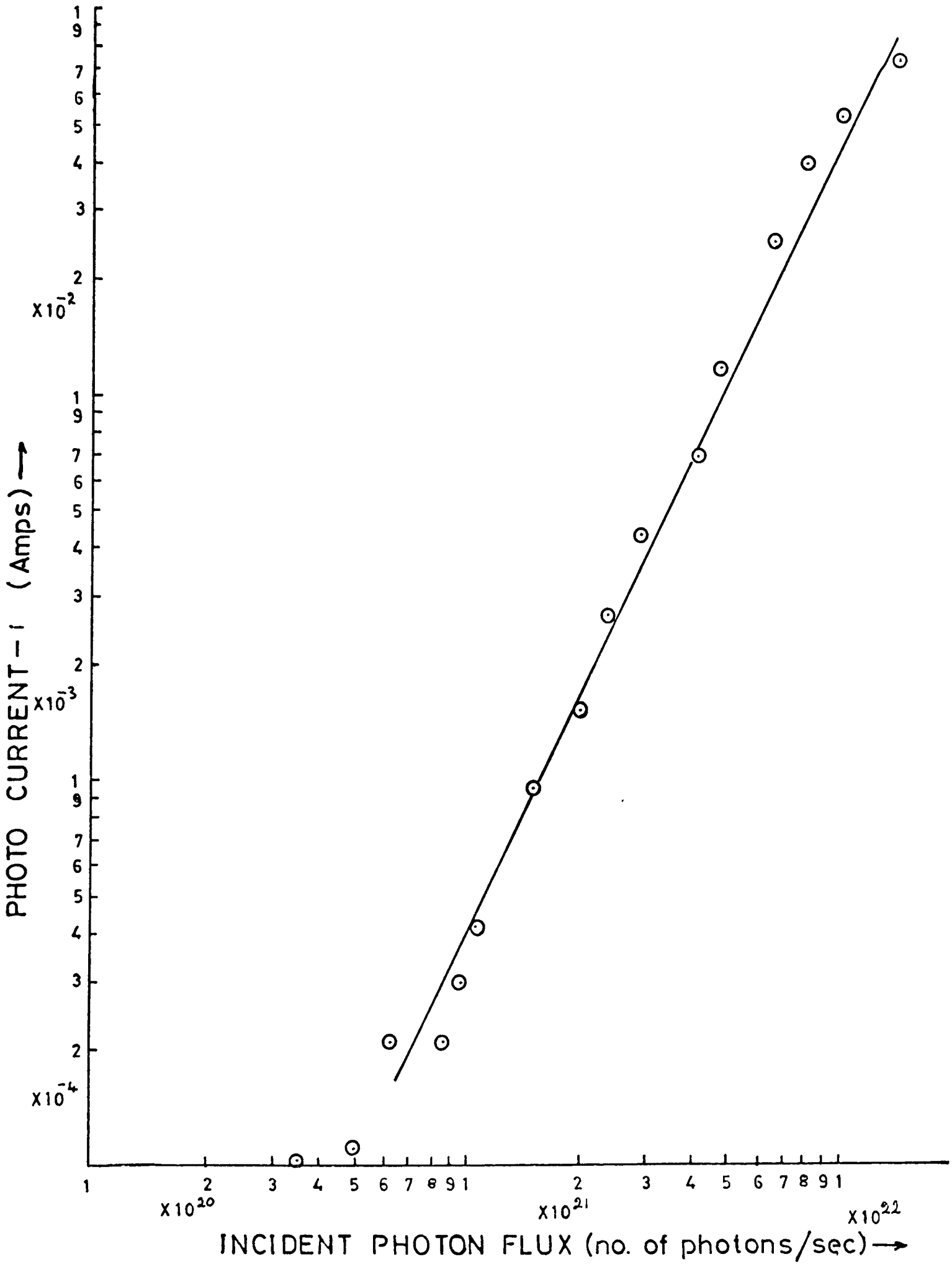
PHOTO CURRENT – I (Amps) →
INCIDENT PHOTON FLUX (no. of photons/sec) →
X10⁻²
X10⁻³
X10⁻⁴
X10²⁰
X10²¹
X10²²

FIG. 8.5.

amps.).

8.5 Discussion of the Results and Conclusions

a) Linear and nonlinear optical absorption in semiconductors have been reported by many workers. The experimental results of Ralston et al. (53) and Geusic et al. (52) with Si indicated a limiting type of intensity-dependent attenuation for high intensity 1.06 μ radiation. They observed linear absorption at low level of incident intensity. The present observation on optical absorption of 0.689 μ radiation in a CdS crystal confirms the above-mentioned results on limiting type transmission in semiconductors. It is suggested that whenever a semiconductor is activated with high intensity Q-switched laser radiation, both linear and nonlinear absorptions have to be considered simultaneously.

The absorption constant A can be calculated from the linear region of the absorption curve. In this region the nonlinear absorption constant can be considered to be negligible, so that a linear transmission equation of the following form can be set:

$$\frac{dN}{dx} = AN \qquad \ldots. (8\text{-}8)$$

From the above equation the constant A can be related to the incident and the transmitted photon fluxes as

$$\ell n\left(\frac{N_t}{N_i}\right) = -A\ell \qquad \ldots. (8\text{-}9)$$

From the results (Fig. 8.2), the value of A was calculated using Eqn. 8-9 and was found to be $\sim$ 20 cm^{-1}. It can be mentioned that the nonlinear absorption constant A calculated for the absorption of 1.06 μ radiation in Si (56) was a factor of 5 higher than this value.

Using the presently calculated value of A in Eqn. 8-3, the two-photon absorption constant B can be calculated at higher photon fluxes (nonlinear region). To compare the result with the Braunstein theory of the double photon absorption in CdS, the value of B was calculated for an incident photon flux of 6×10^{22} photons/ cm^2 sec. At this value of the incident photon flux the transmitted flux (N_t) was found to be 2.39×10^{20} photons/ cm^2 sec. (from Fig. 8.2). The value of B thus calculated was $\sim 1.4 \times 10^{-24}$ cm sec. B has the dimension of cm sec. If it is multiplied by the incident photon flux N_i cm^{-2} sec^{-1}, B can be expressed as

$$B \tilde{\sim} 8 \times 10^{-2} \text{ cm}^{-1}.$$

The value of B calculated by Braunstein (12) for CdS and ruby photons for the same photon flux was slightly more than two orders of magnitude higher than the present value. The discrepancy between the present value of B and the value calculated by Braunstein (12), using a three-band model of the transition, appears to be considerably large. It can be mentioned, however, that the approximations of the different interaction parameters made in Braunstein's calculation were correct only as far as the order of magnitudes were concerned. Thus a large error can easily be introduced in the calculated value of B to account for the observed discrepancy. Considering the magnitude of the values used in the present estimation and the possible errors in Braunstein's calculation of the two photon absorption, it will be justified to conclude that the results of the present experiment conform to a double photon absorption process.

b) The experimental results on photoconductivity in CdS

strongly suggested that at high photon flux the photocurrent is predominantly given by the transition of electrons from the valence band to the conduction band. Such a transition is possible only by the absorption of at least two photons by a single valence band electron. The experimental results strongly supported such a process. From the spectroscopic study of the fluorescence from the laser-illuminated CdS crystal, Braunstein (12) found a reasonable agreement of the observed result with a theoretical model of the double photon absorption.

However, when the incident photon flux was below $\sim 5 \times 10^{20}$ photons/sec. the photocurrent was comparatively much smaller. It can be observed that the appreciable photocurrent is recorded for photon flux above the threshold for linear absorption. Thus it can be inferred that single photon absorption process is intrinsic and is associated with the production of excitons. For the present sample of the CdS it can be concluded that the single photon photoconductivity due to the impurity atoms is negligibly small.

The experiments on optical absorption and photoconductivity in semiconductor both suggested a double photon process at high incident photon fluxes. Such double photon photoelectric emission has also been considered to be an essential characteristic of the laser-surface (metal) interaction. The quantum yield for the production of free electrons by a two photon process in CdS was calculated from the Eqn. 8-7 for a photon flux of 10^{22} photons cm^{-2} sec^{-1}, and was found to be $\sim 2.5 \times 10^{-5}$ electrons/incident photon. If the quantum yield for the production of free electrons from the surface barrier of a metal (e.g. Al has a work function

of ∿ 3.0 eV) is calculated for the similar value of the incident photon flux (from Eqn. 5-3 of Chapter Five) a value of the order of 10^{-10} electrons per photon can be obtained. Such smaller value of the quantum yield of the emission of photoelectrons can be attributed to various factors. The emission process from metal surfaces are contributed by the free electrons of the surface, the concentration of which is much less than the density of atoms pertaining to the interaction process. The metals have very high surface reflectivity compared to the semiconductors. Moreover, for a double photon photoelectric transition in CdS there is a threshold of ∿ 2.4 eV whereas for the surface electrons of Al to be emitted, a minimum energy of ∿ 3 eV is required.

8.6 Additional Experiments

a) I-V characteristic of the photocurrent

A fundamental difference between current flow in the solid and vacuum is that in solids the mobile carriers are continually interacting with the crystal lattice. The presence of recombination centres and impurity atoms will also influence the current flow in the medium. In vacuum, however, the charges are free to move and the current is only limited by space charge. Space charge limited current flow in CdS and CdS_e was reported to take place by Page et al. (57) and Vishchakas et al. (58). In their experiments, an insulating crystal platelet, provided with an emitting contact on one surface and a collecting contact on the other, formed a dielectric diode. In the present experiments, the carriers are produced from a localized volume at the centre of the crystal by the pulsed laser beam. The motion and

collection of these carriers by a suitably biased collector gave rise to the observed photocurrent. If the density of the photoelectrons is kept constant, i.e. if the laser power is the same, the photocurrent should have a linear relation with the applied field E, as given by Eqn. 8-4. In this equation the electron mobility has been considered to be a linear function of the applied field. Thus it was considered necessary to check the linearity of the photocurrent with the applied voltage.

The same experimental arrangement and the crystal as reported in the previous section of this chapter was employed to study the I-V characteristics of the photocurrent. The current was recorded for applied voltage across the crystal ranging from 0 to 500 volts. The I-V plot is shown in Fig. 8.6 for a laser pulse incident on the crystal of $\sim$ 50 kw peak power. For each point in the graph, more than two different readings were taken and the average value of the current was considered.

The I-V curve was found to have two characteristic regions. At low applied field the current was found to increase roughly as the square root of the applied voltage. In this region the slope of the ℓnI-ℓnV plot was found to be $\sim$ 0.6. Above an applied field of $\sim$ 10 V/cm the current was quite linear with the applied field. The slope in this region was found to be $\sim$ 1.07.

The results show that the linearity of the electron mobility must be considered above a certain threshold value of the applied electric field. At low fields the slower increase of the current may possibly be due to the higher electron capture cross-section.

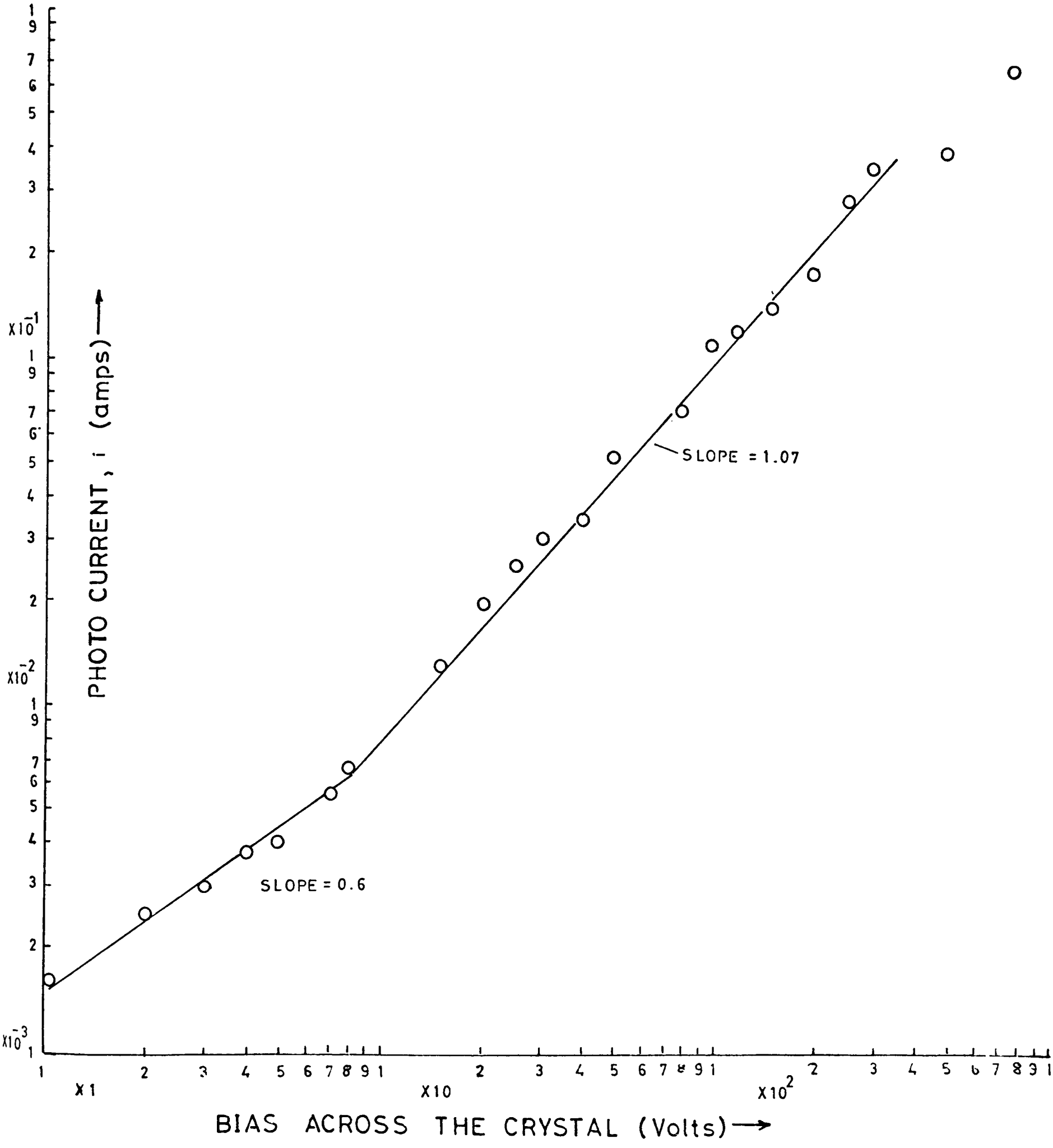
PHOTO CURRENT, i (amps) ⟶
BIAS ACROSS THE CRYSTAL (Volts) ⟶
SLOPE = 1.07
SLOPE = 0.6
X10⁻¹
X10⁻²
X10⁻³
X1
X10
X10²

FIG. 8.6.

It can further be concluded that space-charge limited current flow was not observed in CdS when the carriers were induced by pulsed laser beam. The space-charge limited current would be proportional to the square of the applied voltage (57).

b) Reflection of laser light from the surface of the CdS crystal

The calibrated photodiode (SGD-100) was used to estimate the reflectivity of the CdS crystal used in the previous experiments. The experimental arrangement is as shown in Fig. 8.7. The photodiode P_1 measured the power of the incident beam. The reflected light was received by the photodiode P_2 placed at an angle of θ with the normal to the surface. The laser beam was incident normal to the surface of CdS. Following the treatment in Chapter Four, for the calibration of the photodiode, an expression for the reflection coefficient for the CdS surface can be obtained in terms of the incident power P and the voltage signal obtained in the photodiode P_2. The whole treatment will be similar except the Eqn. 4-2 for the brightness of the incident spot on the CdS surface will be given by

$I = \frac{\gamma P}{2\pi}$, where γ is the reflection coefficient of the surface.

Thus from Eqn. 4-5, the reflection coefficient is given by:

$$\gamma = \frac{2\ d^2 V}{P x b\ \cos\theta . 38.5} \qquad \ldots\ (8\text{-}10)$$

In the experimental set-up the values of the constants were

d = distance of P_2 from the CdS surface

= 0.15 metre.

b = active area of the P.d. = 5×10^{-6} m^2.

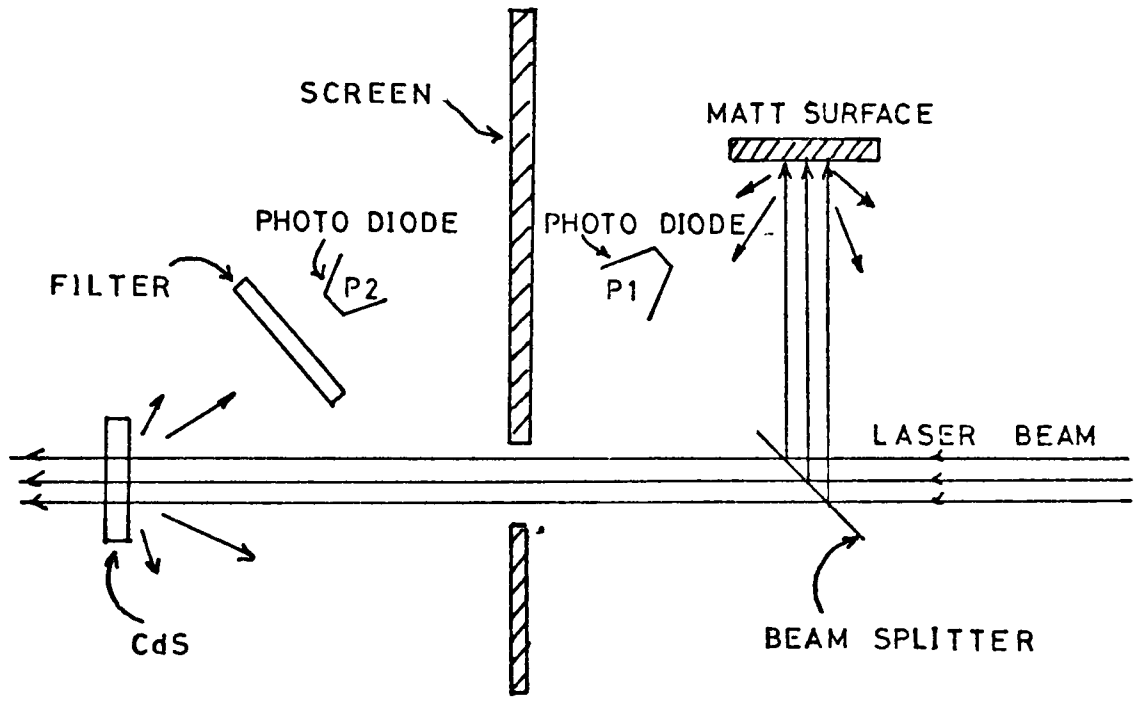

FIG. 8.7. EXPERIMENTAL ARRANGEMENT TO ESTIMATE THE SURFACE REFLECTION OF CdS.

Thus $\gamma = 10^3 \frac{V}{P}$.

The reflection coefficient obtained for different values of the incident laser power is quoted below.

Incident Power P in Watts x 10^3	Voltage at P_2 in Volts	Reflection Coefficient
47.00	4.00	0.080
6.3	0.64	0.101
0.85	0.18	0.097
0.11	0.16	0.145

The results justify the assumption that for the practical purposes the relfectivity of the CdS surface can be considered to be constant for the range of power used in the experiments.

CHAPTER NINE

SUMMARY OF THE RESULTS AND GENERAL CONCLUSIONS

The present investigations have revealed that a Q-switched beam of laser interacts with solids and solid surfaces in a complicated way. Different processes have been found to take place at different stages of the interaction. In the main the interaction with solid surfaces can be classified into two headings, e.g. (a) interaction at low-intensity laser beam (< 30 MW/cm^2), and (b) interaction at high-intensity laser beam.

a) The low-level interaction (for laser intensity below approximately 5 MW/cm^2) is characterized exclusively by the emission of photoelectrons. For materials with work function ϕ greater than the incident photon energy $h\nu$ the emission current was found to be due to a process by which the energy of two photons are simultaneously delivered to a single electron and subsequently ejecting it out of the surface barrier. The amplitude of the current thus obtained was found to depend on the second power of the intensity of the laser pulse. A third order effect was not detected from material with $\phi > 2h\nu$ (e.g. Ta, W, etc.). It is believed that a third order effect will be too small to be detected with the present technique and the lower order effect from the impurity atoms will influence such measurements. For the incident intensity of the laser beam greater than approximately 3 KW/cm^2 the photoconductivity in CdS (band gap Eg > $h\nu$) was also found to be due to a double photon absorption process which results in a band-to-band transition of the valence electrons. From the results it

is concluded that for high incident photon fluxes (compared to the photon flux from ordinary monochromatic sources) on any solid, the absorption process has to be considered in terms of a linear and a nonlinear part. The observed photocurrent in a highly pure semiconductor with Eg > hν and the electrons emitted from metal surfaces with ϕ > hν will be the result of the nonlinear part of the absorption process. In a metal the linearly absorbed photon energy (single photon process) will be dissipated inside the solid as heat, whereas in a semiconductor such absorption may be associated with the production of excitons or free electrons from the impurity atoms.

The effect of the linear absorption in metal surfaces was detected at incident intensity higher than approximately 5 MW/cm^2. For such intensities a delayed emission current with a slower rise time was observed along with the instantaneous photoelectric current. It is suggested that the delayed emission can be treated in terms of the Richardson effect with the concept of a temperature rise of the activated surface.

b) At very high incident intensity (> 30 MW/cm^2) the temperature of the irradiated surface due to linear absorption was found to rise very rapidly above the boiling point of the metal. The result of such high temperature is the ejection of a cloud of ionized material consisting of electrons, ions and neutral particles. The cloud was found to maintain a quasi-neutral property throughout its motion in an applied field. The current signals were generated only when a directed motion of any species of charges was developed very close to a biased collector. The shape of

the current signals was found to depend on the polarity of the biasing collector and its position with respect to the point of origin of the plasma. The current signals were found to be due to the resultant motion of the electrons and ions in their preferred directions. Because of the different reaction times of the electrons and ions when a field acts upon them, the resultant current signal when collected at a large distance from the target was found to consist of two peaks in addition to the initial current peak due to the nonlinear effect.

With such a model of the generation of the current signal from the laser-produced metal plasma, the current due to the reverse motion of the ions (when the collector is biased positive with respect to the target) was found to be comparable to the electron current due to the diffusion of electrons from the plasma boundary to the collector. It was thought that the generation of secondary ions and electrons from the collector surface as a result of the bombardment of the high energy primary particles has a positive contribution to the general shape of the current signal and could also account for the observed high ion current. The measurement of the plasma velocity by the time of flight of the 'plasma drop', making use of the quasi-neutral property of the plasma, gave a value ($\sim 3 \times 10^7$ cm/sec.) which agreed well with the value quoted by other workers, deduced from the hydrodynamical model of the expansion of the laser-produced plasma. The electron temperature of the plasma was measured by Langmuir technique. In this measurement the second current peak which is considered to be due to the diffusion of electrons from the plasma to the

suitably biased collector was plotted against the applied bias voltage. The electron temperature was estimated to be of the order of 10^5 ^oK which seemed to be in reasonable agreement with the theoretical works of Dawson (46) and others.

Another effect which has been considered to have a significant contribution to the current signals is the 'reverse photoelectric process'. In this process the photo-electrons are produced from the surrounding metal parts by the high frequency radiation emitted from the laser-produced metal plasma. When current signal was recorded with a negative bias at the collector so as to repel the initial electrons emitted from the target, the initial peak appear-ing during the laser pulse was found to be due to such a reverse photoeffect.

The mystery of the so-called 'rear-side emission' reported by Knecht (7) was investigated further. The invest-igation revealed that the current detected at a collector placed at the rear of a target when the front surface was irradiated with laser beam was due essentially to an electrostatic coupling effect. When very rapid voltage change between any conductors takes place, the electrostatic coupling through the stray capacitance between them will be important. When charges are produced by a Q-switched laser pulse the displacement current due to a voltage signal dev-eloped across a resistor connected to any neighbouring metal parts will be detected. The observed current signal detected at the rear side was successfully explained in terms of such a displacement current.

Finally, it is concluded that to have a general

theory of the interaction of laser beam with solids much more sophisticated experimental techniques have to be employed. Any theory must take account of the different process, as mentioned above. In the present work, a quantitative theoretical analysis was not attempted because of the uncertainty in the values of the different parameters involved in the interaction. But it is believed that the work gives a correct outline of the interaction process as far as the qualitative behaviour of the end products of the interactions is concerned.

REFERENCES

1. R.E. Honig and J.R. Woolston, "Laser-induced Emission of Electrons, Ions and Neutral Atoms from Solid Surfaces", Appl. Phys. Letters, 2, 138 (1963).

2. D. Lichtman and J.F. Ready, "Laser Beam Induced Electron Emission", Phys. Rev. Letters, 10, 342 (1963).

3. C.M. Verber and A.H. Adelman, "Laser Induced Thermionic Emission", Appl. Phys. Letters,2, 220 (1963).

4. F. Giori, L.A. Mackenzie and E.J. McKinney, "Laser-induced Thermionic Emission", Appl. Phys. Letters, 3, 25 (1963).

5. J.F. Ready, "Mechanism of Electron Emission Produced by a Giant-pulse Laser", Phys. Rev., 137, A620 (1965).

6. J.F. Ready, "Effects Due to Absorption of Laser Radiation", J. Appl. Phys., 36, 462 (1965).

7. Walter L. Knecht, "Initial Energies of Laser-induced Electron Emission from W", Appl. Phys. Letters, 6, 99 (1965).

8. S.H. Khan, F.A. Richards and D. Walsh, "Time Resolution of Laser Induced Electron and Ion Emission", I.E.E.E. Journal of Quantum Electronics QE-1, 359 (1965).

9. F.A. Richards, D.Phil. Thesis, University of Oxford, 1967.

10. H. Sonnenberg, H. Heffner and W. Spicer, "Two-Photon Photoelectric Effect in Cs_3Sb", Appl. Phys. Letters, 5, 95 (1964).

11. M.C. Teich, J.M. Schroeer and G.J. Wolga, "Double Quantum Photoelectric Emission from Sodium Metal", Phys. Rev. Letters, 13, 611 (1964).

12. R. Braunstein and N. Ockman, "Optical Double Photon Absorption in CdS", Physical Review 134, A499 (1964).

13. E.M. Logothetis and P.L. Hartman, "Laser-induced Electron Emission from Solids: Many-photon Photoelectric Effects and Thermionic Emission", Physical Review 187, 460 (1969).

14. E.M. Logothetis and P.L. Hartman, "Three Photon-photoelectric Effects in Gold", Physical Rev. Letters 18, 581 (1967).

15. D. Walsh, "The Photo-electric Emission Time from a Metal Surface", Phys. Letters 24A, 724 (1967).

16. Frank J. Allen, "A Description of Laser-produced Plasma (Electron and Ion Temperature, etc.). Dec. 68, Proj. RDT/E-I-T-06 FLD/GD 20/9, 20/5.

17. E. Archbold and T.P. Hughes, Nature 204, 4959, 670, (1964).

18. D.D. Burgess, B.C. Fawcett and N.J. Peacock, Proceedings of Physical Society 92, 4962 (1966).

19. A.H. Ehler, "Plasma Formed by a Laser Pulse on a Tungsten Target", Journal of Appl. Phys. 37, 4962 (1966).

20. R.V. Ambartsumyan, N.G. Basov, F.A. Bouko, V.S. Zuev, O.N. Krokhin, P.G. Kryukov, Yu. V. Senal-skii and Yu, Yu. Stoilore, Journal of Experimental and Theoretical Physics (U.S.S.R. 48, 1583 (1965); Societ Physics JETP21, 1061 (1965).

21. R.E. Schlier, H.W. Furumoto and H.L. Coccon, "Laser-induced Surface Effects", AVCO Corporation Report, AVSSD-0129-66-RR, 7 May 1966.

22. H. Opower and E. Burlefinger, Temperature Determination of Plasmas Produced by Giant Laser Pulses", Phys. Letters 16, (1), 37 (1965).

23. N.G. Basov, V.A. Boiko, V.A. Dement'ev, O.N. Krokhin and G.V. Slizkov, Journal of Experimental and Theoretical Physics (U.S.S.R.) 51, 989, (1966); Soviet Physics JETP24, 4, 659 (1967).

24. A.J. Alcock, P.P. Dashinin and S.A. Ramsden, "Temperature Measurements of a Laser Spark from Soft X-Ray Emission", Phys. Rev. Letters, 17, (10), 528 (1966).

25. C. David, P.V. Avizonis, H. Welchel, C. Bruce and K.D. Pyatt, "Density and Temperature of a Laser Induced Plasma", I.E.E.E. Journal of Quantum Electronics, Vol. QE-2, No. 9 (1966).

26. C.D. David and P.V. Avizonis, "Optical Interferometry, Diagnostic Techniques", Panel 5.6 Laser Techniques.

27. Walter L. Knecht, "Laser-induced Spontaneous Electron Emission from Rear Side of Metal Foils", Appl. Phys. Letters, 8, 254 (1966).

28. P.W. Li and N.R. Isenor, "Evidence Against Spontaneous Electron Emission from Rear Side of Metal Foils", Appl. Phys Letters 13, 238 (1968).

29. R.E. Honig, "Laser-induced Emission of Electrons and Positive Ions from Metals and Semiconductors", Appl. Phys. Letters 3, 8, (1963).

30. S. Namba, P.H. Kim and A. Mitsuyama, "Ion Emission from Metal Surface Irradiated by Giant-pulse Laser Beam", Lasers, Paris 1967 (p. 113), J. Appl. Physics 37, 3330 (1966).

31. P. Langer, G. Tonon, F. Floux and A. Ducauze, "Laser-induced Emission of Electrons, Ions and X-rays from Solid Targets", I.E.E.E. Journal of Quantum Electronics, Vol. QE-2, No. 9 (1966).

32. H. Opower and W. Press, Zeits. f. Naturf. 21A, 334 (1966).

33. W.I. Linlor, "Some Properties of Plasma Produced by Laser Giant Pulse", Phys. Rev. Letters 12, 383 (1964).

34. J.F. Ready, "Development of Plume of Material Vaporized by a Giant-pulse Laser", Appl. Phys. Letters 3, 11 (1963).

35. W.J. Fader, "Hydrodynamic Model of a Spherical Plasma Produced by a Q-spoiled Laser Irradiation of a Solid Particle", The Phys. of Fluid 11, 10 (1968).

36. Carslaw and Jaeger, "Conduction of Heat in Solids, 2nd Impression.

37. I. Adawi, "Theory of the Surface Photoelectric Effect for One and Two Photons", Physical Rev. 134, 3A (1964).

38. P. Kafalas, J.I. Masters and E.M.E. Murray, "Photosensitive Liquid Used as a Non-destructive Passive Q-switch in a Ruby Laser", J. Appl. Phys. 35, 2349 (1964).

39. D. Hull, "Combination Laser Q-switch Using a Spinning Mirror and Saturable Dye", Appl. Optics 5, 1342 (1966).

40. N.F. Mott and H. Jones, "The Theory of the Properties of the Metals and Alloys", Chap. II (Dover Publications Inc., New York, 1958).

41. Gy. Farkas, I. Kertesz, Zs. Naray and P. Varga, "On the Intensity Dependence of the Nonlinear Electron Emission from Silver Induced by a High Power Laser Beam", 24A, 475 (1967).

42. C.M. Verber and A.H. Adelman, "Laser-induced Thermionic Emission from Tantalum", Jour. Appl. Phys. 36, 1522 (1965).

43. A. Caruso and R. Gratton, "Some Properties of the Plasmas Produced by Irradiating Light Solids by Laser Pulses", Plasma Physics 10, 867 (1968).

44. Allan F. Haught and Donald H. Polk, "High-temperature Plasmas Produced by Laser Beam Irradiation of Single Solid Particles", The Phys. of Fluids, 9, 2047 (1966).

45. Yu. V. Afananyev, O.N. Krokhin and G.V. Slizkov, "Evaporation and Heating of a Substance Due to Laser Radiation", I.E.E.E. Journal of Quantum Electronics, QE-2, 483 (1966).

46. John M. Dawson, "On the Production of Plasma by Giant Pulse Lasers", The Phys. of Fluids 7, 981 (1964).

47. J.F. Ready, E. Bernal and L.T. Shepherd, "Mechanism of Laser-Surface Interaction", (Final Report to Ballistic Research Laboratories, DA18001, AMC1040X.75P, May 1968, Unpublished).

48. L. Spitzer, Jr., "Physics of Fully Ionized Gases (Interscience Publishers Inc., New York, 1962).

49. R.H. Huddlestone and S.L. Leonard, "Plasma Diagnostic Techniques", Academic Press, New York, p. 135, (1965).

50. G. Diemer and W. Hoogenstraaten, J. Phys. Chem. Solids 2119, 47, 220 (1957).

51. T.S. Moss, "Optical Properties of Semiconductors", p.216. Butterworths Scientific Publications, London, (1956).

52. J.E. Geusic, S. Singh, D.W. Tipping and T.C. Rich, "Three Photon Stepwise Optical Limiting in Silicon", Phys. Rev. Letters 19, 1126 (1967).

53. J.M. Ralston and R.K. Chang, "Optical Limiting in Semiconductors", Appl. Phys. Letters 15, 165 (1969).

54. Katsumi Yoshino, Yasutaka Watanbe and Yoshino Inuishi, "Laser-induced Photoconductivity in CdS Crystal", Japan.J. Appl. Phys. 4, 312 (1965).

55. Richard H. Bube and Ching-Tao Ho, "Laser Saturation of Photoconductivity and Determination of Imperfection Parameters in Sensitive Photoconductors", Jour. Appl. Phys. 37, 4132 (1966)

56. A. Hordvick, CLEA 69, Washington, D.C., Paper 3.1 (1969), (Unpublished).

57. D.J. Page, A.A. Kayali and G.T. Wright, "Some Observations of Space Charge Limited Current in Cadmium Sulphide Crystals", Proc. Phys. Soc., Vol. 80 (1962).

58. Yu. K. Vishchakas, A.A. Smilga and G.B. Yushka, "Space Charge Limited Current in Cadmium Selenide Single Crystal Whiskers", Soviet Phys-Semiconductor, 1, 1437 (1968).